PL-TR-95-2106

CASE STUDIES OF SEISMIC DISCRIMINATION PROBLEMS AND REGIONAL DISCRIMINANT TRANSPORTABILITY

Douglas R. Baumgardt

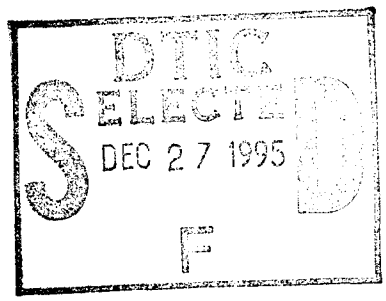

ENSCO, Inc.
Signal Analysis and Systems Division
5400 Port Royal Road
Springfield, Virginia 22151-2312

31 July 1995

Final Report
25 June 1993 - 24 June 1995

PHILLIPS LABORATORY
Directorate of Geophysics
AIR FORCE MATERIEL COMMAND
HANSCOM AFB, MA 01731-3010

SPONSORED BY
Advanced Research Projects Agency (DoD)
Nuclear Monitoring Research Office
ARPA ORDER No. A-128

MONITORED BY
Phillips Laboratory
CONTRACT No. F19628-93-C-0103

The views and conclusions contained in this document are those of the authors and should not be interpreted as representing the official policies, either express or implied, of the Air Force or the U.S. Government.

This technical report has been reviewed and is approved for publication.

JAMES F. LEWKOWICZ
Contract Manager
Earth Sciences Division

JAMES F. LEWKOWICZ
Director
Earth Sciences Division

This report has been reviewed by the ESC Public Affairs Office (PA) and is releasable to the National Technical Information Service (NTIS).

Qualified requestors may obtain additional copies from the Defense Technical Information Center. All others should apply to the National Technical Information Service.

If your address has changed, or if you wish to be removed from the mailing list, or if the addressee is no longer employed by your organization, please notify PL/IM, 29 Randolph Road, Hanscom AFB, MA 01731-3010. This will assist us in maintaining a current mailing list.

Do not return copies of this report unless contractual obligations or notices on a specific document requires that it be returned.

REPORT DOCUMENTATION PAGE

Form Approved
OMB No. 0704-0188

1. AGENCY USE ONLY (Leave blank)	2. REPORT DATE	3. REPORT TYPE AND DATES COVERED
	31 July 1995	Final Report - 25 June 1993 through 24 June 1995

4. TITLE AND SUBTITLE
Case Studies of Seismic Discrimination Problems and Regional Discriminant Transportability

5. FUNDING NUMBERS
PE 62301E
PR NM 93 TA GM WU AC
Contract F19628-93-C-0103

6. AUTHOR(S)
Douglas R. Baumgardt

7. PERFORMING ORGANIZATION NAME(S) AND ADDRESS(ES)
ENSCO, Inc.
Signal Analysis and Systems Division
5400 Port Royal Road
Springfield, Virginia 22151-2312

8. PERFORMING ORGANIZATION REPORT NUMBER
SAS-TR-95-117

9. SPONSORING / MONITORING AGENCY NAME(S) AND ADDRESS(ES)
Phillips Laboratory
29 Randolph Road
Hanscom AFB, Massachusetts 01731-3010

Contract Manager: James Lewkowicz/GPE

10. SPONSORING / MONITORING AGENCY REPORT NUMBER
PL-TR-95-2106

11. SUPPLEMENTARY NOTES

12a. DISTRIBUTION / AVAILABILITY STATEMENT
Approved for public release; distribution unlimited

12b. DISTRIBUTION CODE

13. ABSTRACT *(Maximum 200 words)*

This report describes case studies of regional seismic discriminants, using the Intelligent Seismic Event Identification System (ISEIS), and addresses issues related to the transportability of regional discriminants. Some of the key results of this study include: (1) Observations of large Lg waves from mine blasts. (2) Investigation of the P/S frequency-dependence discriminant. (3) The importance of signal decorrelation in the generation of spectral scalloping by ripplefired mine blasts. (4) Path corrections for the Lg spectral-ratio discriminant using a simple anelastic attenuation model. Also described in this report is a discrimination study of the January 5, 1995 Urals mine event. Because there were no nearby earthquakes or blasts in the Urals mine region, recordings of the event at regional station ARU were compared with WMQ recordings of Chinese nuclear blasts and earthquakes at comparable distance but in a different geographic and tectonic region. This comparison indicated that the January 5, 1995 event had Pn/Lg amplitude ratios more comparable to Chinese earthquakes than nuclear explosions. Based on the analysis of Pn/Lg ratios at NORESS and comparison those produced by PNEs in the same region recorded at NORSAR, we conclude that the January 5, 1995 event produced much stronger shear waves (Sn, Lg) relative to P than did nuclear blasts. We conclude that the event was probably a mine tremor or collapse.

14. SUBJECT TERMS	15. NUMBER OF PAGES
Discrimination, regional seismology, transportability, earthquakes, economic blasts, ripplefire, propagation paths, Lg attenuation	86
	16. PRICE CODE

17. SECURITY CLASSIFICATION OF REPORT	18. SECURITY CLASSIFICATION OF THIS PAGE	19. SECURITY CLASSIFICATION OF ABSTRACT	20. LIMITATION OF ABSTRACT
Unclassified	Unclassified	Unclassified	SAR

TABLE OF CONTENTS

TABLE OF CONTENTS

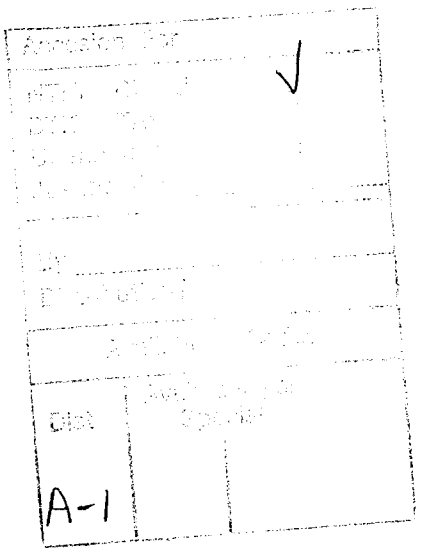

EXECUTIVE SUMMARY

Recent research in seismic discrimination has produced a number of discriminants based on the feature measurements on high-frequency seismic waveforms. Many investigators claim success in discrimination on small numbers of events or events selected from a specific region or mine. A major challenge in developing a system for monitoring world-wide comprehensive testban treaty is to develop discriminants which are "transportable," meaning that they can be made to perform well in different geological and tectonic environments than in the regions where they were developed. This final report describes the results of studies of discriminant transportability, focusing on waveform discriminants for identifying small blasts and earthquakes.

Our studies using the Intelligent Seismic Event Identification System (ISEIS) of many events in different regions and mines have revealed numerous instances where regional waveform discriminants appear to fail or are problematic. Some of these cases have to do with propagation-path effects, but others relate to the differences in physical mechanisms of single nuclear explosions and ripplefired mine blasts and earthquakes. Ripplefired blasts often have waveform characteristics which appear to be more similar to those of rockbursts and earthquakes rather than single nuclear explosions.

The following are the major results and conclusions of this study:

(1) **Large shear waves from mine blasts** - We have frequently observed that *Pn/Sn* and *Pn/Lg* amplitude ratios at high frequency (4-16 Hz) for mine blasts in Scandinavia and Russia have large variation, with many blasts having large shear waves comparable to earthquakes. Most notable are the blasts in the Kiruna mine in Sweden recorded at the ARCESS and FINESA arrays, where most of the events have small *Pn/Lg* ratios at frequencies out to 16 Hz comparable to nearby earthquakes. However, mine blasts with small ratios have also been observed in the Kola Peninsula mines. Evidently, mine blasts can induce large shear waves due to rock fracture and/or

spalling of rock fragments at the bench face. Perhaps mine blasts should be classified as another kind of rockburst if they induce significant shear. Nuclear explosions do not appear to induce large shear waves and thus, the discriminant may be safe for identifying single nuclear blasts.

(2) ***P/S* frequency dependence** - Recent investigators have suggested that the frequency dependence of the regional *P/S* ratio may be a discriminant, with explosions having increasing *P/S* ratio with frequency but earthquakes having very little dependence on frequency. This may be due to strong *Rg*-to-shear scattering from shallow explosions at low frequency. However, a number of examples can be found where this lack of frequency dependence does not hold for earthquakes. For example, the Steigen earthquake swarm in Norway has increasing *Pn/Lg* ratios with frequency, like mine blasts, although the *Pn/Lg* ratios are usually lower for the earthquakes. Also, unusual frequency dependencies have been observed where the ratio does not change consistently with frequency. For example, the recent Ural event of January 5, 1995 had low *Pn/Lg* ratios at low and high frequency, like earthquakes, and high ratios in the 2-5 Hz band, like explosions. We have also studied the frequency dependence of *Pn/Lg* amplitude ratios for Russian and Chinese nuclear blasts and earthquakes recorded at the Chinese station WMQ. The events have the expected frequency dependence after correction for distance, i.e., the nuclear explosions have increasing ratios with frequency whereas the earthquakes have very little frequency dependence.

(3) **Ripplefire induced spectral scalloping** - The time-independent spectral scalloping observed in many mine blasts results from the superposition of multiple source-time functions which are correlated. However, time-independent scalloping is not always observed in ripplefired blasts. Source finiteness may cause this lack of spectral scalloping due to decorrelation of the source-time functions, perhaps due to spatially distributed source or differences in the time-source functions of the individual blasts.

(4) ***Lg* spectral ratios** - The *Lg* spectral ratio discriminant has worked for discriminating blasts and earthquakes in western U.S. However, this discriminant often fails to discriminate blasts and earthquakes in Scandinavia. This discriminant appears to work when the blasts occur in shallow

rocks which couple poorly at high frequency, such as the NTS high gas porosity rocks, and the earthquakes occur at greater depths. In regions where the surface geology and deeper crustal rocks are more homogeneous, such as in the Scandinavian shield regions, there appears to be little spectral difference between explosions and shallow earthquakes. We have also implemented a distance correction scheme which accounts for affects of anelastic attenuation on the *Lg* spectral ratio and have found that this correction reduces much of the observed distance-dependent scatter in the *Lg* spectral ratios recorded at GERESS for earthquakes, mineblasts, and rockbursts.

These examples serve as caveats for using a straight statistical approach to discrimination which relies on the same unified discriminants to identify all events. Any discrimination approach needs to consider regional variations in the performance of discriminants when making event identifications.

1.0 INTRODUCTION

Past studies of regional seismic discriminants have revealed that certain simple seismic measurements can be used as discriminants between classes of known earthquakes and explosions, including conventional economic explosions (mine blasts) and nuclear explosion tests. These include frequency dependent ratios of amplitudes of different phases, in particular, regional *P/S* (e.g., Bennett et al, 1989; Baumgardt and Young, 1990; Kim et al, 1993), spectral ratios on individual regional seismic phases (Murphy and Bennett, 1982; Bennett and Murphy, 1986; Taylor et al, 1988; Taylor et al, 1989; Walter et al, 1994), and the detection of ripplefire by the identification of spectral scalloping (Baumgardt and Ziegler, 1988; Hedlin et al, 1989; Hedlin et al, 1990; Kim et al, 1994). Our development of the research discrimination system Intelligent Seismic Event Identification System (ISEIS) (Baumgardt et al, 1991) has implemented these discriminants and tested them on many mine blasts and earthquakes in Scandinavia, recorded at the regional arrays NORESS, ARCESS, FINESA, and GERESS (Baumgardt et al, 1991; Baumgardt et al, 1992), and single-station recordings of earthquakes and nuclear blasts in China and Russia (Baumgardt and Der, 1994). These studies have all generally produced positive results for the discriminants. However, we have observed regional variations in the performance of the discriminants. In some instances, they fail and causes of the failures need to be understood for the discriminants to be effective in any future comprehensive test ban treaty monitoring system.

The project described in this final report has addressed issues related to "discriminant transportability," that is, the problem of using discriminants developed with training events in a "known" region, consisting of both earthquakes and explosions, to a new "unknown" region where many such training events of known earthquakes and explosions may be available. These issues arise in the context of monitoring compliance with a comprehensive test ban treaty, which may involve many countries in the world and where there will be limited historical data for certain rare seismic source types, such as nuclear explosions. In monitoring a non-proliferation treaty, the

"first test" scenario must be considered, where a possible nuclear weapons test must be detected and identified in a country which has never tested before. This country may be located far from countries which have historically tested nuclear explosions, and regions which differ in terms of the tectonic source mechanisms of the earthquakes, and geological effects, both in the potential source regions as well as along propagation paths from the sources to monitoring stations. We must be sure that discriminants found for training events in the known regions can be "transported" to the new, unknown regions accounting for differences in geology and propagation path effects on the discriminants. Our earlier report, completed during this project (Baumgardt and Der, 1994) addressed the transportability of the *Pn/Lg* amplitude discriminant and investigated methods for correcting the discriminant for distance and for calibrating it to different tectonic regions, using geological and crustal structure information.

Another issue in discriminant transportability relates to the reliability in the performance of discriminants. Can the waveform discriminants, such as the *P/S* amplitude ratio, the frequency dependence of the *P/S* amplitude ratio, *Lg* spectral ratio, and the spectral scalloping ripplefire discriminant, produce false identifications, based on training sets of events in known regions, and can the causes of these false identifications be understood and accounted for in event identification? This report documents some examples of instances from these studies where regional discriminants seem to fail, or appear to provide problematic discriminatory capability.

In Section 2.0, we describe an interesting set of known mine blasts at the Kiruna mine in Sweden which have high-frequency *P/S* ratios which look like nearby earthquakes. Other examples of mine blasts with earthquake-like have been found in our earlier research (e.g., Baumgardt, 1993 a, b) but never quite so concentrated set in one mine. We suggest that mineblasts may be just another kind of rockburst, which may be more earthquake-like rather than explosion-like in terms of the amount of shear-wave energy they produce.

In Section 3.0, we present results of a study of a new discriminant developed with western U.S. earthquakes and NTS nuclear explosions. This discriminant, which has been a recent focus

of attention to investigators at Lawrence Livermore Laboratories (e.g., Walter et al, 1994), relies on the frequency dependence of the *Pn/Lg* ratio. Differences in frequency dependence of *Pn/Lg* ratio have been observed for earthquakes and nuclear explosions in the western U.S. Other studies (e.g., Bennett et al, 1989; Baumgardt and Young, 1990; Kim et al, 1993) have hinted at the same discriminant since they show better discrimination between blasts and earthquakes using high-frequency *P/S* ratio than low-frequency measurements. We suggest that this discriminant behaves quite differently for mine blasts than for nuclear blasts. We also show how this discriminant is complicated by frequency-dependent propagation path effects, and study further the performance of the distance correction schemes introduced by Baumgardt and Der (1994) as they relate to the frequency dependence of the *Pn/Lg* ratio for mine blasts, nuclear explosions, and earthquakes.

Section 4.0 discusses the performance of the spectral scalloping ripplefire discriminant which has been an area active of observational and theoretical research since it was first suggested as a regional discriminant by Baumgardt and Ziegler (1988). We point out the importance of an apparently overlooked factor, signal decorrelation, on the character of spectral scalloping. Ripplefire signal correlation, not source finiteness, is the cause of ripplefire-produced spectral scalloping. If the signals of the ripplefire pattern can be decorrelated, the spectral scalloping will not be observed. Furthermore, the observed degree of decorrelation which can be discerned from the character of the spectral scalloping may be useful in characterizing the ripplefiring itself.

Section 5.0 addresses again the *Lg* spectral ratio discriminant for mine blasts, nuclear explosions and earthquakes. In this and earlier studies (e.g., Baumgardt, 1993b) we have found this discriminant to be marginal for discriminating mine blasts and earthquakes, although it does appear to work in certain regions. We discuss possible reasons for this variability of performance of the discriminant and present a method for correcting the discriminant for distance using an anelastic attenuation model.

Section 6.0 summarizes the results of this project and the overall conclusions.

2.0 The Kiruna Mine Blasts of Northern Sweden: Case Study of the Failure of the P/S Ratio Discriminant

2.1 Background

The regional *P/S* ratio discriminant has long been investigated as a possible discriminant between explosions and earthquakes, because intuitively, earthquakes being shear, dislocation type sources should produce more shear-wave energy than explosions (Pomeroy et al, 1982). Thus, *P/S* ratios should be lower for earthquakes than for explosions. Early studies in the 1970's and early 1980's demonstrated the potential of the discriminant (e.g., Blandford et al, 1981) for separating explosions and earthquakes. Bennett et al (1989) demonstrated improved separation of nuclear explosions and earthquakes on the basis of high frequency *S/P* ratios. Baumgardt and Young (1990) studied mine blasts and earthquakes which were in the same region in Scandinavia and showed that mine blasts have significantly higher *Pn/Lg* ratios at high frequency than earthquakes. This research led to the implementation of this discriminant in the Intelligent Seismic Event Identification System, or ISEIS (Baumgardt et al, 1991), and the discriminant has proven to be effective in a number of regions of Scandinavia and Europe monitored by the NORESS-type arrays (Baumgardt, 1993). Kim et al (1993) demonstrated the success of this discriminant at high frequencies for discriminating quarry blasts and earthquakes in eastern U.S.

It has commonly been assumed that this discriminant will usually separate mine blasts and earthquakes at high frequency. When the ratio is taken as P to S, the blasts should have larger ratios than earthquakes since they should underexcite shear waves. Recently, this discriminant has rarely been shown to fail, although earlier work of Nuttli (1981) indicated it was a problematic discriminant in Iran. Recently, Lynnes and Baumstark (1991) studied this discriminant for many events in eastern and western U.S. and argued that its performance can be vitiated by propagation path effects.

The purpose of this study is to show examples of the failure of high-frequency *P/S* ratios to discriminate small blasts in the Kiruna mine in northern Sweden from nearby earthquakes. These events can be identified by other means. However, we present these results as a caveat against over relying on this discriminant. We have studied 45 events, mostly recorded at the ARCESS array and some at the FINESA array, shown plotted on the map in Figure 1. These events occurred near the Steigen earthquake swarm in Norway (Atakan, 1992) as well as other presumed earthquakes and mine blasts in the area. The location clustering of these events was discussed by Rivière-Barbier (1993). Figure 1 shows the locations of these blasts along with locations of other nearby earthquakes and explosions. In Rivière-Barbier's report, the IMS locations of these events were assigned to her designated Area 24 between 67.5-68° N latitude and 18-22° E longitude. Most of the IMS local magnitudes were between 1.5 and 2.0. These magnitudes are well below the level of 2.5 generally thought to be the lower limit of concern for a 5 kt decoupled nuclear explosion. However, monitoring "mini-nuclear explosions" may require consideration of events this small. Rivière-Barbier (1993) indicated the consistency of origin times for these events of 22:35 in the summer months and 23:35 in the winter months which were consistent with the known blasting practice at the Kiruna mine. Based on consistency of origin time and location, these events were most likely mine blasts. Waveform discriminants extracted for the ARCESS and NORESS data should confirm that these events are mine blasts.

2.2 Failure of the *P/S* Ratio Discriminant

These events have been processed by ISEIS using the incoherent beam method of computing log RMS amplitudes in 9 frequency bands and measuring *P* and *S* amplitudes in each of the frequency bands. Examples of the incoherent beams for one of the blasts are shown on logged and unlogged plots in Figures 2 (a) and (b), respectively. The traces have all been shifted for display purposes. Phase identifications from the IMS are shown in Figure 2. The maximum RMS amplitude was measured on the first regional *P* phase, usually *Pn*, and the largest regional *S*,

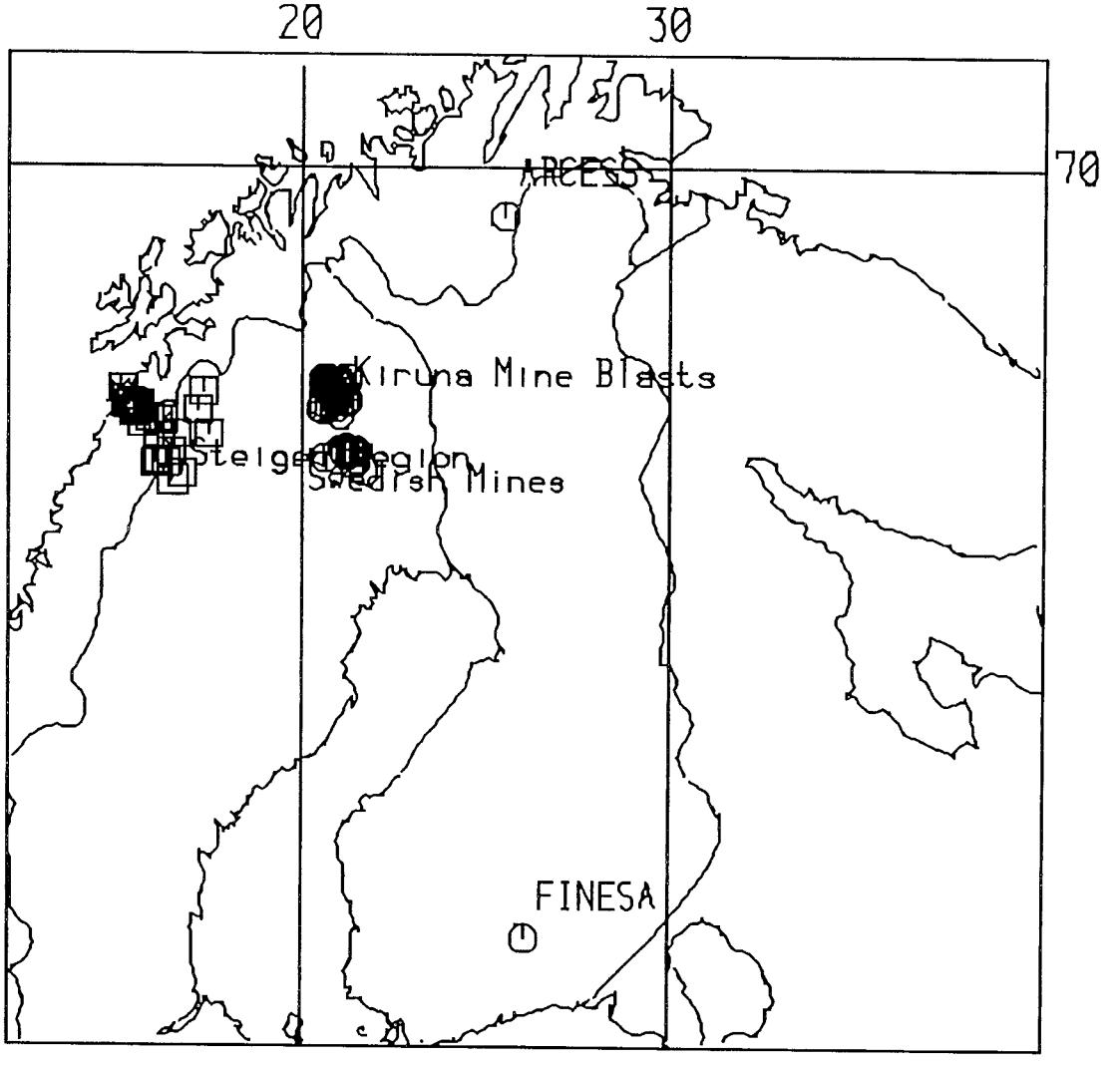

Figure 1: Map showing locations of Kiruna mine blasts, nearby mine blasts, and earthquakes in Northern Sweden, earthquakes in the Steigen region of Norway, and the ARCESS and FINESA arrays.

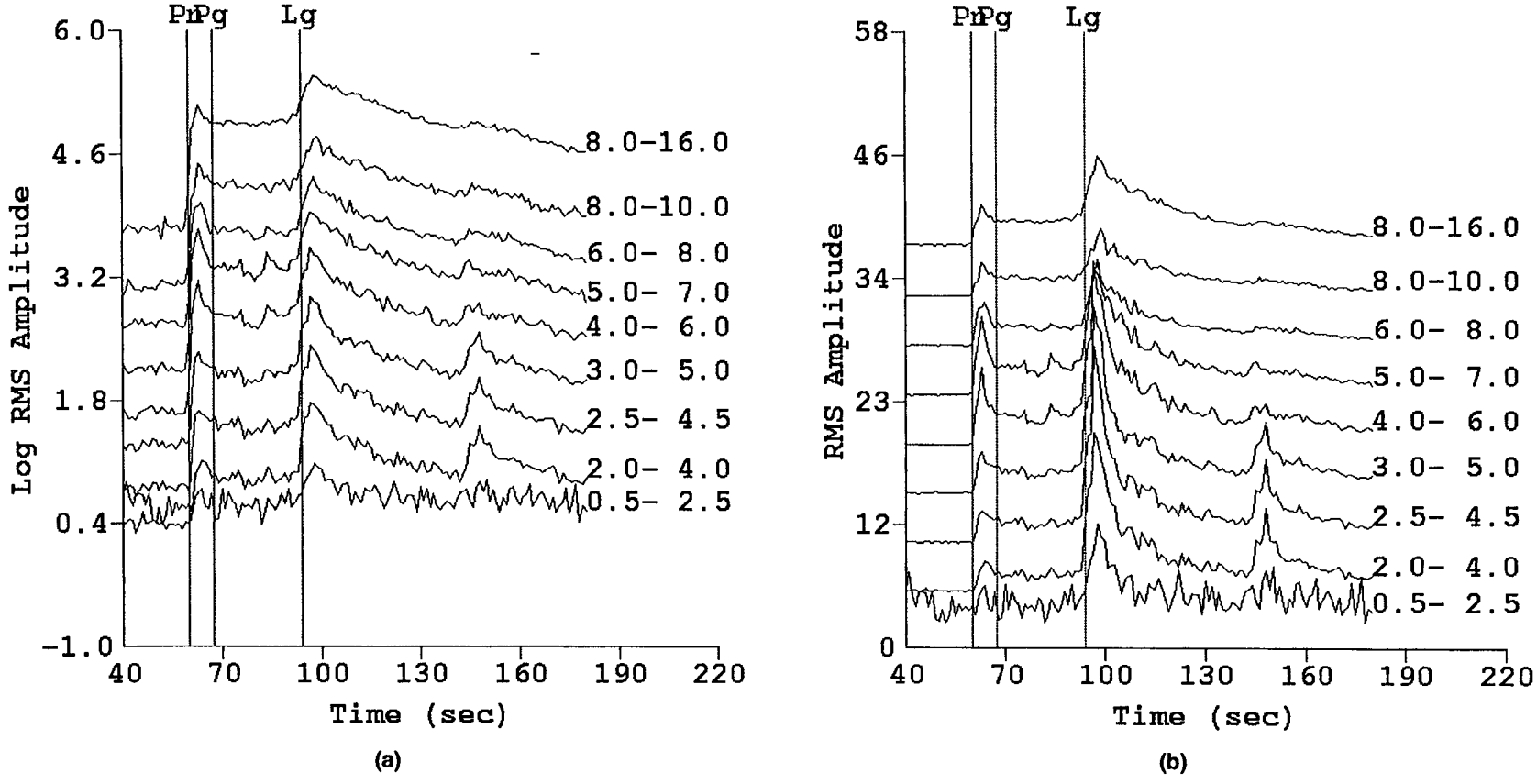

Figure 2: (a) Incoherent beams of a Kiruna mine blast - log RMS, (b) Incoherent beams of a Kiruna mine blast - unlogged RMS. Lines indicate phase picks. All beams shifted for display purposes.

identified as *Lg*. The amplitude ratios, *Pn/Lg*, have been computed for all the events in the 9 consistent frequency bands and stored in the Oracle database.

Figure 3 shows the *Pn/Lg* ratios in the 8 to 16 Hz filter plotted as a function of distance for the events recorded at ARCESS (Figure 3a) and FINESA (Figure 3b). The *Pn/Lg* ratios for Kiruna events are plotted as triangles, and the other nearby mine blasts are plotted as circles and the earthquakes are plotted as squares. Each of the groups of event type are labeled in Figure 3. The epicentral distances of the Kiruna blasts from ARCESS are around 280 km as compared to about 740 km from FINESA. Because of the much greater distance of the blasts from FINESA, only measurements for the larger events could be made for that array.

The *Pn/Lg* ratios of the Kiruna mine blasts as a group overlap the earthquake group in the 8 to 16 Hz band and are well below those observed for other mine blasts in the region. This observation holds for measurements at both the ARCESS and FINESA arrays. As shown in Figure 3(a), most other mine blasts in the region have higher *Pn/Lg* ratios than these events, with log ratios at ARCESS between -0.2 and 0.3, and most earthquakes, which typically have low *Pn/Lg* ratios, with ratios below -0.2. The Kiruna blasts as a group have ratios between - 0.3 and - 0.8, well below the values of nearby blasts and overlapping the values of the Steigen earthquakes. Propagation path differences cannot explain this overlap since all the events are in the same region and the propagation paths are all nearly identical. We have also plotted a "Scandinavian distance correction line," empirically derived using events recorded at the Scandinavian arrays, to correct the *Pn/Lg* ratio for distance in the Scandinavian shield (Baumgardt and Der, 1994). Even though the Kiruna blasts are closer to the arrays than the earthquakes, the distance correction between the Kiruna and Steigen events would be insignificant.

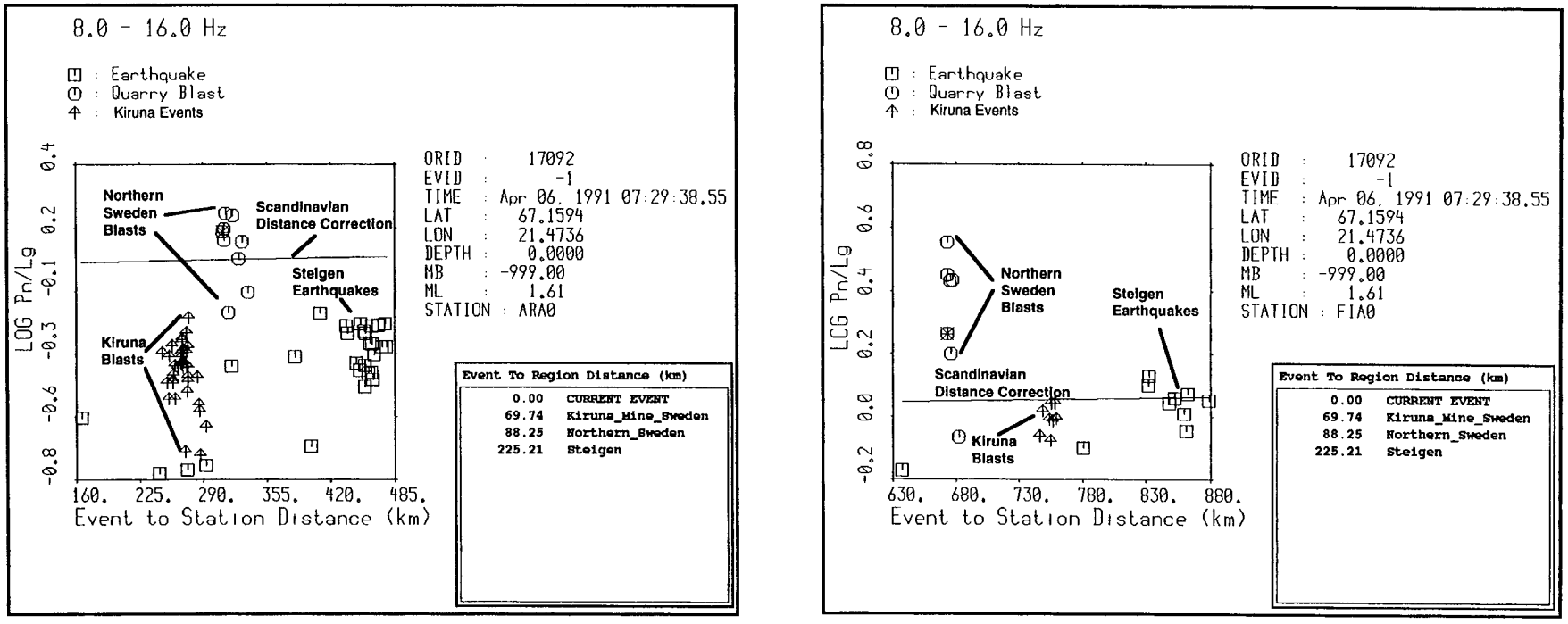

Figure 3: Scatter plots versus distance of *Pn/Lg* ratios in the 8 to 16 Hz filter band of the Kiruna blasts and other nearby earthquakes and explosions. (a) ARCESS data, (b) FINESA data. The line indicates the *Pn/Lg* distance correction derived for ratios based on measurements of Scandinavian data. Note that the *Pn/Lg* ratios for the Kiruna blasts overlap those of the earthquakes.

We observe this overlap in all frequency bands, as shown in Figures 4 and 5 for ARCESS and FINESA, respectively. These plots show the same scatterplot of *Pn/Lg* ratio versus distance in four frequency bands, 2-4 Hz, 3-5 Hz, 5-7 Hz, and 8-10 Hz. As frequency band increases, the non-Kiruna explosion and earthquake classes separate. However, the Kiruna mine blast points seem to decrease with increasing frequency, as do the earthquakes. There is some overlap between the Kiruna blasts and the explosion group, but the bulk of the events fall below the explosion group. Many of the Kiruna mine blasts have ratios which are below the earthquakes.

These results show that for some reason the Kiruna mine blasts excite strong shear waves relative to compressional waves and have *Pn/Lg* ratios which more closely resemble earthquakes than explosions. Yet, we know that the events are mine blasts. Clearly, the *Pn/Lg* ratio feature alone would fail to identify these events. This raises the question of why the discriminant fails so clearly to identify these events and if there are any other means of identifying the events besides location and the consistency of origin times.

2.3 Ripplefire and Coda Discriminants

One of the surest ways to identify mine blasts is with the "ripplefire" discriminant, where mine blast ripplefiring can be identified on the basis of observation of time-independent spectral modulations (Baumgardt and Ziegler, 1988; Hedlin et al, 1989; 1990). Our study of these events using the ISEIS-based Multiple Event Recognition System (MERSY) has identified many of the events as mine blasts. Figure 6 shows an example of a sonogram for one of the blasts. Clearly, this event has time independent spectral scalloping beginning at the *Pn* onset and extending well into the coda.

Figure 7 shows the MERSY output for the event. MERSY computes cepstra for these spectra, as described by Baumgardt and Ziegler (1988), and then automatically identifies the locations of the peaks which are consistent for all the phases. Figure 7 shows the MERSY cepstral

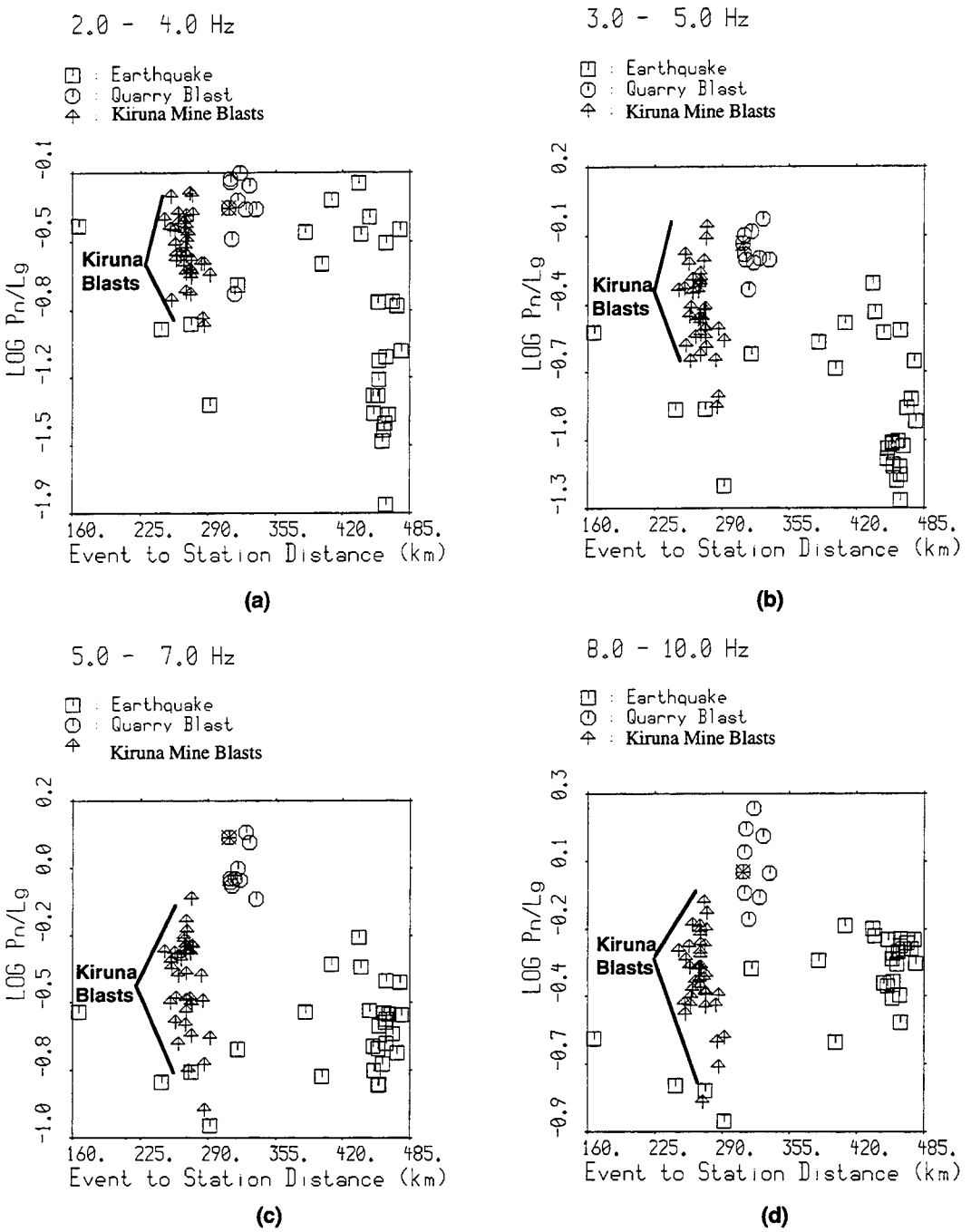

Figure 4: Scatter plots of *Pn/Lg* in 4 frequency bands versus distance for the ARCESS array. (a) 2-4 Hz, (b) 3-5 Hz, (c) 5-7 Hz, (d) 8-10 Hz. Kiruna mine blasts are plotted as triangles. These points overlap earthquakes in all frequency bands.

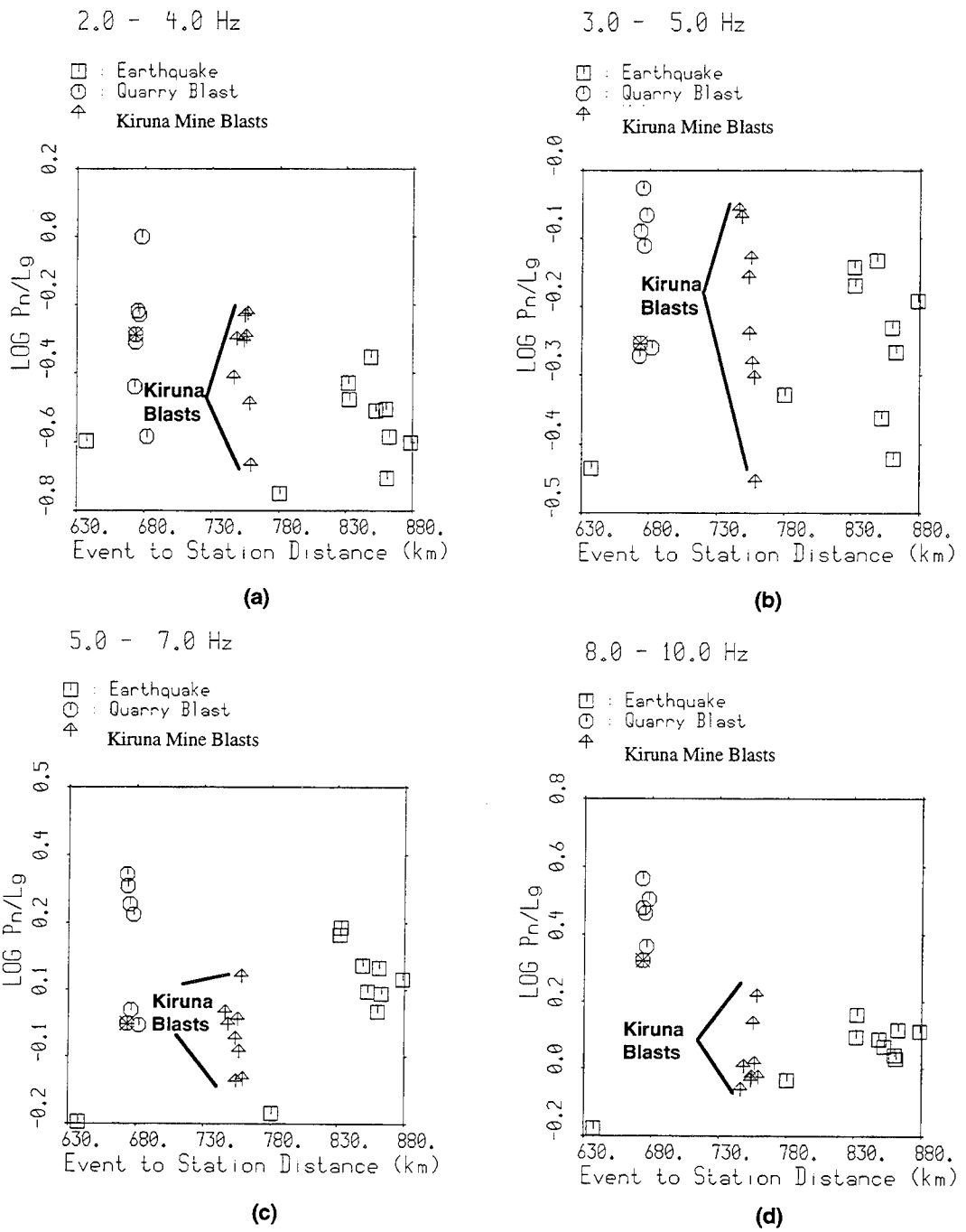

Figure 5: Scatter plots of *Pn/Lg* in 4 frequency bands versus distance for the FINESA array. (a) 2-4 Hz, (b) 3-5 Hz, (c) 5-7 Hz, (d) 8-10 Hz. Kiruna mine blasts are plotted as triangles. These points overlap earthquakes in all frequency bands.

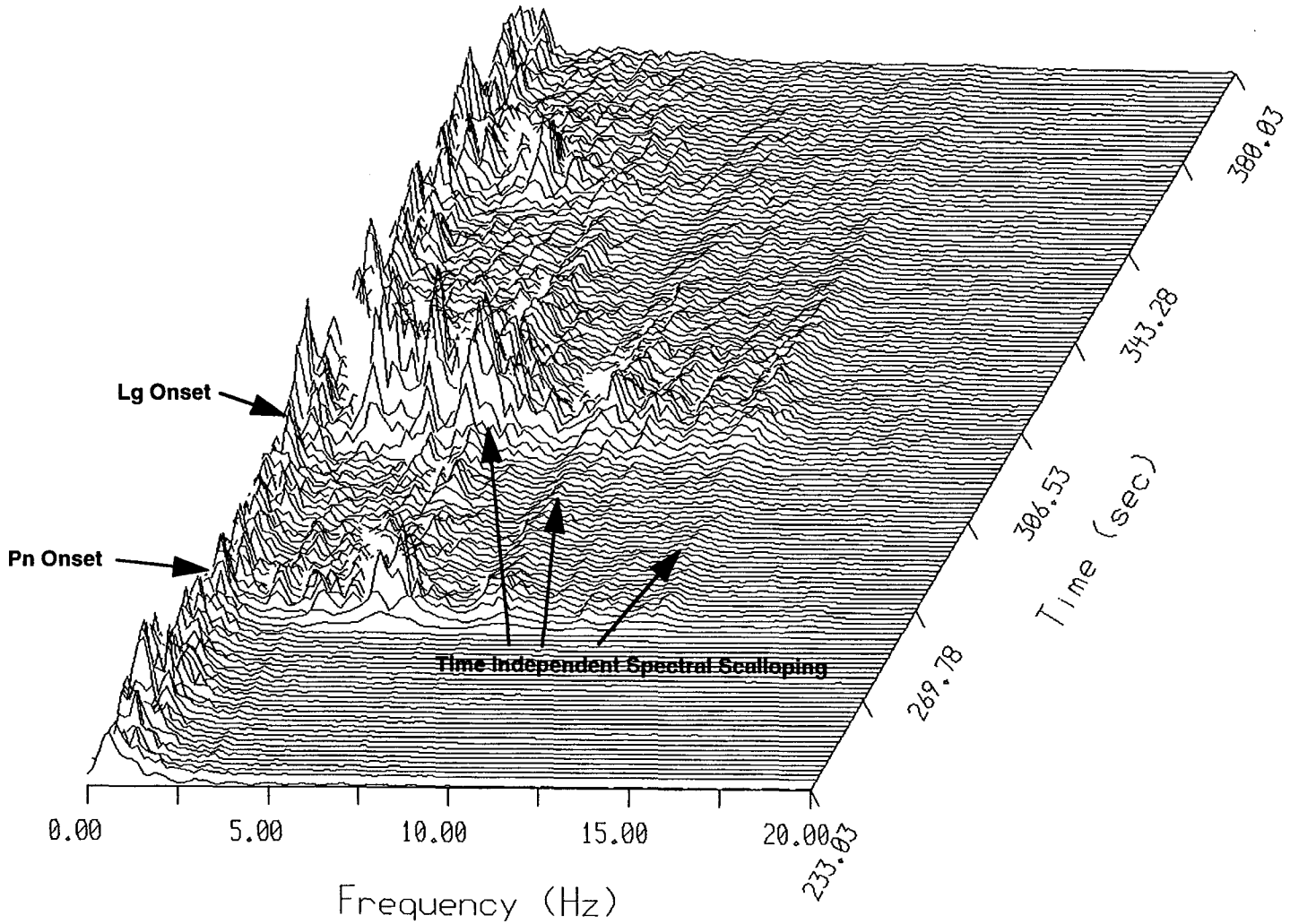

Figure 6: ISEIS array-averaged spectrogram (sonogram) of a Kiruna (Northern Sweden) mine blast which shows obvious time-independent spectral scalloping.

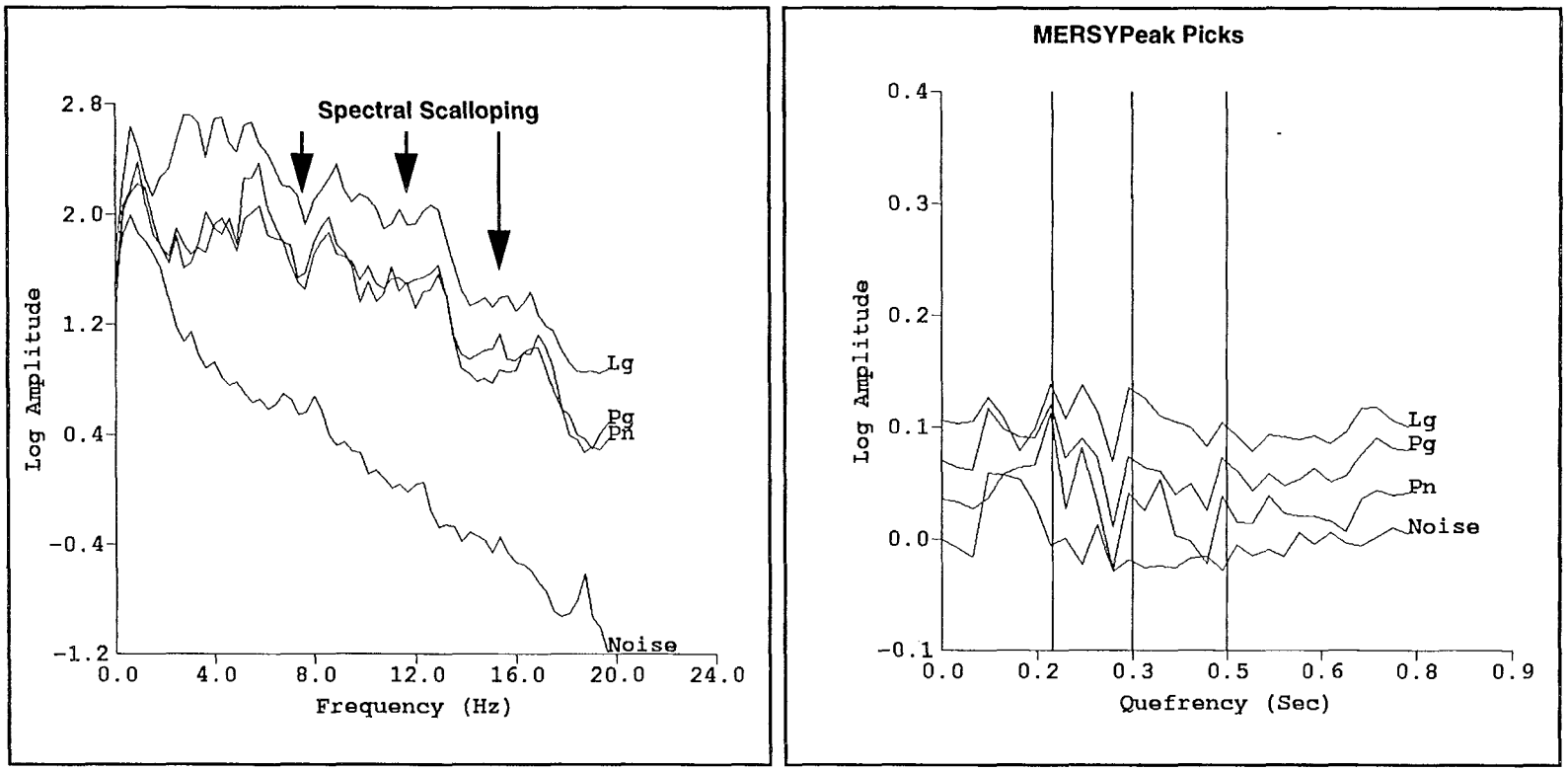

Kiruna Mine Blast Array-Averaged Spectra
ARCESS Array

(a)

Kiruna Mine Blast Array-Averaged Cepstra
ARCESS Array

(b)

Figure 7: (a) Array stacked amplitude spectra for a ripple fired blast at the Kiruna mine, Northern Sweden. (b) MERSY display of cepstra for the 3 regional phase spectra and noise. Cepstra have been shifted for display purposes.

plots for the spectra and the peaks which were identified by the system. Of the 45 events analyzed, 30 events had time independent spectral scalloping and were identified by MERSY as mine blasts.

We have also considered another potential discriminant for these events based on observations of coda shape. Recently, Blandford (1993) has suggested that the complexity discriminant, which was originally developed for teleseismic data, would discriminate regionally recorded earthquakes and explosions. The idea of the coda complexity discriminant is that earthquakes might be expected to produce emergent *Pn* waves and stronger codas than explosions. Earthquake sources may produce stronger shear waves and *Rg* waves than explosion sources, which in turn may excite stronger coda waves by mode conversion of the shear and *Rg* waves from lateral heterogeneities.

In our analyses of mine blasts, earthquakes, and nuclear explosions in different regions, we have noted a difference in coda shape between blasts and earthquakes. Examples of coda shapes in ISEIS incoherent beams (log rms) for a southern Norway mine blast and earthquake recorded at the NORESS array and a Tien-Shan earthquake and a Lop Nor nuclear explosion, recorded at the CDSN station WMQ, are shown in Figure 8. These plots reveal that explosions have different coda shapes than earthquakes. Explosions have a highly peaked *P* signal and then a curved coda which often decays to a low value before the onset of the *S* wave. It is interesting that both the mine blast in Norway and nuclear explosion in China exhibit this same distinctive coda shape. Earthquakes, on the other hand, appear to have relatively flat codas.

Figure 9 shows examples of ARCESS incoherent-beam codas from four Kiruna mine blasts. Each of the incoherent beams have the phase identifications labeled. Note that in all cases, the *Lg* waves have larger RMS amplitudes than the *Pn* waves at high frequency as we expect for earthquakes. However, we believe by visual inspection that their coda shapes are more typical of the blast codas for mine blasts recorded at NORESS and shown in Figures 8 (a) and 8 (c).

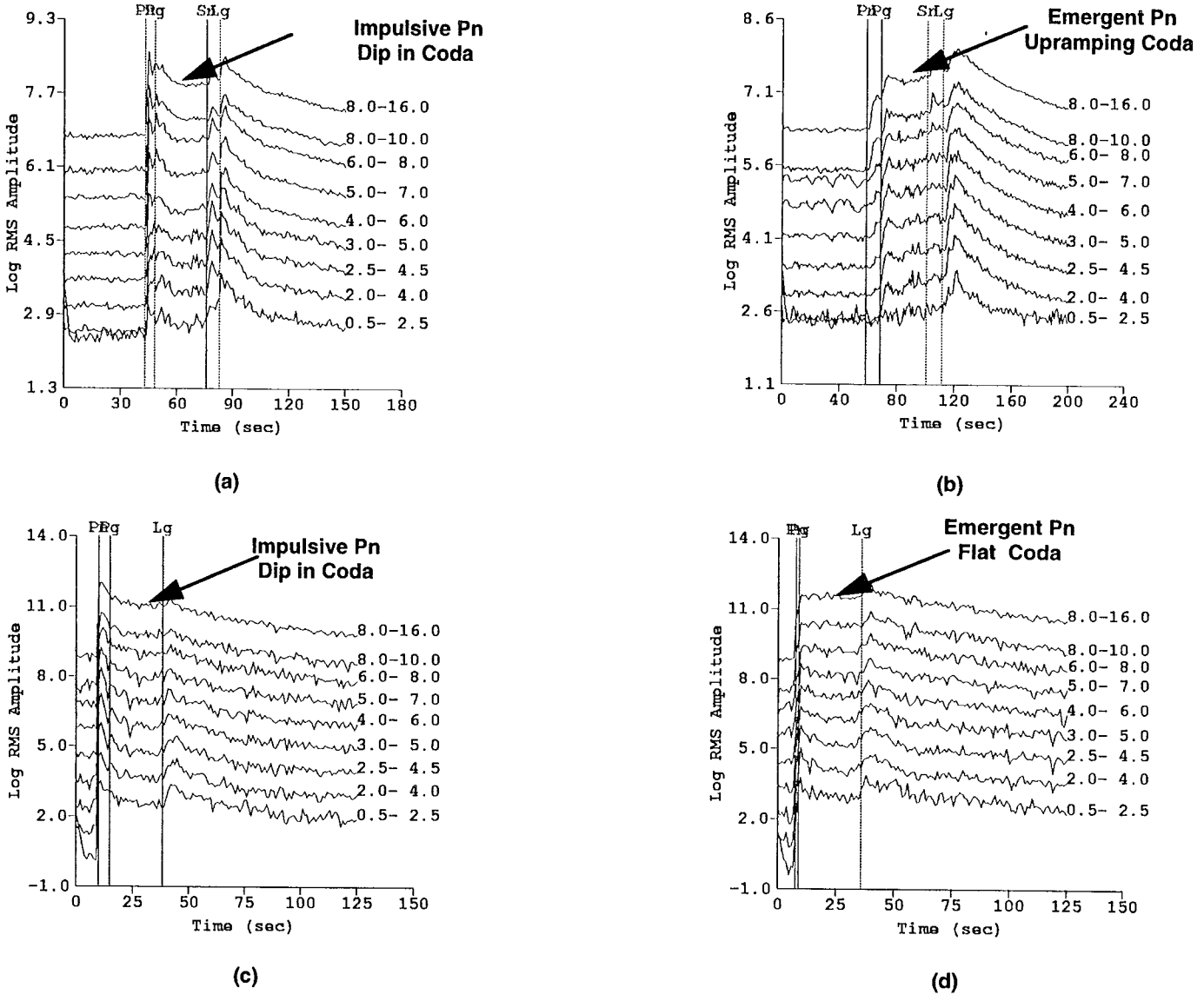

Figure 8: Examples of log-RMS incoherent beams which demonstrate a new coda discriminant. (a) Mine blast in southern Norway recorded at NORESS. (b) Earthquake in southern Norway recorded at NORESS. (c) Nuclear explosion recorded at WMQ. (d) Earthquake in Tien Shan recorded at WMQ. Explosion codas have a dip whereas earthquake codas are flat.

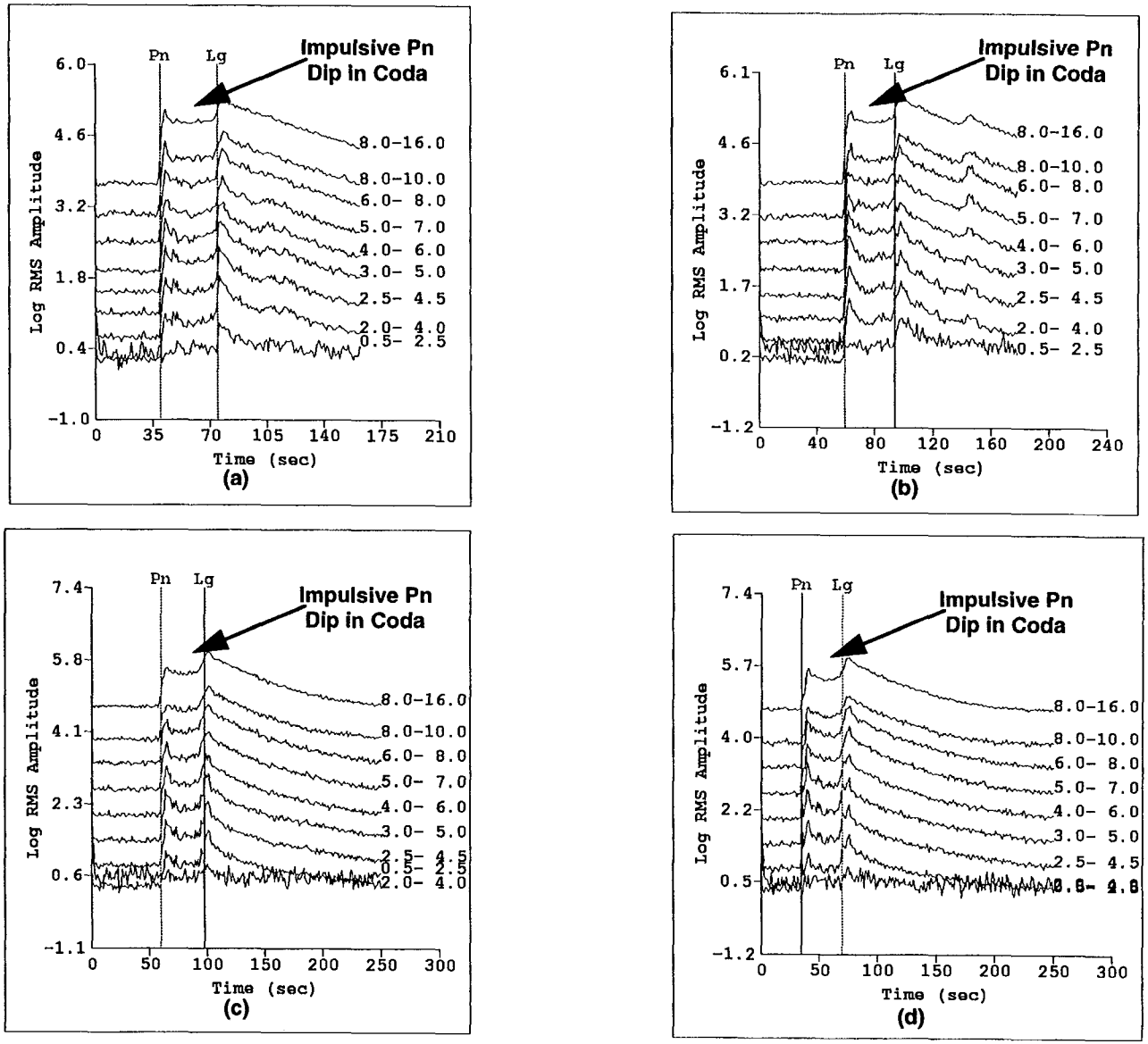

Figure 9: Examples of log-RMS incoherent beams for 4 Kiruna mine blasts. These events have an impulsive Pn onset and a coda "dip" in the high-frequency band, which are characteristic of mine blasts like the NORESS codas in Figures 8 (a) and 8(c). Local magnitudes of the events are (a) 1.8, (b) 1.76, (c) 1.64, and (d) 1.65.

Although the *Pn* waves have low amplitudes relative to *Lg*, in all cases they appear impulsive and the coda dips prior to the *Lg* onset, as shown by the arrows in Figure 9.

Figure 10 shows examples of coda shapes for earthquakes in northern Sweden. As indicated by the arrows, these codas are quite different in that they do not exhibit the "coda dip" in the high frequency band. Rather, their codas appear to be more flat or upramping than mine blasts. These codas may be the characteristic of earthquakes caused by mode conversion of stronger shear waves and *Rg* waves. Also, the earthquakes often have more distinctive *Pg* phases than the blasts. These events have similar values of *Pn/Lg* ratios as the Kiruna blasts, but their coda shapes are not blast like.

We have made a subjective estimate of the coda shape for the Kiruna events. We identified the event as "blast like" if the characteristic coda dip of the blast could be observed visually on the 8-16 Hz incoherent beam. The discriminant appears to work best on the high-frequency incoherent beam. This coda shape characteristic can be observed in about 31 of the 45 Kiruna blasts studied. Many of the events which could not be identified on the basis of coda shape were very small or their codas were contaminated by signals from other events which occurred nearby and close in time to the Kiruna events. However, we were able to identify the blast-like character of the codas for a number of Kiruna events which did not have apparent ripplefire scalloping.

2.4 Conclusions

This study has shown that the high-frequency *Pn/Lg* ratio discriminant fails to identify presumed blasts in the Kiruna mine as being blast like. In the absence of other information, the Kiruna events recorded at both the ARCESS and FINESA arrays would have been identified as earthquakes with relatively high confidence based on these events having small ratios caused by large *Lg* waves relative to the *Pn* waves. However, combining the ripplefire and coda shape discriminants would confirm the identity of most of the events as mine blasts.

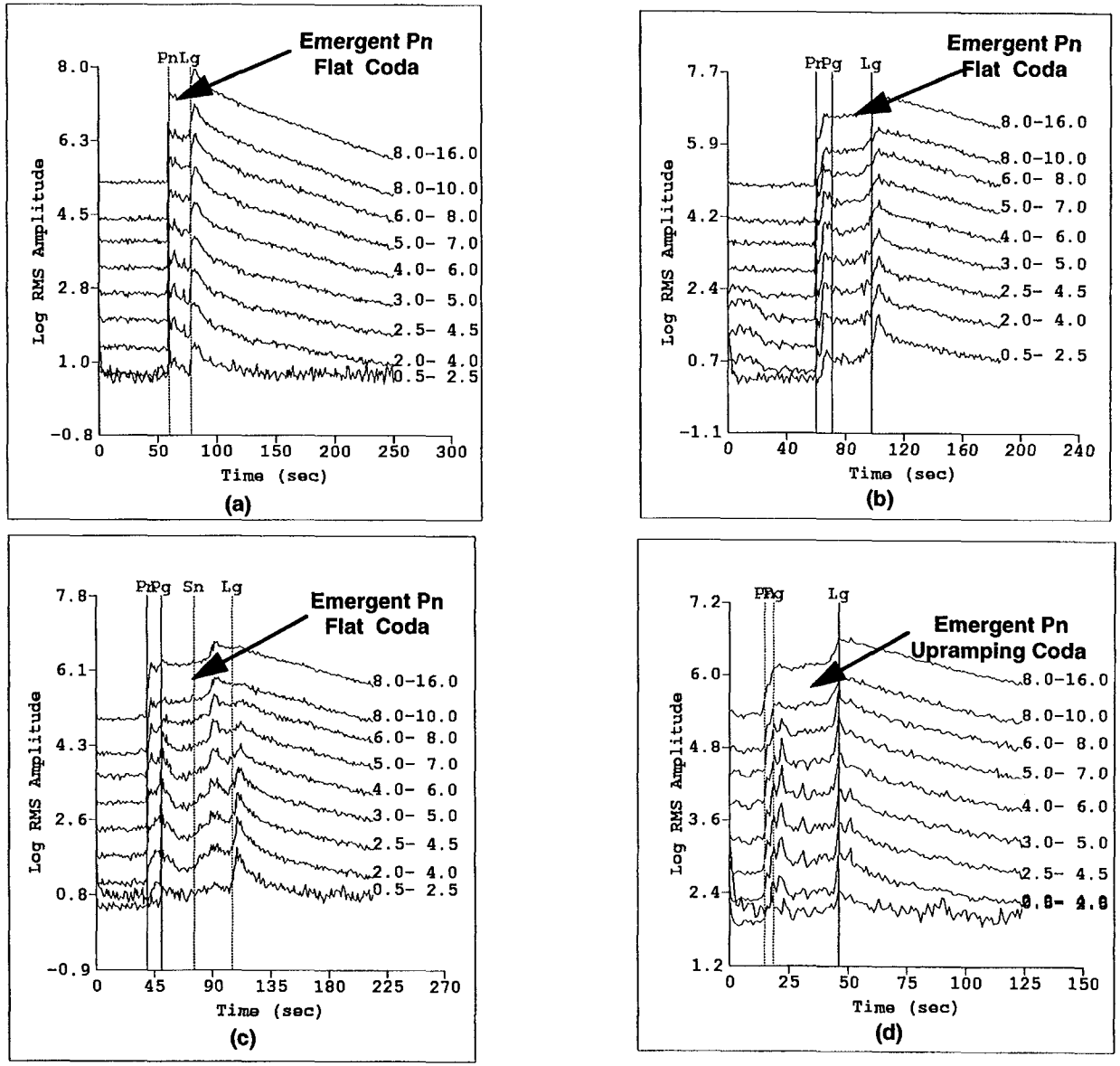

Figure 10: Four examples of ARCESS incoherent beam codas for earthquakes in northern Sweden showing the emergent Pn and "flat" or "upramping" codas which seem characteristic of earthquakes and unlike the Kiruna codas. Local magnitudes of the events are (a) 2.04, (b) 2.48, (c) 2.71, and (d) 2.27.

Why these particular events look like earthquakes on the basis of the *Pn/Lg* ratio is not well known. It obviously cannot be due to propagation path effects because mine blasts in other mines and nearby earthquakes can be discriminated. We speculate that blasting practice in the Kiruna mine may be responsible. Recent modeling studies (Barker et al, 1993; McLaughlin et al, 1994) have suggested a *P* wave defocusing mechanism caused by the bench face of the mine. These events may have reduced *Pn* amplitude caused by defocusing although in most cases, the *Pn* waves are still very impulse-like on the incoherent beams. Another possible explanation is that the Kiruna blasts may have been designed to produce stronger spall than other mine blasts in the region. The spall source mechanism may have had a radiation pattern that produced more enhanced shear waves at the ARCESS and FINESA arrays producing more earthquake-like *Pn/Lg* ratios.

Furthermore, ripplefired blasts are intended to cause fracturing and rubblizing of the rock at the bench face. Since rocks are being cracked and fractured, this process itself may induce large shear waves, in the same way in which mechanisms of tectonic release and induced block motions produce strong shear waves and surface waves in certain nuclear explosions.

This study has shown the importance of using a combination of techniques to identify small events. Although the amplitude ratio discriminant has proven to be very successful in certain regions, it can fail, as we have shown above. Perhaps we should expect small blasts to fail to discriminate since they may occur closer to the bench face of the mine and the *P* waves may be defocused. Clearly, the discriminant cannot be considered one hundred-percent foolproof for identifying all mine blasts of small magnitude.

3.0 FREQUENCY DEPENDENCE OF THE *Pn/Lg* RATIO

In this section, we discuss a new discriminant proposed by Walter et al (1994) based on the frequency dependence of the *Pn/Lg* ratio. As in the previous section, we consider whether this discriminant can be expected to work as well for small economic blasts and earthquakes as it did for larger nuclear blasts and earthquakes. We also consider how this discriminant is affected by differences in distances of blasts and earthquakes. To correct such effects, we investigate again the distance correction schemes developed by Baumgardt and Der (1994). We also present results from a study of the January 5, 1995 Southern Urals mine event, described in more detail in a topical report by Baumgardt (1995b) which presents an interesting example of unusual frequency dependence of the *Pn/Lg* amplitude ratio discriminant.

3.1 The *Lg* Transfer Function

Many investigations (e.g., Bennett et al, 1989; Baumgardt and Young, 1990; Kim et al, 1993) of the regional *P/S* ratio discriminant have argued that the discriminant performs best at high frequency. Recently, a discriminant between nuclear explosions and earthquakes using the frequency dependence of the *Pn/Lg* ratio has been proposed by Walter et al (1994), based on an argument that the *Lg/Pn* ratios can be thought of as "transfer functions" for explosions. This idea is illustrated schematically in Figure 11.

In essence, explosions are assumed to be pure compressional sources whereas earthquakes may intrinsically produce broadband shear waves. Thus, explosions should produce no intrinsic *Lg* waves whereas earthquakes may intrinsically produce broadband shear waves. This being so, the *Lg/Pn* ratio for explosions is a kind of "transfer function" since most of the *Lg* waves must have been derived by mode conversion of other waves produced by the explosion source to shear waves, which in turn become *Lg* waves.

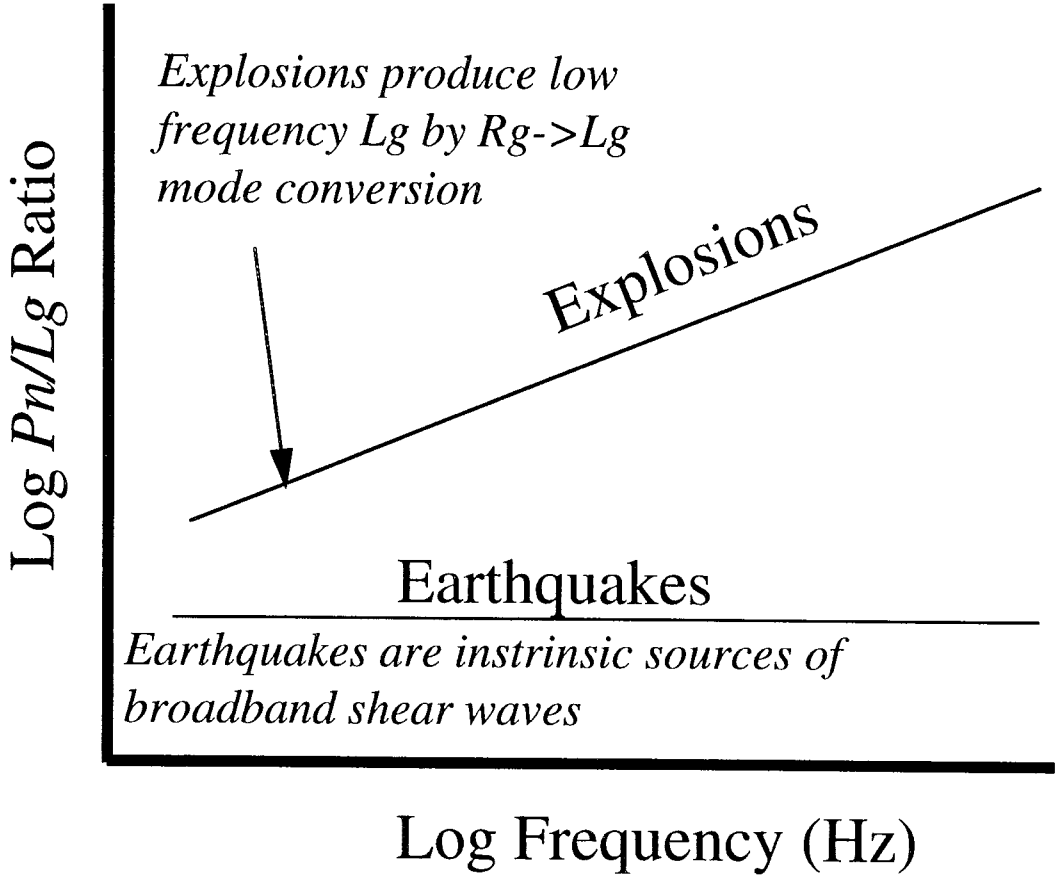

- Explosions are pure compressional sources.
- Earthquakes instrinsically generate broadband shear waves.
- *Lg/Pn* ratio for explosions is *S->P* transfer function.
- Explosions produce low frequency *Lg* waves by *Rg->Lg* mode conversion.

Figure 11: *Pn/Lg* frequency dependence based on the *Lg* transfer function concept (Based on Walter et al, 1993).

One possible source of *Lg* waves from explosions, which has been advocated by Gupta et al (1991), is mode conversion from *Rg*. Since nuclear explosions are shallow, they may excite stronger *Rg* waves than earthquakes and these waves would forward scatter into shear waves from lateral heterogeneities in the crust or from topography. Although the *Rg* waves may be strongly attenuated by this process and may not be observed, the scattered shear waves may further interfere to become *Lg* waves. This conversion process is strongest in the 0.5 to 2 Hz spectral band, thus the resultant *Lg* waves from nuclear explosions will be strong in this band and *Pn/Lg* ratios will be comparable to earthquakes. Thus, we would expect that the *Pn/Lg* ratio should strongly increase with frequency for explosions, since the *Lg* waves would be primarily produced at low frequency, but the ratio would be frequency independent for earthquakes because earthquakes are intrinsic broadband *Lg* sources.

Walter et al (1994) showed that this frequency dependence discriminant worked for NTS nuclear explosions, the Non Proliferation Experiment (NPE) event, and nearby earthquakes. Some of our recent studies of ISEIS measurements have also suggested that such a discrimination result holds for mine blasts and earthquakes. Examples have been observed for the Vogtland mine blasts and earthquakes in Germany (Baumgardt, 1993a), and for mine blasts on the Kola Peninsula and Novaya Zemlya nuclear explosions (Baumgardt, 1993b). In these cases, we have observed *Pn/Sn* and *Pn/Lg* ratios to increase with frequency, whereas for earthquakes, the ratios are comparatively unchanging with distance. In this section, we show some examples of where this discriminant has not performed in this way.

3.2 Frequency Dependence of *Pn/Lg* Ratio for the Kiruna Mine Blasts

In the last section, we suggested that mine blasts themselves may in fact be intrinsic sources of shear waves produced by cracking or by rock spallation. This may explain the low values of the ratios at high frequency, which we observed for the Kiruna mine blasts. We now investigate how these ratios depend on frequency.

Frequency dependent plots of the *Pn/Lg* ratio recorded at ARCESS and FINESA for the events studied in the last section are shown in Figures 12 (a) and (b). The circles show average ratios measured for known Swedish mine blasts (not in the Kiruna mine), the squares are for the Steigen earthquakes, and the triangles are the values for the Kiruna blasts. The symbols are plotted at the mean values of the ratios in each band and the error bars indicate twice the standard deviation (i.e., 2σ) for the events in the three groups.

In the case of the ARCESS array, shown in Figure 12 (a), we observe very little frequency dependence for the *Pn/Lg* ratio for the Kiruna blasts, a behavior expected for the *Lg* transfer functions of earthquakes. However, both the non-Kiruna mine blasts and Steigen earthquakes exhibit a strong frequency dependence, with the ratios increasing with frequency. This behavior suggests that both earthquake and non-Kiruna mine blasts are stronger sources of *Lg* at low frequency than at high frequency. In the case of the FINESA recordings, all three groups have similar frequency dependence, which tends to increase sharply with frequency. Why the Kiruna blasts are different for FINESA and ARCESS is not clear. It is notable that the Kiruna log ratios are less than 0 (i.e., *Lg* is bigger than *Pn*) at ARCESS all across the band whereas at FINESA, they increase gradually to 0 in the 8 to 10 and 8 to 16 Hz. Perhaps this results from greater attenuation of *Lg* at FINESA compared with ARCESS because the former is at a greater distance from the mine.

Thus, we conclude from this study that the Kiruna mine blasts, recorded at high signal-to-noise ratio at ARCESS, have *Pn/Lg* amplitude ratios with much less frequency dependence than other mine blasts. This is consistent with our conclusion in the last section that the Kiruna blasts may be intrinsic sources of shear waves. We've also observed that the Steigen swarm itself has a strong frequency dependence in the *Pn/Lg* ratio. This must be related to the source mechanism of the Steigen earthquakes, which may have underexcited *Lg* waves at high frequency. The distinction between small, intraplate earthquakes and ripplefired mineblasts may not be as great in terms for *Pn/Lg* frequency dependence as that between earthquakes and nuclear explosions.

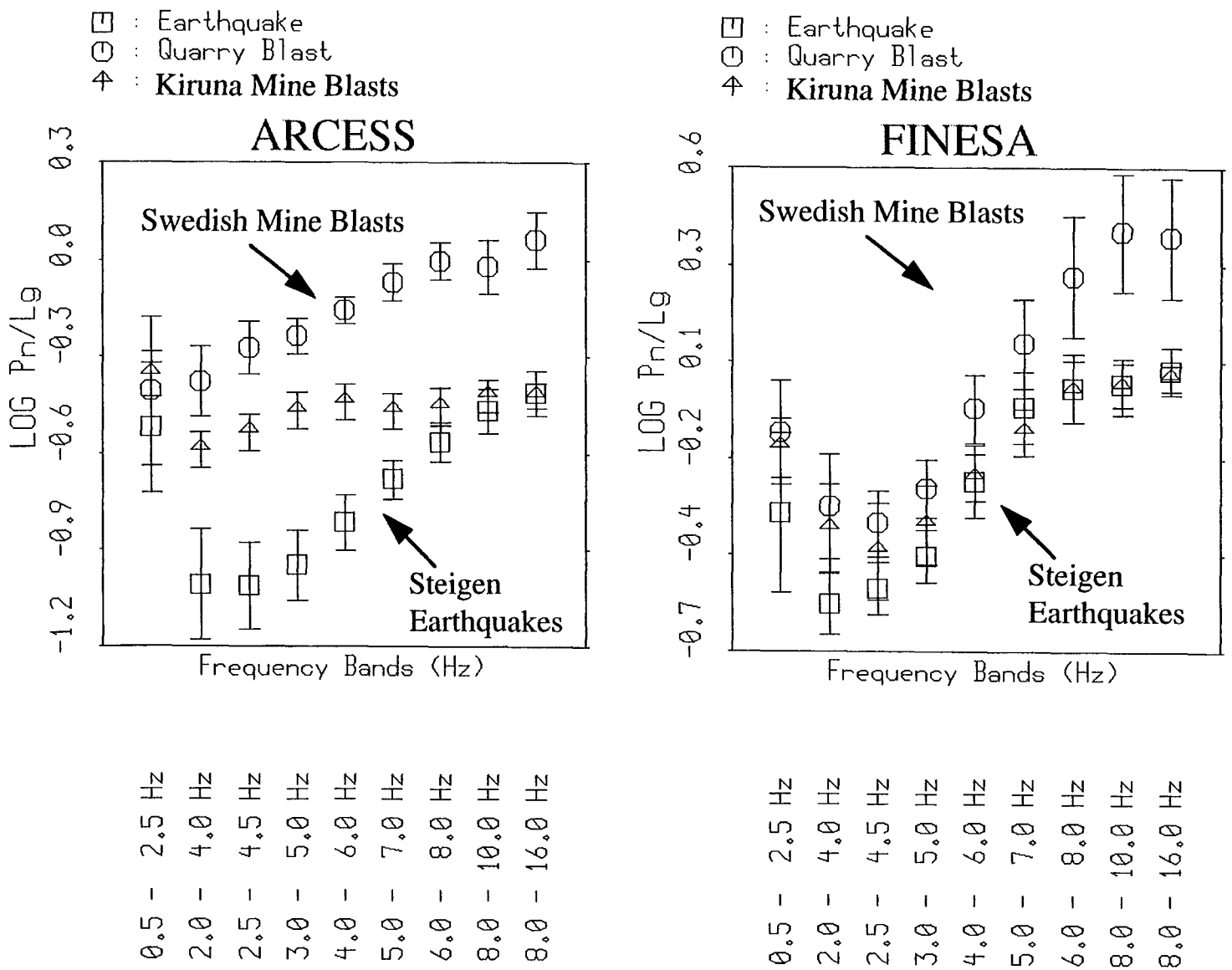

Figure 12: Comparison of frequency dependence of *Pn/Lg* ratio for ARCESS and FINESA recordings of the Kiruna and other nearby events in northern Scandinavia. Note the Kiruna events overlap the Steigen events at high frequencies.

3.3 Frequency Dependence of *Pn/Lg* for the January 5, 1995 Southern Urals Event

On January 5, 1995, an event occurred in Russia near the southern Urals which raised much interest because of its location in a region where there had been Soviet detonations of PNEs (Baumgardt, 1995a). Figure 13 shows the location of the event, nearby historical PNEs, and the IDC alpha stations which recorded the event. Baumgardt (1995a) studied this event in much detail and compared it with other nearby PNEs and concluded that the event was a rockburst perhaps accompanied by a mine collapse.

One result of this study, which relates to the discussion in this section, was that the recording of this event at the nearest station, Arti (ARU), had unusual frequency characteristics and the *Pn/Lg* ratios had unusual frequency dependence. This is evident in Figure 14, which shows the ARU vertical component seismogram passed through 5 filters. The phase picks, made on the top broadband trace, are indicated on each of the bandpass filtered traces by the vertical lines. The interesting feature is that the *P* waves are large in the mid bands (2 to 6 Hz) but appear diminished in the high and low frequencies. The reverse appears to hold for the shear waves, which are large at low frequency (up to 2.5 Hz) and high frequency (8-10 Hz) but smaller in the frequency bands in between.

Because of the lack of reference events in the region recorded at ARU (no PNEs have been recorded at ARU), Baumgardt (1995a) compared the event with earthquakes and explosions in China and Russia recorded at the station Urumchi (WMQ) in China, originally studied by Baumgardt and Der (1994) and shown on the map in Figure 15. The justification for this comparison, even though the Ural and Chinese events occurred in different regions and were recorded at different stations, is that the distances and propagation paths in the ARU and WMQ regions are similar. Also, because we are comparing ratios between phases in the same frequency band, the difference in the ARU and WMQ instrument response is not a factor. However, we may

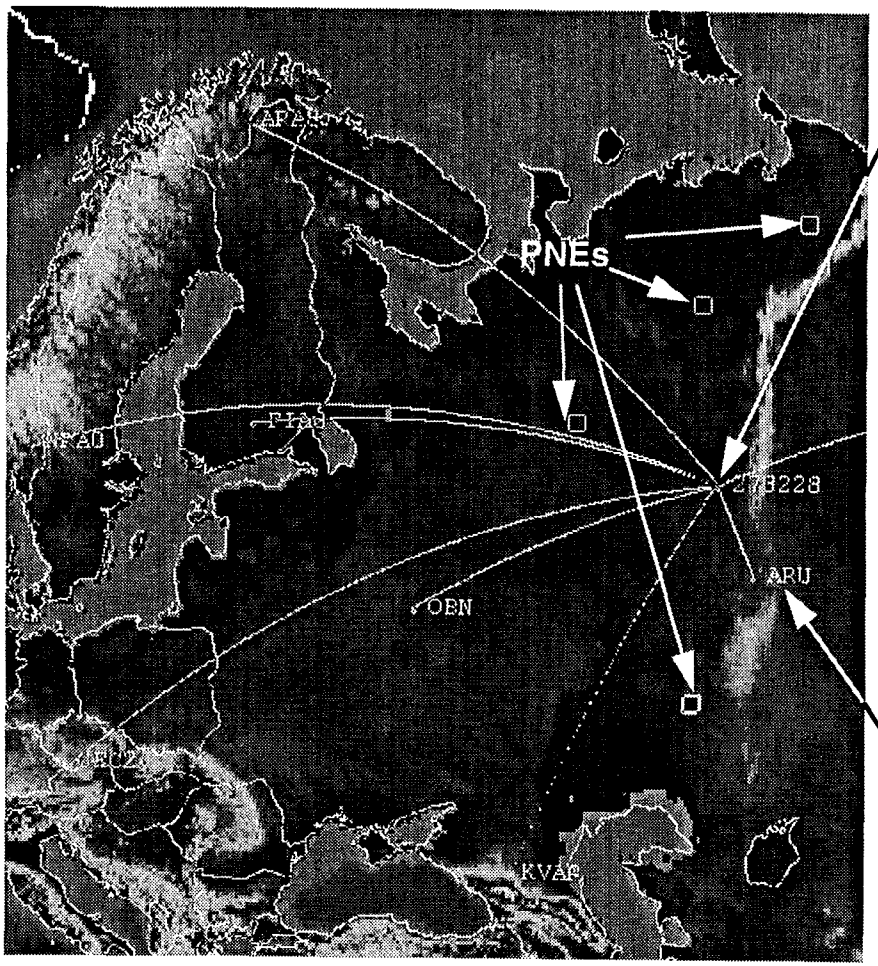

- Magnitude 4.3 event which occurred in a Russian mine.
- Announced by Russians as "tectonic" rock burst or collapse.
- Closest recording Alpha station was ARU.

Figure 13: Map showing location of the January 5, 1995 S. Urals events and the alpha stations which recorded the event. Also shown are location of nearby PNEs. (Note: This is a black-and-white rendering of a color original.)

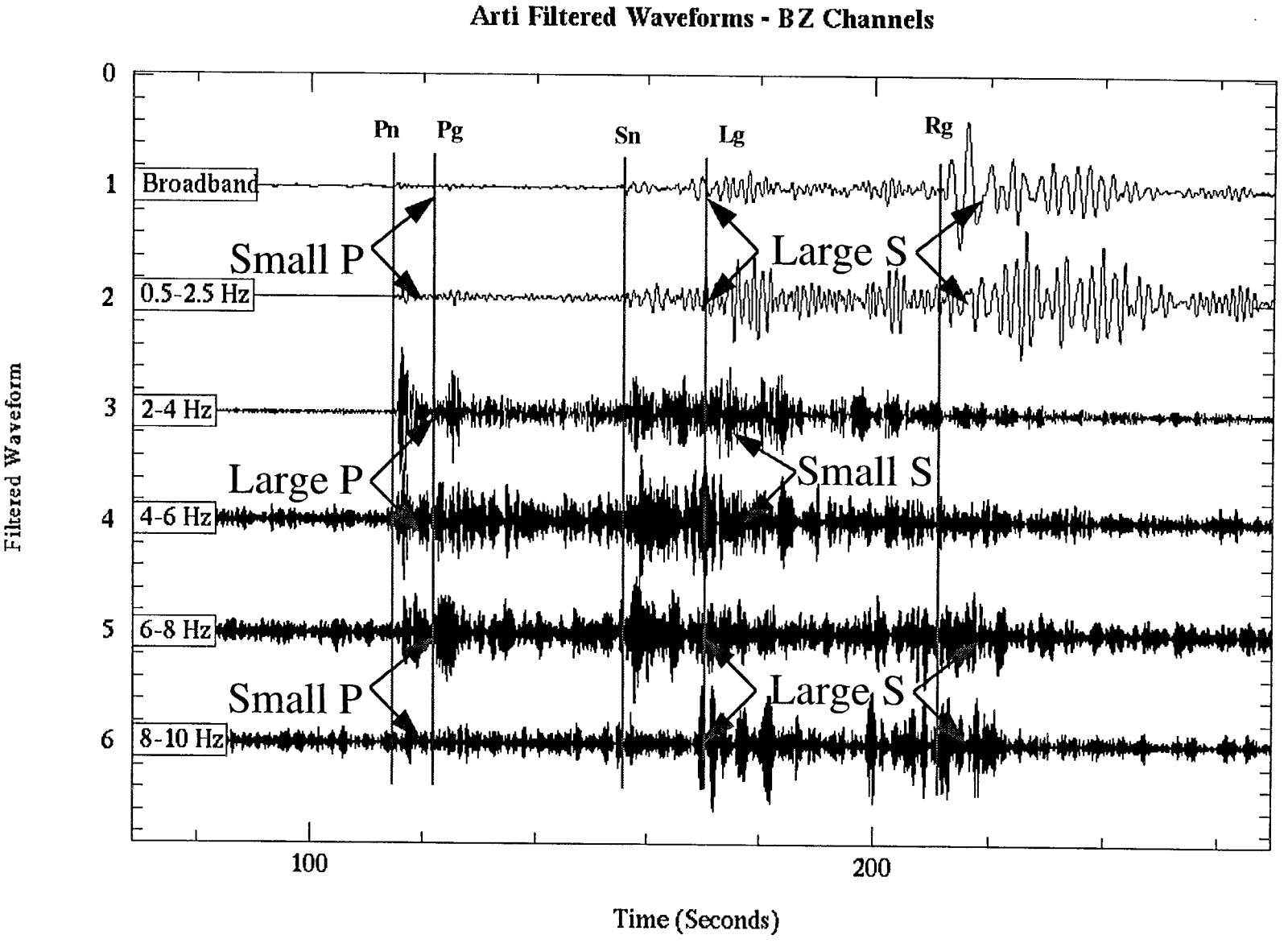

Figure 14: Bandpass filtered traces for the Janurary 5, 1995, Southern Ural event. The *P/S* ratio behavior exhibits unusual frequency dependence.

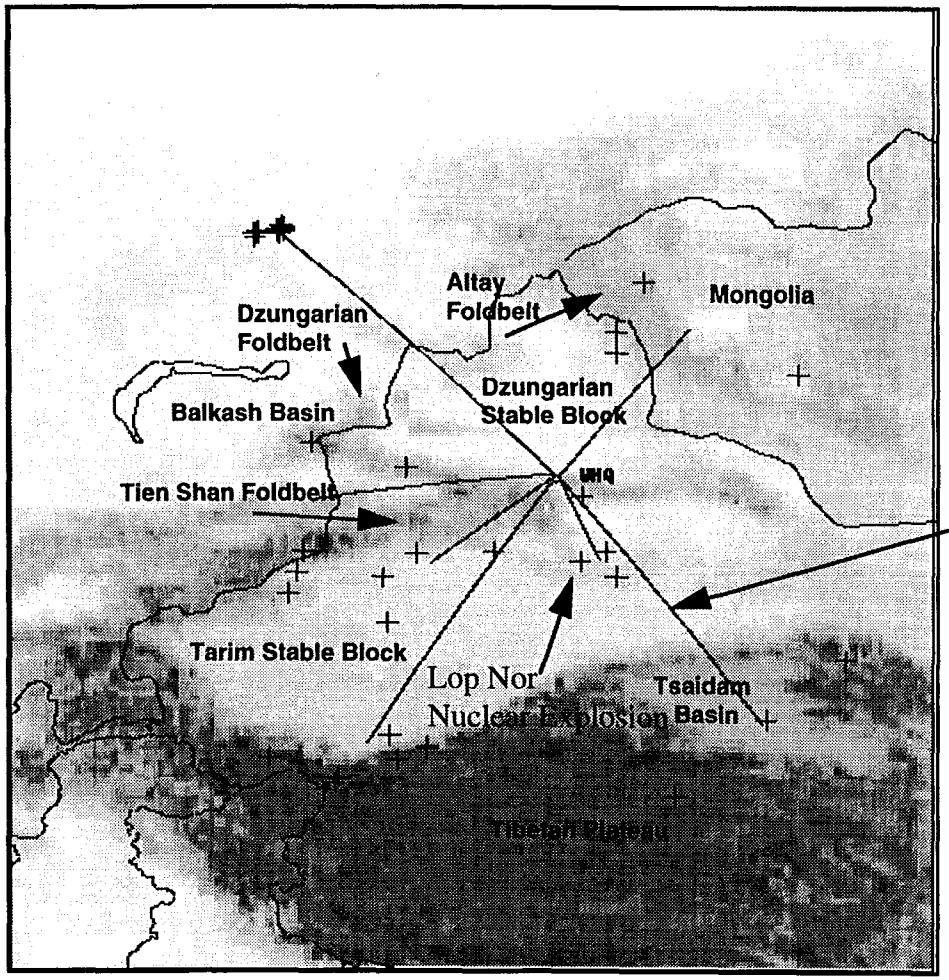

- Lack of reference events in Eurasia for Urals event requires comparison with Chinese events.
- Geology of propagation paths from earthquakes to Chinese station WMQ comparable to Urals path to ARU.
- Greater attenuation in China may produce larger *Pn/Lg* ratios (greater *Lg* attenuation) than in Russia.

Figure 15: Chinese events recorded at the stations WMQ which are compared to the S. Urals event recorded at ARU.

expect greater attenuation in the crust of China than in the more shield-like Russian Platform, which may result in large *Pn/Lg* ratios in China than in Russia at the same distances.

We consider two different distance corrections for *Pn/Lg* ratios, studied by Baumgardt and Der (1994); one derived from a detection study of regional phases by Sereno (1990) and the second inferred by Baumgardt and Der (1994) directly from measurements of *Pn/Sn* and *Pn/Lg* amplitude ratios from seismic events in Scandinavia and Europe. Both these curves may be considered to be shield type curves, although as was pointed out by Baumgardt and Der (1994), they have very different distance dependence.

Figure 16 shows a distance plot of the measured *Pn/Lg* ratios in the 6 to 8 Hz band from the Ural event at ARU and the WMQ recordings of Chinese earthquakes and nuclear explosions recorded at the WMQ station. In Figure 16 (a), the distance-dependence of the Baumgardt and Der (1994) correction is superimposed. Figure 16 (b) shows the result of applying the distance corrections. Figure 17 shows the same thing but with the Sereno (1990) correction. Comparison of these two curves shows that the Sereno curve has a much stronger distance dependence in the 6 to 8 Hz band than the Baumgardt and Der curve which in turn has a much stronger effect when the correction is applied. The Sereno correction pulls the Kazakh nuclear explosions down closer to the Urals point. Also, the Sereno correction moves the Lop Nor point to a much higher value than the Kazakh explosions. The Baumgardt and Der curve is less severe and after correction, the Urals event still falls below the nuclear explosions and appears to be more comparable to the earthquakes. Moreover, the corrected Lop Nor nuclear explosion point has a value closer to those of the Kazakh nuclear explosions. Thus, in this single 6-8 Hz band, the Baumgardt and Der corrections would classify the event as earthquake-like whereas the Sereno corrections would classify the event as an explosion.

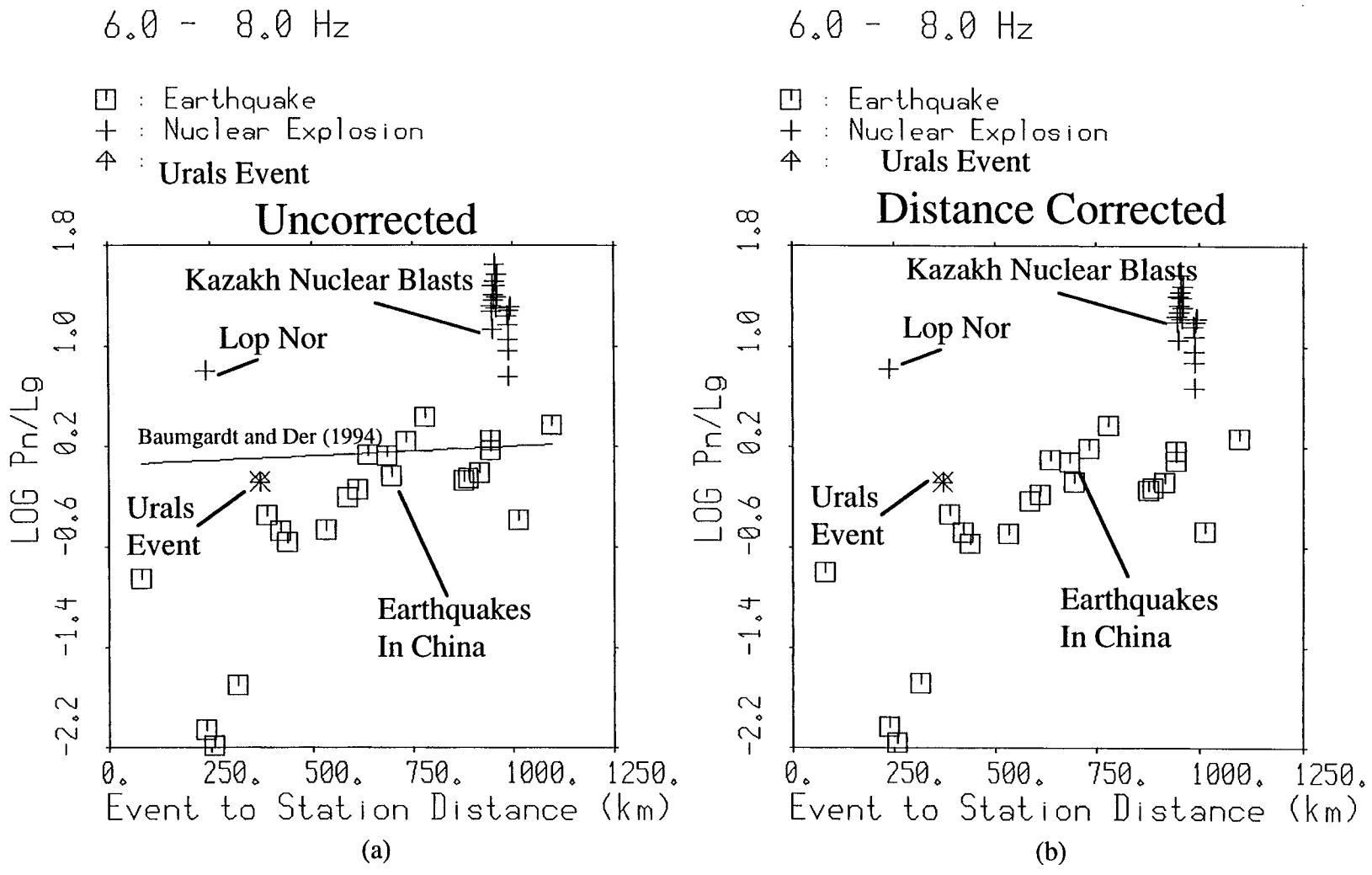

Figure 16: *Pn/Lg* ratios plotted versus distance for the WMQ recordings of Chinese earthquakes and Lop Nor and Kazakh nuclear blasts recorded at WMQ compared with the January 5, 1995 Urals event recorded at ARU. Distance correction of Baumgardt and Der (1994) is shown on the left and applied on the right.

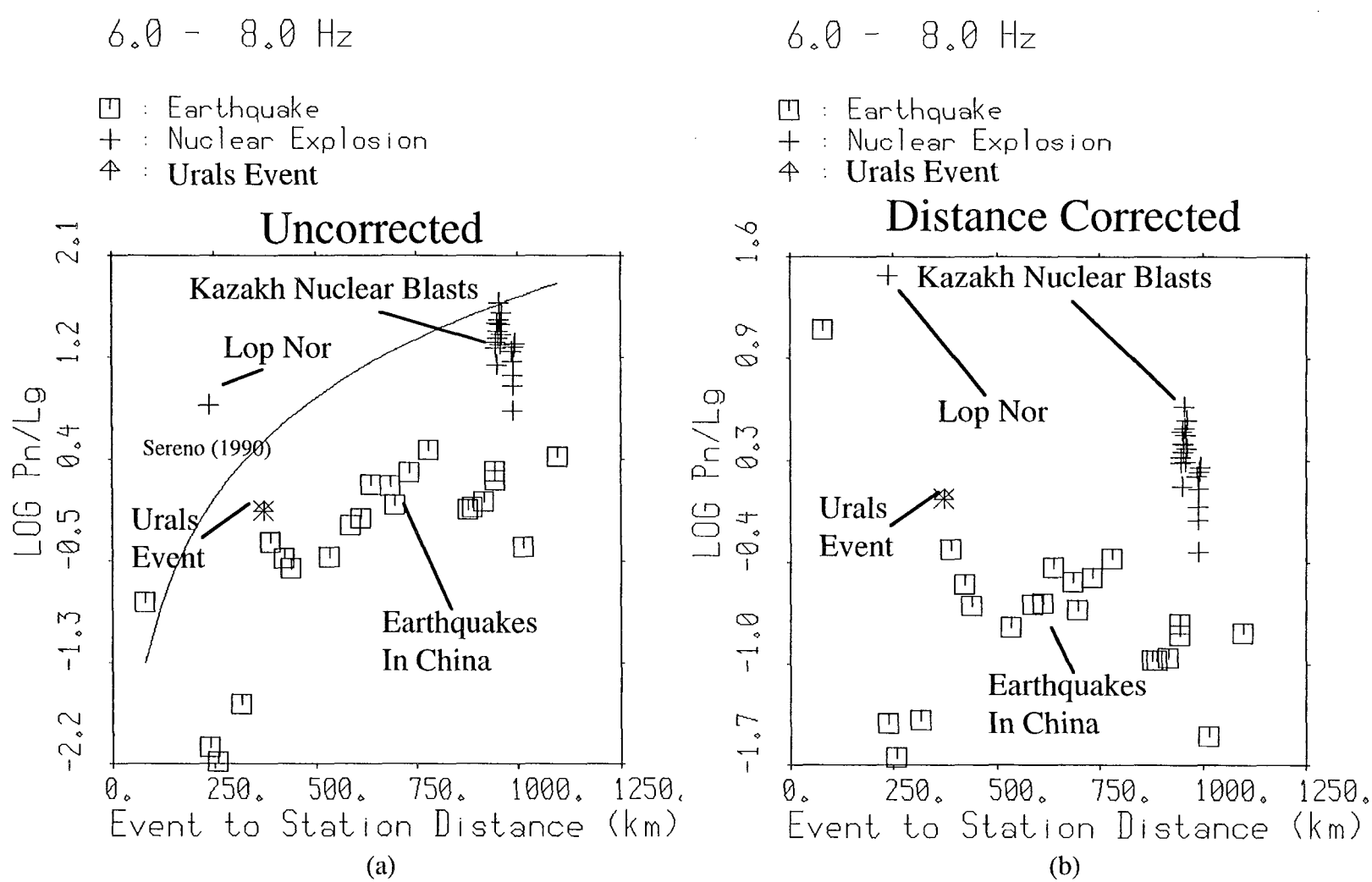

Figure 17: *Pn/Lg* ratios plotted versus distance for the WMQ recordings of Chinese earthquakes and Lop Nor and Kazakh nuclear blasts recorded at WMQ compared with the January 5, 1995 Urals event recorded at ARU. Distance correction of Sereno (1990) is shown on the left and applied on the right.

We now consider the frequency dependencies for these points and the two correction method. Figure 18 shows the frequency dependence of the *Pn/Lg* ratios for these events, corrected by the Baumgardt and Der distance correction curves, and Figure 19 shows the same corrections using the Sereno corrections. All the points are shown in Figures 18 (a) and 19 (a) and the mean values and 2 σ standard deviations are shown in Figures 18 (b) and 19 (b). The frequency dependence can be better observed in the plots of the mean values. Both sets of plots show that the earthquake points have very weak frequency dependence. For the nuclear explosions, the ratios in Figure 18 increase with frequency 6 to 8 Hz band where the ratios hit the "noise ceiling" which is the frequency where the *Lg* disappears below the noise level. Baumgardt and Der (1994) pointed out that the *Lg* is not observed from the nuclear explosions at frequencies above 6 Hz. (The Russian nuclear explosions at Kazakh were over 900 km away from WMQ, whereas the Lop Nor nuclear explosion and the Chinese earthquakes were much closer. Therefore, the *Pn/Lg* amplitude-ratio noise ceiling for the Russian explosions results from the attenuation of the *Lg* wave energy below noise at frequencies above 6 Hz.) Thus, the *Pn/Lg* ratios above the 6 to 8 Hz band for the Russian nuclear explosions are actually *Pn*-to-noise ratios.

The frequency dependence of the Ural event, plotted as asterisks in these two plots, differs greatly after these two corrections. However, its unusual frequency dependence is quite evident. Using the Baumgardt and Der correction in Figure 18 (b), the Ural event appears to fall closer to the earthquake group, as we observed in the filtered plots in Figure 14. The Sereno distance correction in Figure 19 tends to move the Urals points up closer to the nuclear explosion curve. Also, the Sereno distance correction seems to make the nuclear explosion frequency dependence look more like the earthquake frequency dependence, whereas in reality, we know that the trend is very different for the nuclear explosions; i.e., we know that *Lg* amplitude does not increase above the 3 to 5 Hz band.

Baumgardt and Der (1994) Distance Corrections

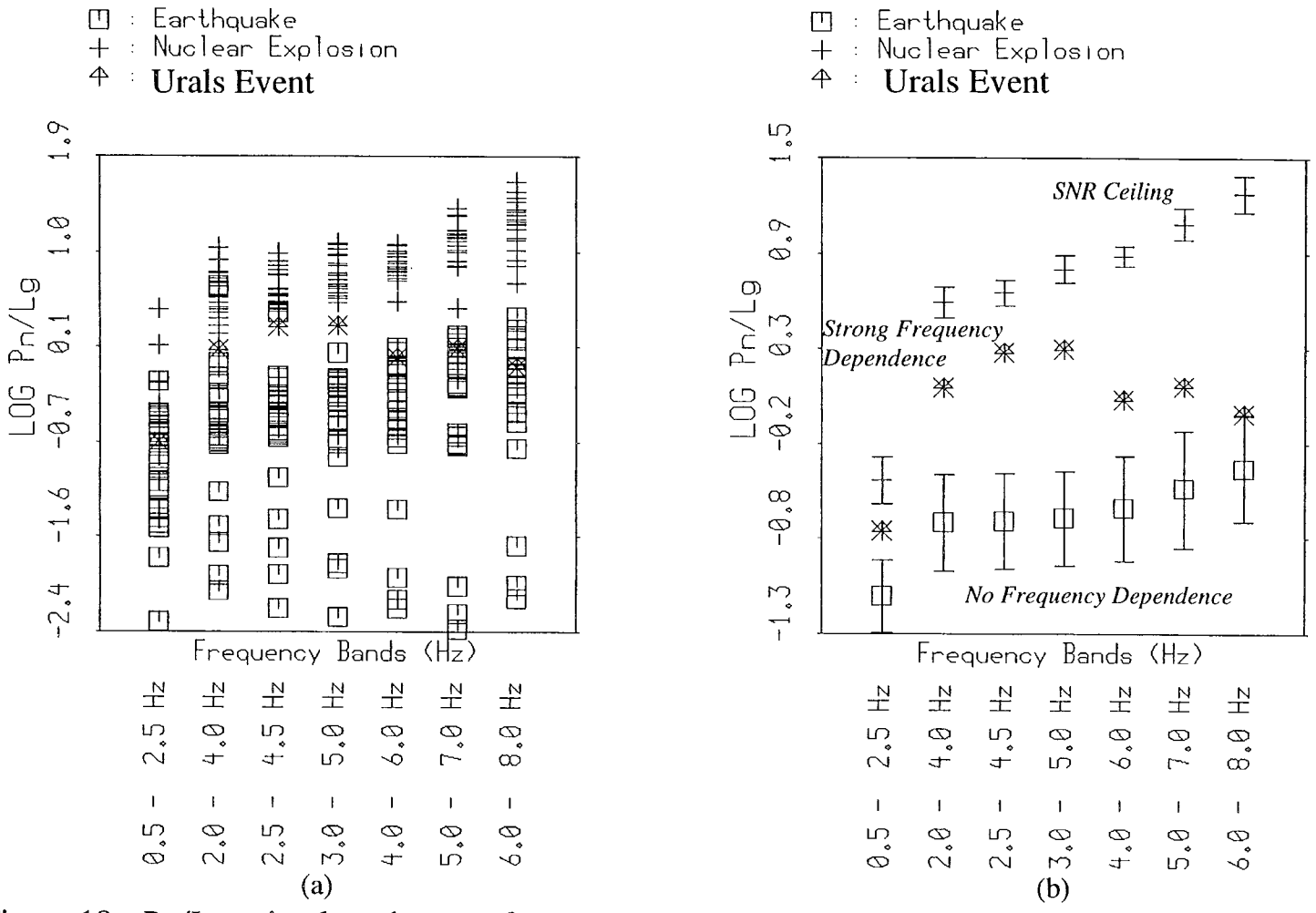

Figure 18: *Pn/Lg* ratio plotted versus frequency for the events plotted in Figure 16 with the Baumgardt and Der (1994) distance corrections applied, all points plotted on the left and the average and standard deviations on the right. These corrections are less severe, but the Urals event has unusual frequency dependence.

Sereno (1990) Distance Corrections

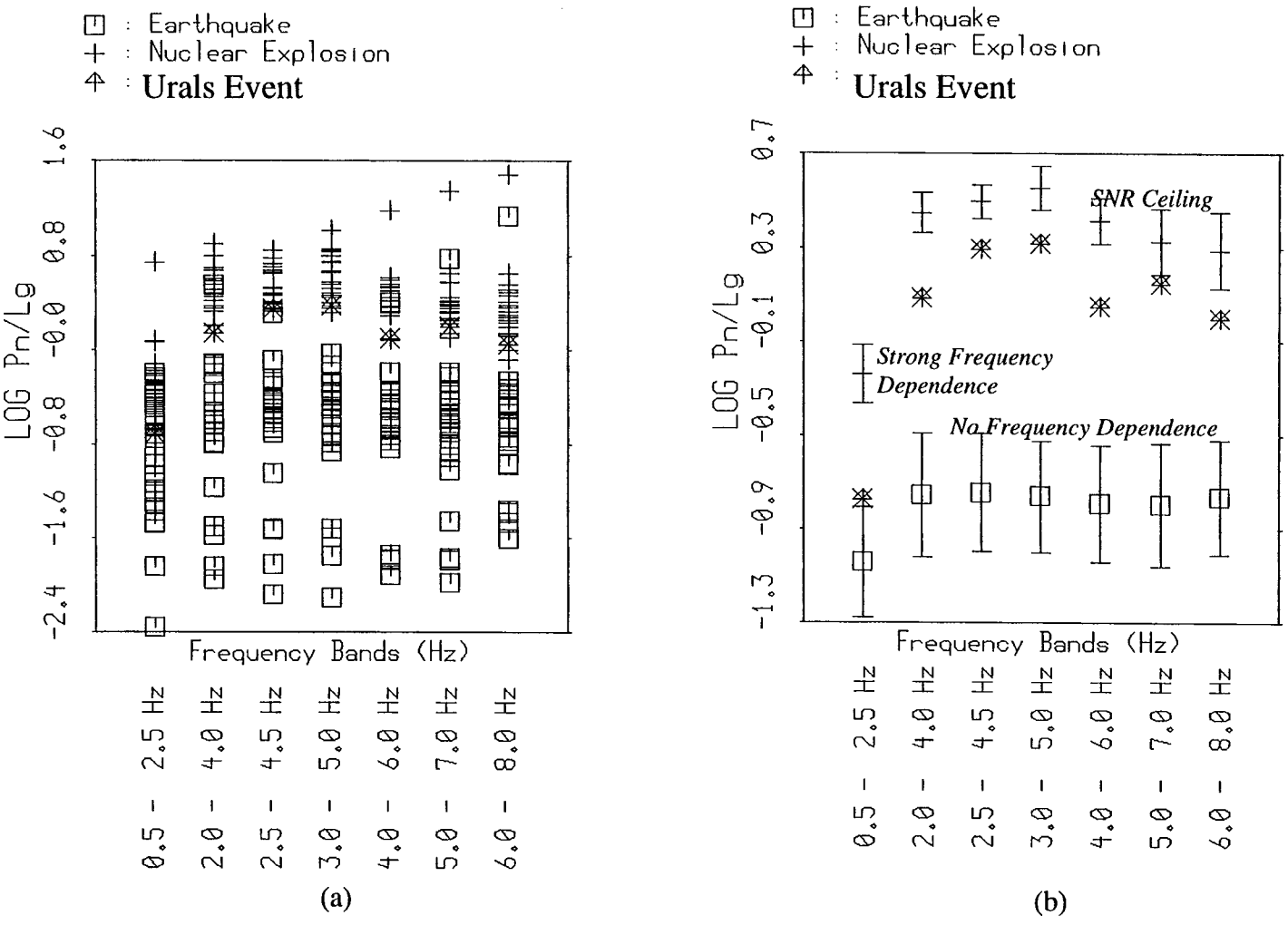

Figure 19: *Pn/Lg* ratio plotted versus frequency for the events plotted in Figure 18 with the Sereno (1990) distance corrections applied, all points plotted on the left and the average and standard deviations on the right. These corrections are severe and move the Urals event into the explosion group in terms of frequency dependence.

Based on this analysis, we conclude that the Ural event frequency dependence resembles earthquakes in that it appears to be an intrinsic source of shear waves at high frequency. However, the frequency dependence is still unusual, and Baumgardt (1995a) has questioned whether the high-frequency *Lg* energy comes from the same source as the low-frequency energy. Using the Baumgardt and Der corrections, our observations of frequency dependence in the *Pn/Lg* ratio agree with the ideas of Walter et al (1994). However, the Sereno corrections seem to be rather extreme and do not produce the expected behavior in the frequency dependence of nuclear blasts. Although we favor the Baumgardt and Der curves, more analysis of the *Pn/Lg* change with distance needs to be done for events in this region. Neither of these shield curves may be appropriate for the tectonically active mobile belts of China.

3.4 Conclusion

Our analyses of frequency dependence of *Pn/Lg* ratios in ISEIS for these selected cases indicates that the *Lg* transfer function concept of Walter et al (1994) depends critically on the nature of the source mechanism of explosions and earthquakes. Nuclear explosion source mechanisms are probably more purely compressional than mine blasts, which may be intrinsic sources of shear waves. We observe the expected difference in frequency dependence between nuclear explosions and earthquakes in China. However, we have observed very different kinds of frequency dependence for events associated with mines. As we argued in Section 2.0, ripplefired mine blasts are designed to fracture rocks and induce spallation near the mine bench face. Thus, we may expect shear waves to be produced intrinsically by mine blasts. Thus, the discriminant should work to identify nuclear explosions and single explosions in mine. However, ripplefired mine blasts may often be identified as earthquakes.

4.0 THE RIPPLEFIRE DISCRIMINANT

4.1 Time Independent Spectral Scalloping

The discrimination of mine explosions and earthquakes relies critically on the observation of time-independent spectral scalloping caused by ripplefiring (Baumgardt and Ziegler, 1988; Hedlin et al, 1989, 1990). Currently, this appears to be the only method, other than precise locations of events to known mines, to identify mine blasts. The Multiple Event Recognition System (MERSY) applies the method of Baumgardt and Ziegler (1988) to automatically identify time-independent spectral scalloping by finding time-independent cepstral peaks in cepstra of individual phases derived from the spectra of the phases (Baumgardt et al, 1991). Experience with processing numerous events over a number of years has demonstrated that MERSY can usually detect any spectral modulations which can be seen visually in spectra. However, there are instances of known mine blasts which have not produced strong spectral scalloping and for which this discriminant fails to work.

Figure 7 in Section 2.0 shows an example of a MERSY analysis of one of the Kiruna mine blasts. On the left is shown spectra computed for the three phases associated with the event, *Pn*, *Pg,* and *Lg*. These three spectra show scalloping which indicates that the events were probably ripplefired. On the left are plotted the cosine cepstra for the events computed by Fourier transformation of the spectra. The spectral modulations produce cepstral peaks which can be easily identified. MERSY picks "consistent" cepstral peaks, i.e., peaks which show up in all phases but which do not show up in the noise, at quefrencies above 0.5 seconds, the lowest quefrency resolvable at a sampling rate of 40 Hz. When such peaks appear, they probably indicate ripplefired mine blasts or bubble pulses produced by underwater explosions (e.g., see Baumgardt, 1995b) because such features have never been reported for small earthquakes.

4.2 Why the Ripplefire Discriminant Fails

However, spectral modulations often do not appear in known chemical blasts, examples of which were documented by Kim et al (1994). They suggest that these blasts were either single shots with no delays or had delays too short to be resolved with the sampling rate of the digital data. They further argue that a fundamental delay less then 4 times the sampling interval of the data cannot be resolved by spectral analysis as time-independent spectral scalloping.

Figure 20 compares two sets of spectra for a mine blast in southern Norway recorded at NORESS (left) and one on the Kola Peninsula recorded at ARCESS (right). The NORESS spectra on the left exhibit strong modulations whereas the Kola spectra on the right exhibit very weak or non-existent modulations. A vertical line indicates a possible first null at about 3 Hz in both cases. This may be an indication of a fundamental delay in excess of 0.2 seconds, which is well in excess of 4 times the sampling interval of the recordings systems at NORESS and ARCESS, which are 0.025 seconds. However, the Kola event produced no noticeable spectral scalloping.

In this section, we suggest that another factor, signal *decorrelation*, can also cause spectral modulations not to be observed even for ripplefires with large enough delay times to be observed within the bandwidth provided by the sampling rate of the digital data. To understand how this happens, the cause of spectral scalloping in ripplefired chemical explosions must be understood.

4.2.1 The Origin of Spectral Scalloping in Ripplefired Blasts

A misconception has arisen, primarily in the conclusions of some recent ripplefire modeling studies (e.g., Barker et al, 1993; McLaughlin et al, 1994), that "Quarry blast spectral scallops are primarily due to the finite size and duration of the source and are insensitive to the details of the ripplefiring timing." Although size and duration are certainly related to the cause of scalloping, the cause-and-effect statement "finite duration causes spectral scalloping" is imprecise. Spectral scalloping can only be produced by the superposition of two or more pulses which are spectrally

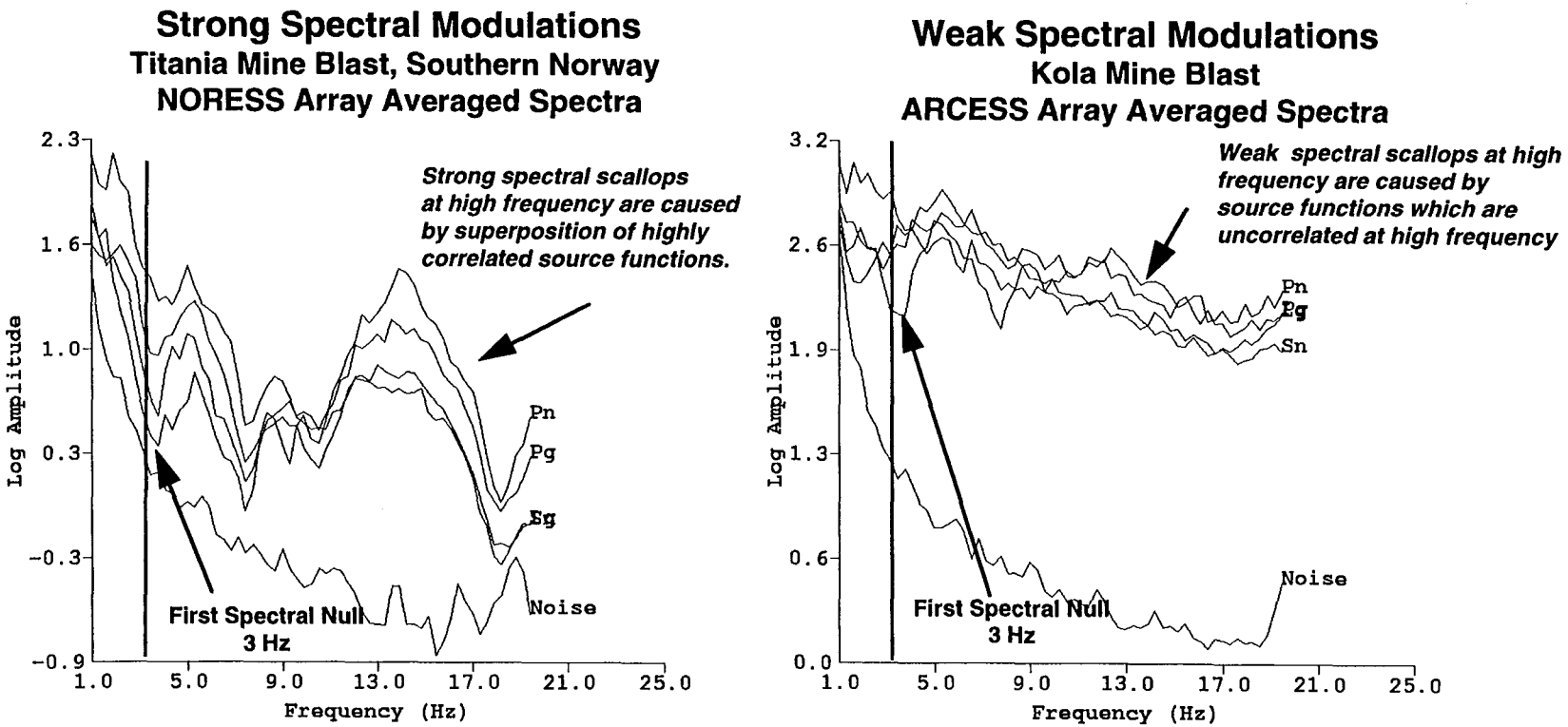

$$y(t) = \sum_{j=1}^{N} x_j(t-\tau_j)$$

Ripple Fire Modeled As Superposition of Delayed Source Functions

$$|Y(\omega)| = \sum_{i=1}^{N} |Xi(\omega)|^2 + 2 \sum_{j=1}^{N} \sum_{k=j+1}^{N} |Xj(\omega)Xk(\omega)| \cos\omega(\tau_j - \tau_k)$$

Power Spectral Density

Cross Correlation Terms *Spectral Modulation Terms*

Figure 20: This figure compares examples of strong and weak spectral scalloping. Spectral scallops are produced by the cosine term which multiplies the correlation term. Decorrelation of the signals reduces spectral scalloping.

correlated, and the timing precision directly controls the strength of the spectral scalloping. This is important in understanding why, in many cases, ripplefired blasts may not produce spectral scalloping.

Consider the simple double-delayed pulse model. Generalizing from the discussion of Baumgardt and Ziegler (1988), we assume that a signal, *Y(t)*, consists of the sum of *x1(t)* and *x2(t)* with *x2* delayed by time τ. Baumgardt and Ziegler (1988) assumed that *x1(t)* and *x2(t)* were essentially the same signal but having different amplitudes. In the following, we consider that they may be completely different signals. Thus, we have for the composite signal

$$Y(t) = x1(t) + x2(t-\tau). \tag{1}$$

Computing the Fourier transform of (1), we have,

$$Y(\omega) = X1(\omega) + X2(\omega)e^{-j\omega\tau}, \tag{2}$$

where $Y(\omega)$, $X1(\omega)$, and $X2(\omega)$ are the Fourier transforms of *y(t)*, *x1(t)* and *x2(t)*, respectively and ω is the frequency. We now compute the power spectral density of (2), which is $Y(\omega)Y(\omega)^*$ and where * refers to complex conjugation. We then have

$$\begin{aligned} Y(\omega)Y(\omega)^* = X1(\omega)X1^*(\omega) \; + X2(\omega)X2^*(\omega) \; + \cos\omega\tau\left[X1^*(\omega)\; X2(\omega) + X1(\omega)X2(\omega)^*\right] \\ + i\sin\omega\tau\left[X1(\omega)X2^*(\omega) - X1^*(\omega)X2(\omega)\right] \end{aligned} \tag{3}$$

Letting $Y(\omega)Y^*(\omega) = |Y(\omega)|^2$, which is the power spectral density, and

$X1(\omega)X2^*(\omega) = X1(\omega)^* X2(\omega) = |X1(\omega)X2(\omega)|$, which is the cross-spectral density, we have

$$|Y(\omega)|^2 = |X1(\omega)|^2 + |X2(\omega)|^2 + 2|X1(\omega)X2(\omega)|\;\cos\omega\tau. \tag{4}$$

Note that in the third term of (4) the coefficient $cos\ \omega\tau$ introduces the spectral scalloping, and it is multiplied by the cross-spectral density term. Thus, the strength of the spectral scalloping is controlled by the value of the cross-spectral density between the two signals. If the signals are uncorrelated and the cross-spectral density is small or zero at all frequencies, the composite spectral density is simply the sum of the two individual spectral densities and there is no spectral scalloping. The duration of the delay, τ, does not control whether or not there will be spectral scalloping. The duration in this case only determines the periodicity of the scalloping, which is $1/\tau$, when the signals are correlated.

We now consider the general expression for a ripplefire pattern consisting of many delays. A signal of N delays can be written as follows:

$$y(t) = \sum_{j=1}^{N} x_j(t - \tau_j), \tag{5}$$

where we assume the ripplefire pattern consists of a discrete sum of the individual source functions of the ripplefire pattern. Note that in this general form, it is invalid to use the continuous expression, like that of Smith (1993), where the ripplefire pattern is represented as the convolution over a finite time window of a source function $s(\tau)$ with a the ripplefire delay function, or "comb function," $r(\tau)$, written as

$$s(t) = \int_{\tau=o}^{t_N} r(\tau)u(t - \tau)d\tau. \tag{6}$$

In the general case, a ripplefire pattern is not a continuous sum over a finite time interval, as written above, but rather a discrete sum as in (5). In the limit of infinite number of shots, (5) converges to (6). However, most ripplefire patterns which have been observed do not warrant the assumption that the number of shots being large enough for (6) to hold in general. The continuous integral (6) would only apply if the individual shots were delta functions delayed in time, in which case the individual signals all correlate.

The power spectrum of (5) can be written in general as

$$|Y(\omega)|^2 = \sum_{i=1}^{N} |Xi(\omega)|^2 + 2\sum_{j=1}^{N}\sum_{k=j+1}^{N} |Xj(\omega)Xk(\omega)| \cos\omega(\tau_j - \tau_k) \tag{7}$$

In this general form, the degree of modulation of the power spectrum is controlled by the product of the correlation of the individual source functions, $|Xj(\omega)Xk(\omega)|$, multiplied by the cosine of the difference of the time delays between the source functions, $\cos\omega(\tau_j - \tau_k)$. This expression makes clear the fact that the individual source functions must be correlated in order to produce spectral scalloping.

It has been argued that the "corner frequency" of a ripplefired mine blast is controlled by the time duration of the ripplefire time sequence. However, this is not strictly true for a discrete sequence, as expressed in (5). The null frequencies of the spectral scalloping or modulation are given by the expression

$$\omega_n = \frac{n\pi}{2(\tau_j - \tau_k)}, \tag{8}$$

where n is an odd integer. The lowest frequency null, which determines the "corner frequency," should occur at,

$$\omega_1 = \frac{\pi}{2(\tau_{\max} - \tau_{\min})}, \tag{9}$$

that is, at the reciprocal of the nominal duration of the ripplefire pattern, $T = \tau_{\max} - \tau_{\min}$. However, this lowest possible null, controlled by the ripplefire duration, will be strongly visible only if the two signals corresponding to earliest and latest times of the entire ripplefire pattern are correlated, and the strength of the spectral peak before this null, which defines the corner frequency, is controlled by the degree of correlation. Ripplefire patterns can be very complicated and be spread across a large spatial area. It is entirely possible the first and last shots, which may

be the most separated shots, may not be strongly correlated. Thus, the corner frequency may not be well defined at the frequency of the reciprocal of the time duration of the ripplefire sequence.

One can certainly conceive of many source-time functions, $x(t)$, which have a finite duration but do not produce scallops; the simple exponentially attenuated periodic function, $x(t) = e^{-\beta t}\sin(k_o x - \omega_o t)$, is an example. The absorption coefficient β, spatial wavenumber k_O, and temporal frequency ω_O, are constants. This function can have a long duration if the constant coefficient β is small, and its spectrum is a broadened Delta function centered at frequency ω_O. However, the spectrum will not be scalloped no matter what its duration. Scalloping can only result from the superposition and time delay of two or more correlated time series.

Baumgardt and Ziegler (1988) first showed examples of time-independent strong scalloping produced by ripplefiring of mine blasts in Scandinavia. Spectral scalloping with deep nulls have been observed for a number of events, perhaps indicating that simple, long-delay ripplefire patterns were detonated. More recent studies have suggested more complex ripplefire patterns which produce less deep nulls than were observed in Scandinavia (e.g., Stump and Reinke, 1988; Smith, 1989). Baumgardt and Ziegler (1988), Stump and Reinke (1988), Smith (1989, 1993), and Gitterman and van Eck (1993) have shown how more complex scalloping can be produced by signal interferences between the different signals in the ripplefire pattern and that the positions of the various peaks and nulls of the scalloping will be caused by the cosines of the different delay times and their differences. The values of the delay times control the nature of the interferences and the scalloping. Stump and Reinke (1988) and Gitterman and van Eck (1993) have shown how the strength of the modulations will be controlled by the accuracies of the individual timing delays of the ripplefire. However, no matter how large the variance of the timing delays, spectral modulations of some form will be present if the individual pulses of the ripplefire are coherent. If the signals are uncorrelated, there will be no spectral scalloping irregardless of the precision of the firing delays of the ripplefire.

4.2.2 Signal Decorrelation and Spectral Scalloping

Generalizing from the discussion above, the total power spectrum, $P(\omega)$, of a multiple shot sequence can be expressed as the sum of the auto- and co-spectra between all unique source pairs in the ripplefired sequences,

$$P(\omega) = \sum_{i,j} S^{k}{}_{i,j}(\omega) \tag{10}$$

where $S_{i,j}{}^{k}(\omega)$ is the cross-spectral power function for source i and j in the ripplefire sequence for seismic phase k, (i.e., *Pn*, *Pg*, *Sn*, or *Lg*). The cross spectral power function is represented as in terms of a spectral coherence function as

$$S_{i,j}{}^{k}(\omega) = a_i a_j C(\omega, x_i - x_j, s_k) \exp \omega[t_i - t_j + (x_i - x_j)], \tag{11}$$

where s_k is the phase slowness in sec/km, a_i is the source amplitude term (usually 1), x_i is the location of source i, and $C(\omega, x_i\text{-}k_j, s_k)$ is the coherence function defined as

$$C = Factor \times \exp(-\alpha\omega\Delta x). \tag{12}$$

Δx is the spatial separation $(x_i\text{-}x_j)$, ω is the angular frequency, *Factor* is a constant, and α is the phase dependent decorrelation function. These functions are defined in terms of observed decorrelations of different phases across the regional array NORESS, which are known to be a function of array geometry and are different for different phases (Mykkeltveit et al, 1983). Generally, high-frequency *Pn* and *Pg* phases are more coherent than the shear phases, *Sn* and *Lg*. To reflect this variation in decorrelation, the decorrelation terms are set as follows:

$$Pn\text{ - }\alpha = 0.0146,\ Pg\text{ - }\alpha = 0.02,\ Sn\text{ - }\alpha = 0.08,\ Lg\text{ - }\alpha = 0.167.$$

The effect of this model on spectra are shown in Figures 21 and 22. The model assumes 50 sources in a 56 m square grid are fired with 7 ms delay between sources. The maximum delay for this model is 50 times 7 ms, or 350 ms. We assume no propagation delays in this instance of the model. Thus, for 350 ms fundamental delay, the spectral scallop nulls should be separated by 2.5 Hz.

In Figure 21 (a), we assume no decorrelation by setting the value of *Factor* to 0. All four phases show equally strong spectral modulation, with peaks and troughs separated by 2.5 Hz as expected. In Figure 21(b), the value of *Factor* is set to 1 and the decorrelation factor in (12) is in effect. This figure shows that decorrelation visibly decreases the strength of the modulations for the *Lg* wave compared to the others. Also, the strength of decorrelation decreases with increasing frequency. In Figures 22(a) and (b), the effect of the decorrelation has been made much stronger by increasing the value of *Factor* to 100 and 500, respectively. In Figure 22 (a), the modulations have been completely eliminated for *Sn* and *Lg* and strong frequency dependence of the strength of the spectral modulations is evident for *Pn* and *Pg*. In Figure 22 (b), the high decorrelation has eliminated all spectral scalloping.

Thus, this discussion shows that if a ripplefire pattern can be designed such as to make the individual signals uncorrelated, spectral scalloping can be destroyed. Different phases in the regional seismogram, such as *Lg* waves, tend to be less spatially correlated than *Pn* which could result in *Lg* spectra being less scalloped than *Pn* spectra. Examples of this kind have phenomena that have been found by Der and Baumgardt, 1994. Moreover, if different rows of shots are fired in different geologic media, or at a significantly different depth in the mine, such that they produce different source-time functions, coherence between signals can be destroyed and no spectral scalloping will be observed. This may happen, for example, if a decoupled explosion or mini nuclear explosion is fired at the same time as a ripplefired pattern, but at a different depth and in a

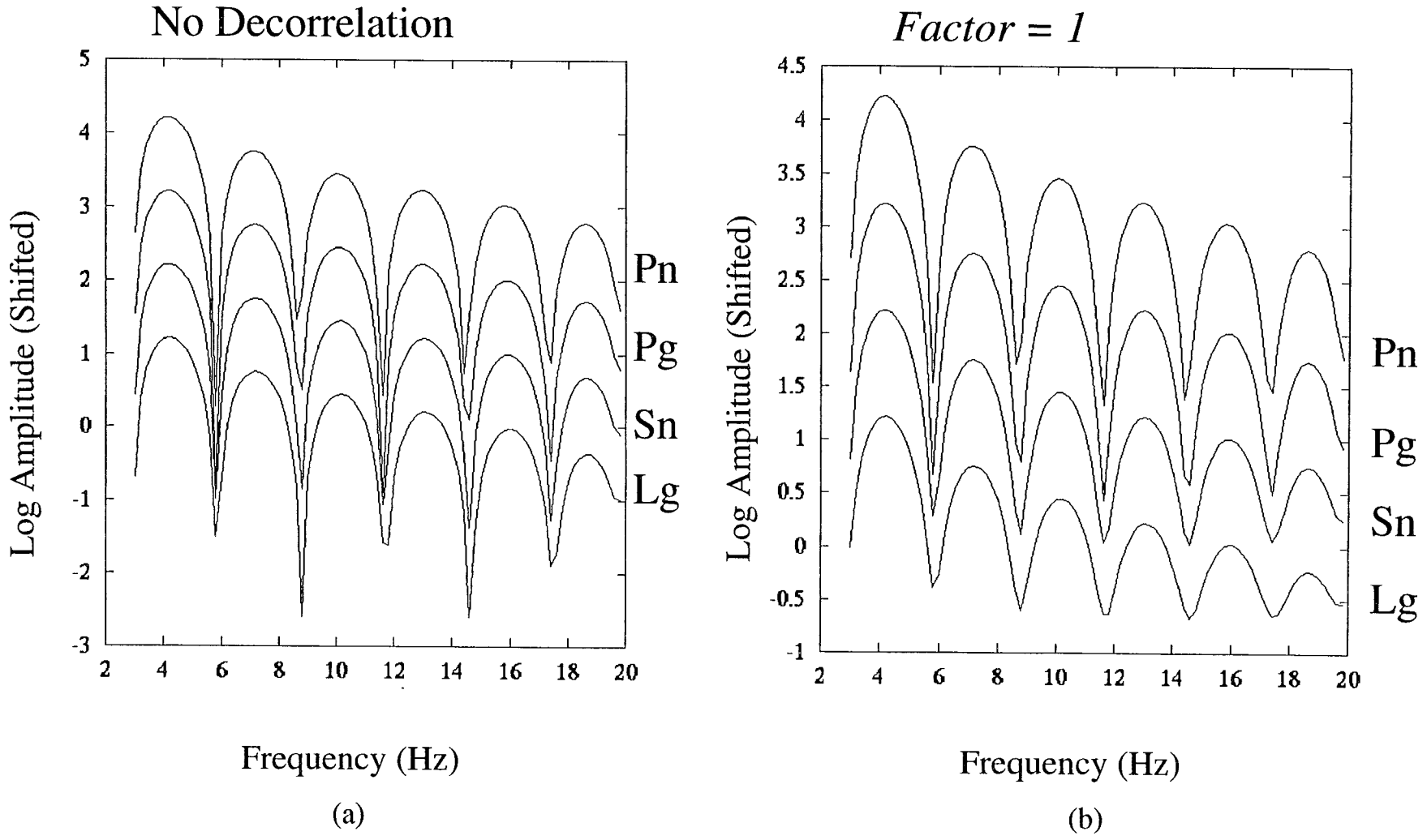

Figure 21: Examples of two theoretical scalloping models with weak decorrelation. 50 sources in 56 m square grid fired with 7 ms delay between sources.

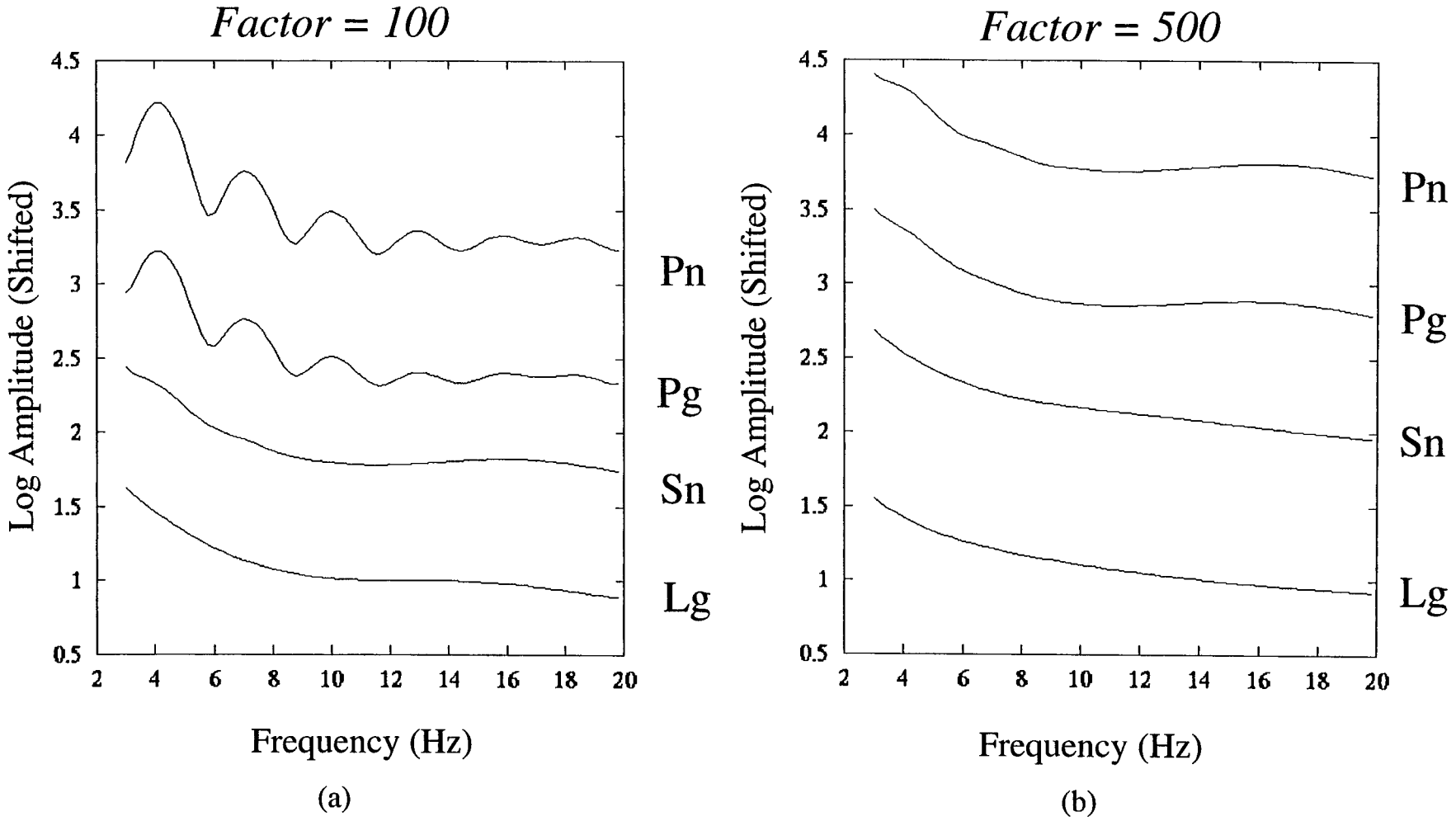

Figure 22: Same model as in Figure 22 with much stronger decorrelation. Note that scalloping can be destroyed by the decorrelation.

different medium, so that no spectral scalloping may occur. Also, differences in the intrinsic source function (amplitude, spectral content) of the nuclear explosion and individual blasts can destroy spectral scalloping, as demonstrated by Barker et al (1993) and McLaughlin et al (1994), because of the decorrelation of the resulting seismic pulses produced by the different source functions. Thus, lack of spectral scalloping combined with a large signal may be a feature which could indicate an attempted hide-in-ripplefire evasion attempt.

5.0 *LG* SPECTRAL RATIOS

In this section, we revisit issues of whether discriminants based on spectral characteristics of regional phases can reliably and consistently identify small blasts and earthquakes. We first discuss the empirical and theoretical basis for the discriminant based on recent studies at Lawrence Livermore Laboratories. We then re-examine spectral characteristics of regional signals which have been studied by ISEIS in light of these new studies, including continued analysis of the January 5, 1995 Southern Urals event. Finally, we discuss a new method for correcting regional phase spectral ratios for propagation distance.

5.1 Physical Basis for the *Lg* Spectral Ratio Discriminant

Measurements of ratio of spectral levels between low and high frequency in the *Lg* phase has been shown in studies to discriminate closely located nuclear explosions and earthquakes in the western U.S. (Murphy and Bennett, 1982; Bennett and Murphy, 1986). The separation was based on the explosions being deficient in high frequencies compared to earthquakes. However, these two studies did not fully address possible magnitude-scaling of the discriminant. Taylor et al, (1988) and Taylor et al, (1989) also studied this discriminant for events in western U.S. and found that it worked for the regional phases *Pn* and *Pg* as well as *Lg*. However, the earthquakes were not closely located to the explosions and propagation-path effects were not considered.

Studies of small mine blasts and earthquakes with ISEIS have found mixed results for the *Lg* spectral discriminant. The discriminant fails to discriminate small mine blasts and earthquakes (ML < 3.0) in Scandinavia but did separate explosions and earthquakes in the Vogtland region of Germany using narrow band data from the GERESS array (Baumgardt, 1993a). The separation indicated that the Vogtland explosions were peaked at low frequency and deficient in high frequencies, and that the earthquakes had broader spectra with more energy in the high frequency

band than the explosions. The latter result confirmed the study of Wuster (1993), who used an ARMA spectral discriminant on broader-band GERESS data.

Recently, Walter et al (1995) have found marginal performance the discriminant for small NTS explosions and earthquake swarms in the vicinity of the Lawrence Livermore Laboratory NTS network. Spectral ratios in the phases *Pn, Pg*, and *Lg* discriminated best at magnitudes greater than 3.5 and showed strong magnitude dependence. Figure 23 shows a plot of their results for the 1-2Hz/6-8Hz *Lg* spectral discriminant versus ML along with source model calculations recently made by Walter (1995). This plot shows the basis for the discriminant in terms of magnitude scaling and differences in source characteristics of nuclear blasts in high and low gas porosity rocks and earthquakes. Obviously, the spectral ratio for *Lg* increases with ML. The source models predict differences in spectral ratio for high and low gas porosity, with higher gas porosity producing higher spectral ratios. Evidently, detonations in highly gas porous rocks do not couple as efficiently at high frequencies as those in less porous rocks. However, detonations in both types of geologies produce less high frequency energy relative to low frequency than do earthquakes. This depends on the material properties of the rocks and the assumptions in the source models. Perhaps detonations in hard, non-porous rocks produce comparable spectral ratios as earthquakes.

Figure 23 also shows marginal performance of the discriminant at low magnitudes (ML< 3.0) where the theoretical curves converge and the empirical data points for earthquakes and explosions become more mixed. Notably, shallow earthquakes do not appear to discriminate at all from high gas-porosity explosions. In attempting to discriminate shallow earthquakes and mine blasts, we may be dealing with a similar situation.

5.2 Magnitude Scaling of the *Lg* Spectral Ratio Discriminant in Eurasia

In light of the results in Figure 23, we have reinvestigated the ISEIS measurements of regional discriminants in Eurasia referenced earlier. A map showing the locations of the events

Diagram By William Walter, LLNL

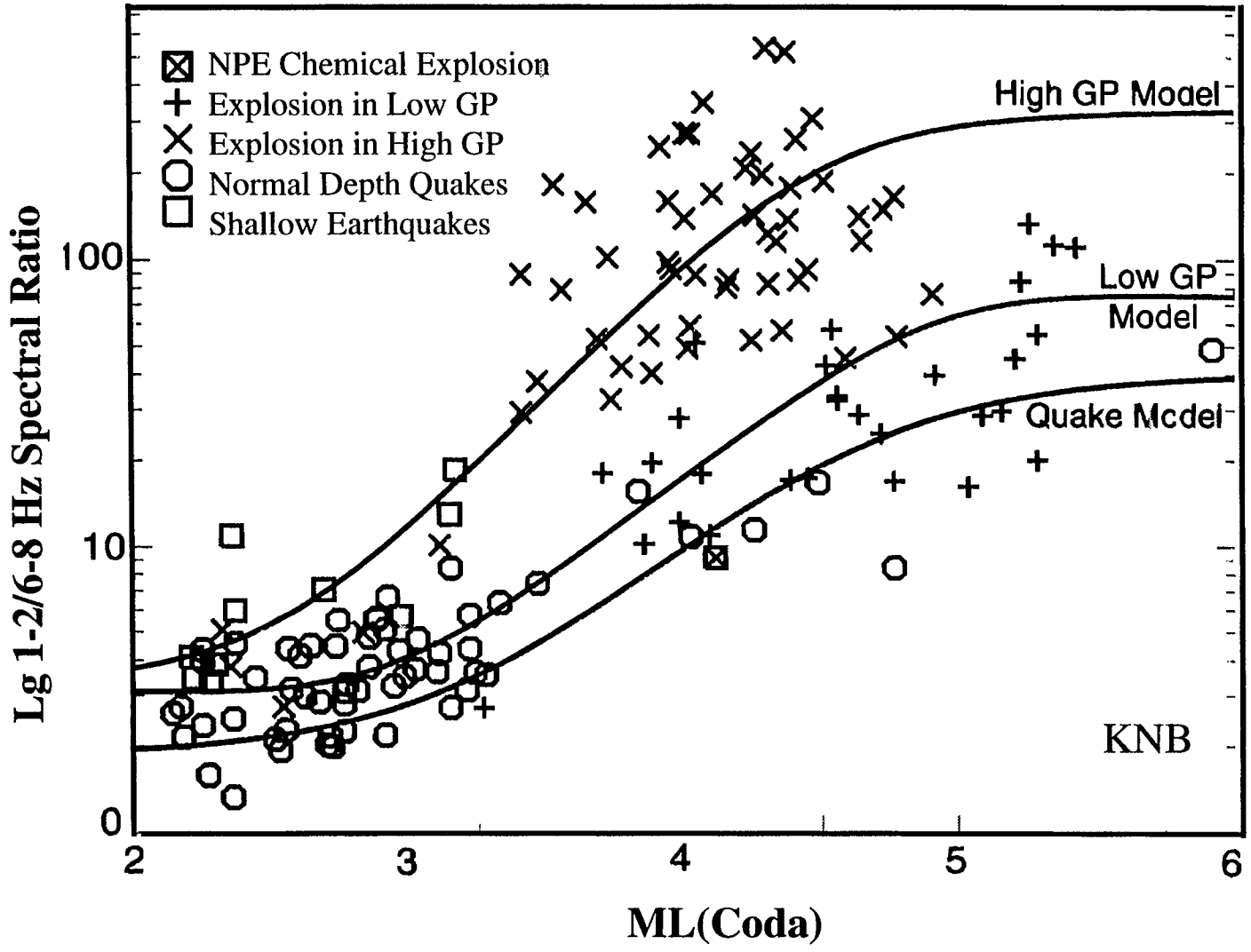

Figure 23: Spectral ratio data from Western US explosions and earthquakes, studied originally by Walter et al (1994). Explosions apparently have higher ratios than explosions at the same value of local magnitude.

originally studied by Baumgardt (1993a) is shown in Figure 24. These events were earthquake and quarry blasts in the Vogtland region of Germany and rockbursts in two regions of Poland, Lubin and Upper Silesia. Also shown in Figure 24 are the locations of an earthquake swarm in Switzerland, studied by Baumgardt and Der (1994). We also study spectral ratios for the Scandinavian events recorded at ARCESS (Kiruna mines, Northern Sweden mines, and earthquakes, Steigen earthquake swarm) discussed in Section 2.0 and shown on the map in Figure 1.

Figure 25 shows plots of 2-4Hz/4-6Hz *Lg* spectral ratios for GERESS and ARCESS recordings of events in two different regions, Germany (a) and Scandinavia (b). These ratios are the logs of the rms spectral level in the two spectral band. The spectra are corrected for instrument amplitude-spectrum response prior to computing the ratios. Figure 25 (a) shows the spectral ratios plotted versus distance for the Vogtland earthquake and explosions, originally studied by Wuster (1993), and some additional rockburst data from the ground truth database of Grant et al (1993). Also, for comparison, the *Lg* spectral ratio measured at the Chinese station WMQ for the Chinese nuclear explosion at Lop Nor is plotted. All the spectra were corrected for instrument response, so differences in the instrument type should not be an issue. However, the Lop Nor event occurred in a very different region and is a very different kind of source than the Vogtland events. Considering this, however, it is interesting that the event had comparable spectral ratio as the Vogtland blasts. The Vogtland earthquakes and blasts are at comparable distance, and their separation is clearly evident, with explosions producing *Lg* waves with deficient high frequencies and higher spectral ratios than the earthquakes. The rockbursts at greater distance have greater scatter, which may be related to their greater propagation distance. We consider propagation effects on spectral ratio in the next section.

The spectral ratio differences are due to differences in spectral characteristics, not to ripplefire spectral scalloping in the mine blasts. In Figure 26, plots of the *Lg* spectra are overlaid. All spectra have been corrected for the instrument response. (Note: This figure is a black-and-white rendering of an original color picture. The spectra of the Lop Nor nuclear blast and mine

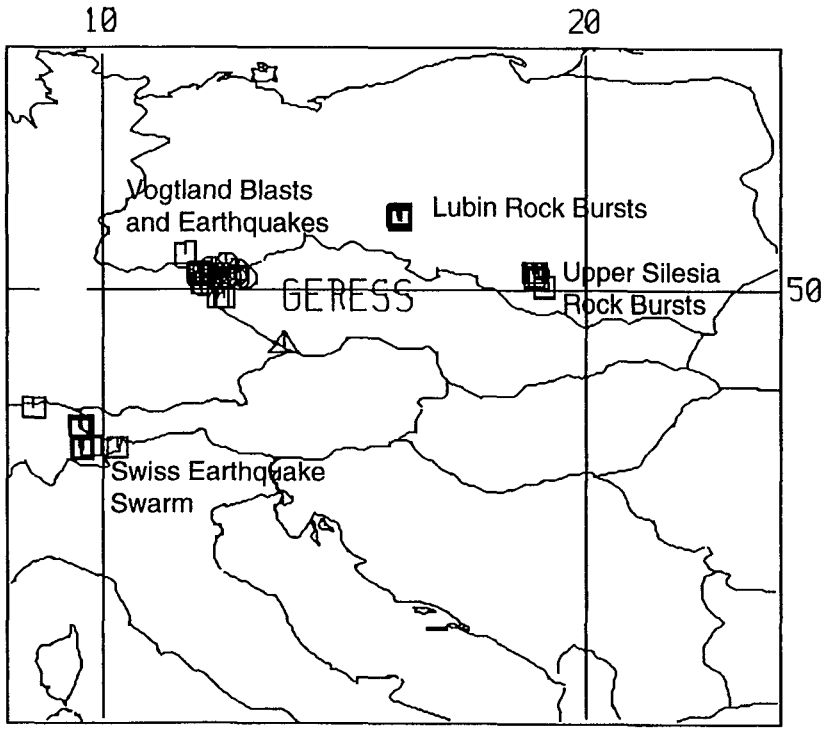

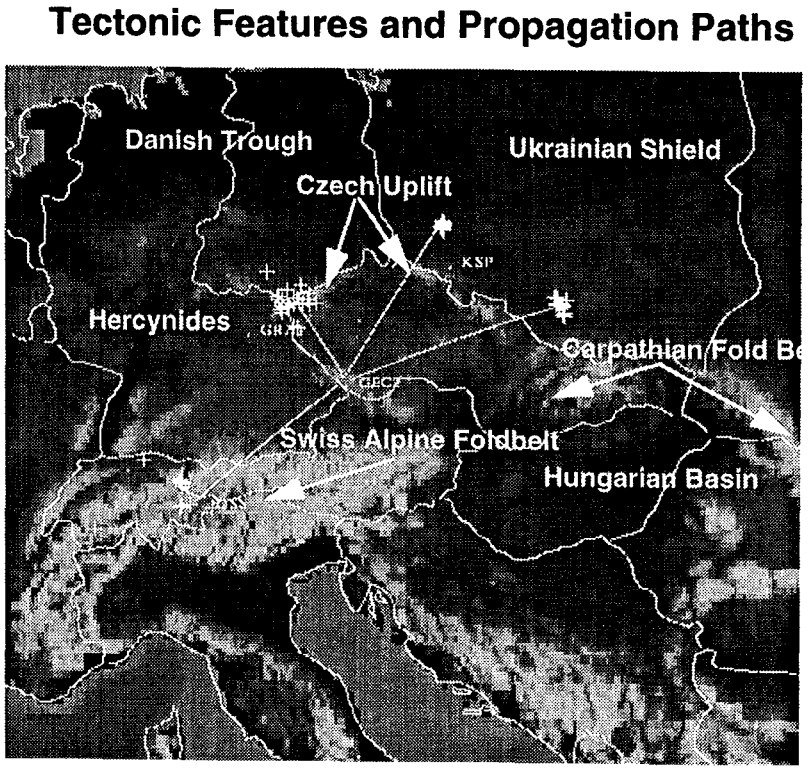

Figure 24: These maps show the locations of the Vogtland earthquakes and mine blasts, the Lubin rockbursts, the upper Silesia rockbursts, and a Swiss earthquake swarm. All events were recorded at the array GERESS.

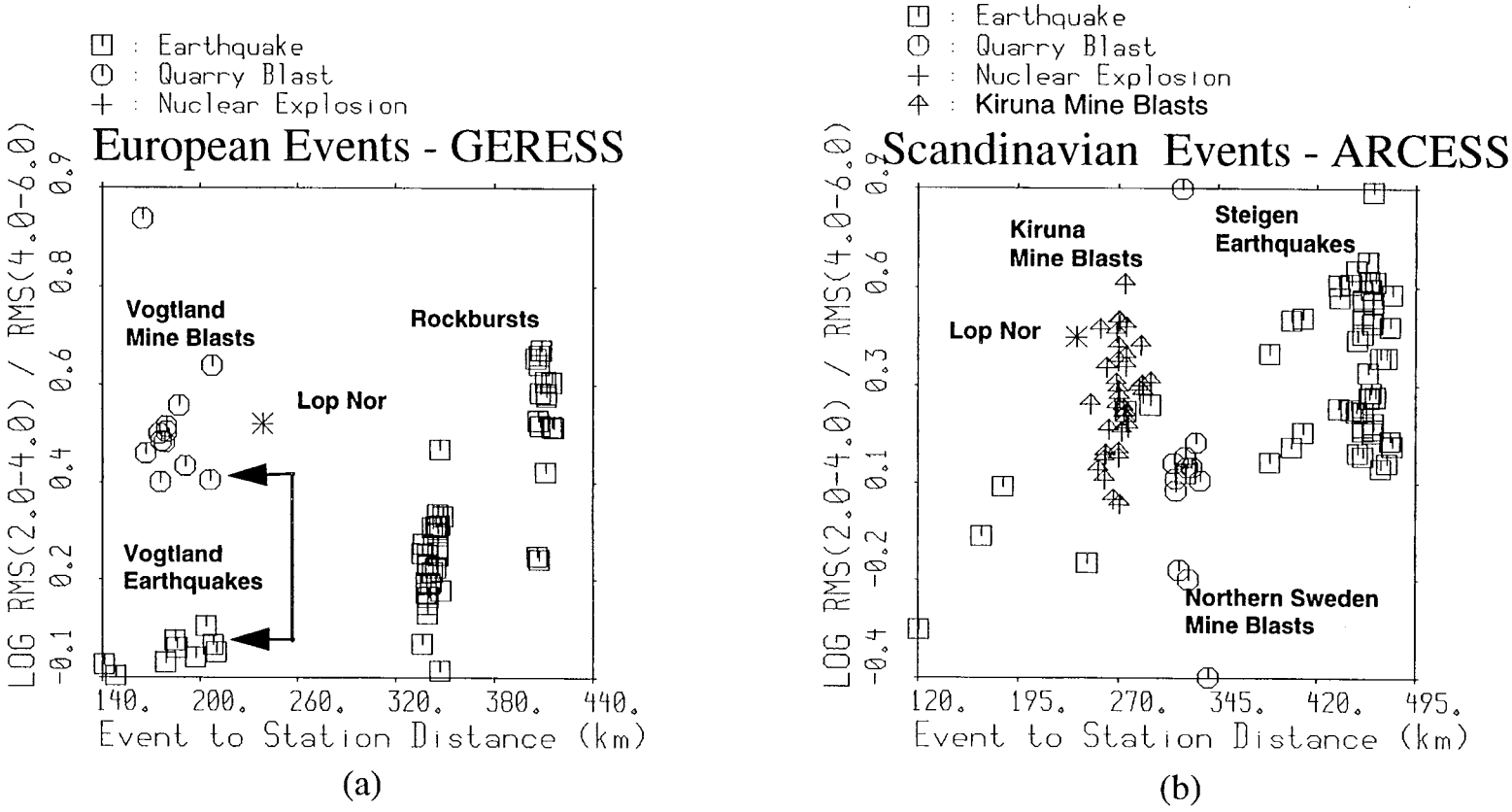

Figure 25: (a) *Lg* spectral ratios measured at GERESS for German mine blasts, earthquakes, and Polish rockbursts compared to the Lop Nor nuclear explosion at WMQ. (b) *Lg* spectral ratios measured at ARCESS for Scandinavian mine blasts and earthquakes compared to the Lop Nor nuclear explosion at WMQ. In both cases, the Lop Nor event is plotted as an asterisk. All spectra were corrected for instrument response before computing spectral ratios. The spectral ratio discriminant worked in the Vogtland regions and discriminates rockbursts and mine blasts. It does not work in Scandinavia.

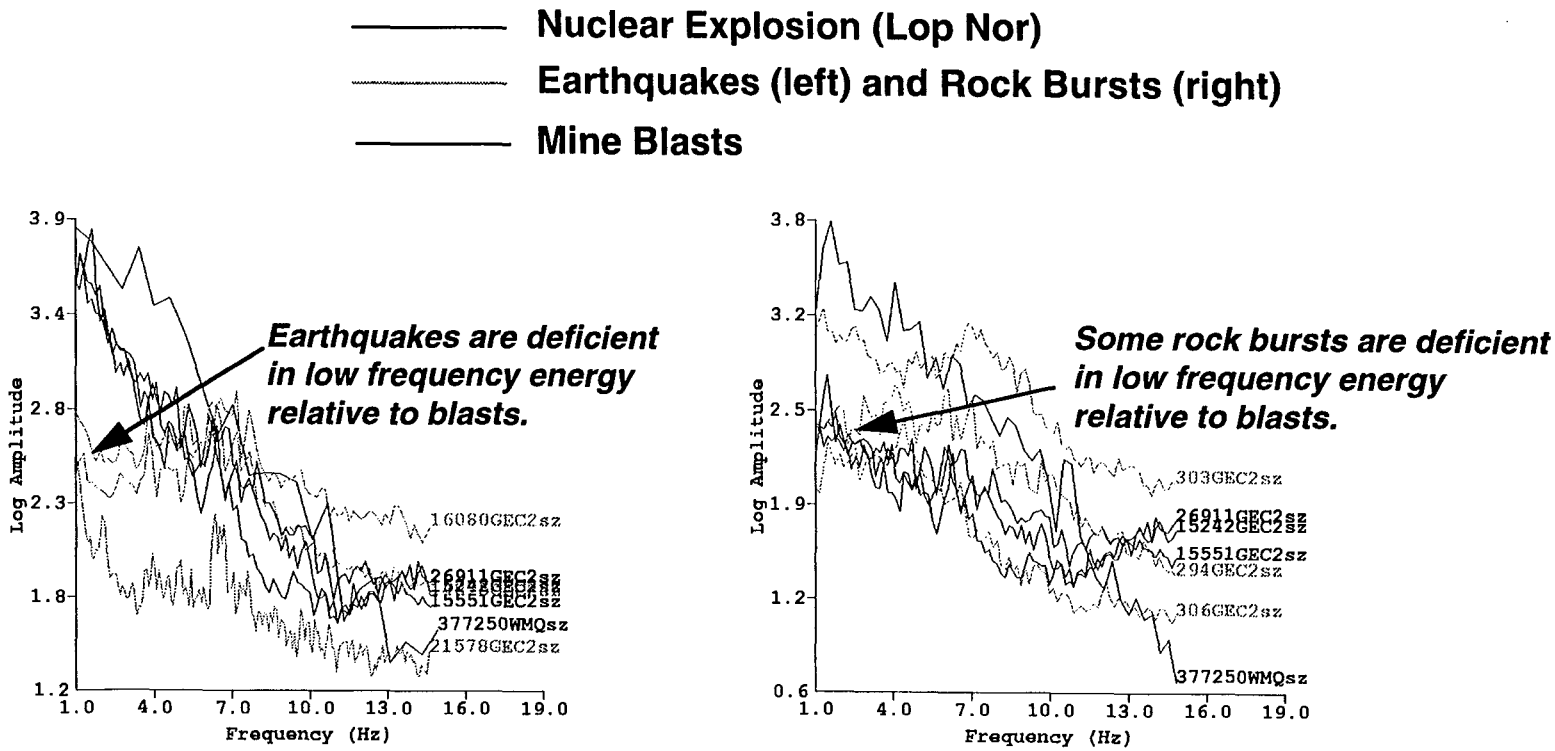

Comparison of *Lg* spectra measured at GERESS for mine blasts (black) and earthquakes (gray) with *Lg* spectrum measured at WMQ for the Lop Nor nuclear explosion. Earthquakes are deficient in low frequency energy compared to blasts.

Comparison of *Lg* spectra measured at GERESS for mine blasts (black) and earthquakes (gray) with *Lg* spectrum measured at WMQ for the Lop Nor nuclear explosion. Some, but not all rock bursts are deficient in low frequency energy compared to blasts.

Figure 26: Comparison of spectra for mine blasts, rockbursts, and earthquakes in Germany and the Lop Nor nuclear blast recorded at WMQ. Spectral ratio works because earthquakes are deficient in low frequency energy.

blasts are the darker colored spectra and the earthquakes and rockbursts are colored gray.) Figure 26 (a) shows that the earthquake spectra are deficient in low frequency energy. A similar comparison is shown in Figure 26 (b) between Vogtland blasts and some of the rockbursts, which also shows the same deficiency in low frequency energy in the rockbursts. Thus, the spectral ratio difference reflects real differences in the spectral shapes. There is no evidence of spectral scalloping from ripplefire in any of these spectra.

Figure 25 (b) shows the distance scaling for the Kiruna and northern Sweden mine blasts and the Steigen and northern Sweden earthquakes recorded at ARCESS. The Steigen earthquakes and Kiruna mine blasts overlap in spectral ratios. However, the Steigen earthquakes are over 200 km more distant than the Kiruna blasts. The Kiruna blasts have comparable spectral ratios as the Vogtland mine blasts. There are earthquakes at comparable distance as the Kiruna blasts which tend to have lower ratios. The Steigen earthquakes have comparable values of spectral ratio as the Kiruna blasts and therefore do not seem to discriminate. However, these events are also at a greater distance. Thus, like the rockbursts recorded at GERESS, these higher ratios for the Steigen events may be caused by higher attenuation over the larger distance

We now consider how these small-event spectral ratios scale with magnitude. Figures 27 (a) and (b) show plots as a function of ML for the 2-4Hz/4-6Hz and 2-4Hz/6-10Hz spectral ratios for the events recorded at GERESS which were plotted versus distance in Figure 25 (a). The squares include the Vogtland earthquakes and Polish rockbursts and the circles are the Vogtland mine blasts. The Vogtland earthquakes and mine blasts clearly separate but do not seem to scale with magnitude. The rockburst points are quite scattered and no strong magnitude dependence is evident.

Figures 28 (a) and (b) show the two spectral ratios plotted versus ML for the Scandinavian events recorded at ARCESS. Although these events cover a comparable magnitude range as the GERESS spectral ratios in Figure 27, the Steigen events have a systematic variation magnitude,

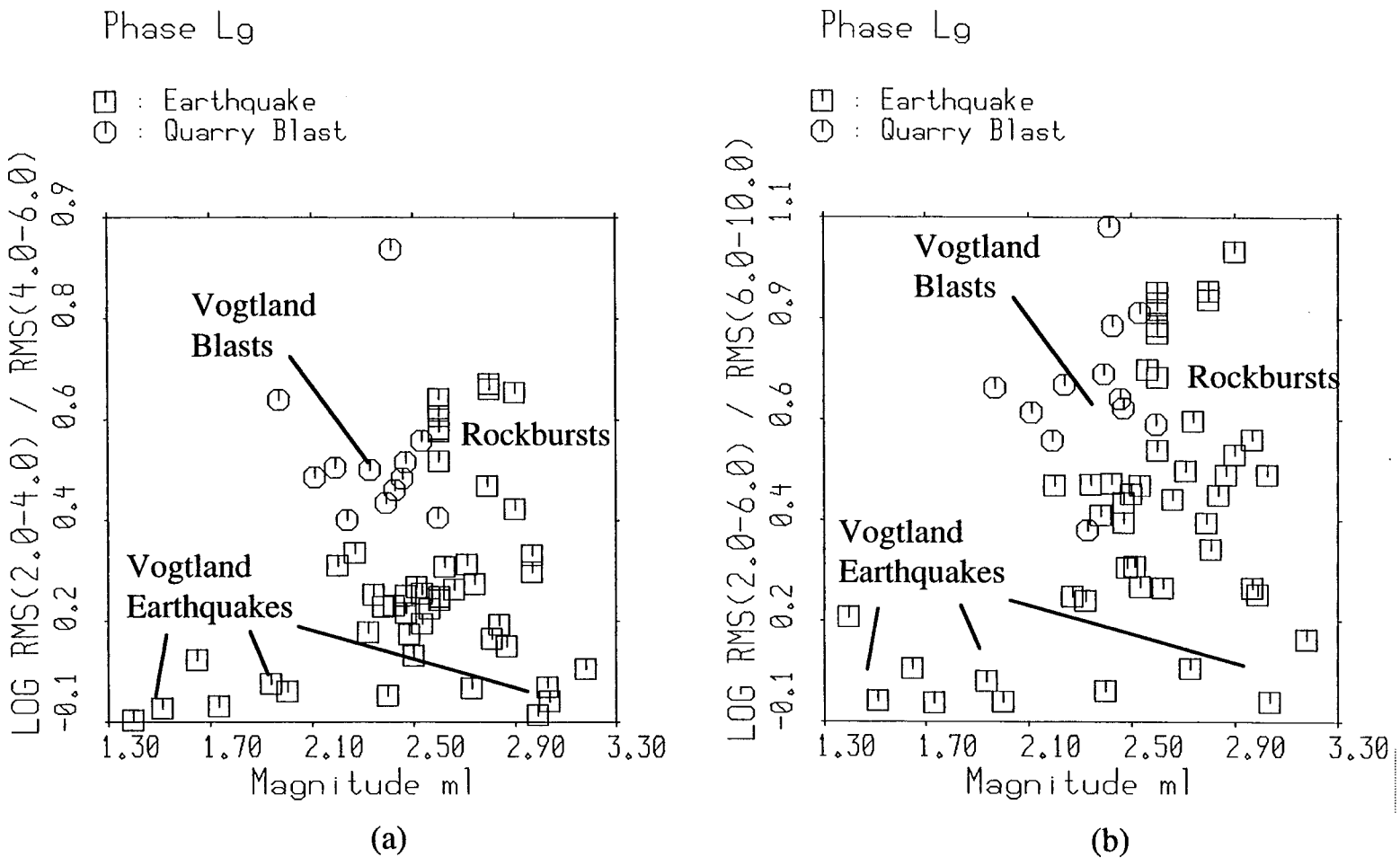

Figure 27: Two spectral ratio scatter plots versus ML for GERESS recordings of Vogtland earthquakes and explosions and rockbursts in Poland. Vogtland earthquakes have low ratios (higher frequencies) than the blasts. Rockbursts have a wide range of values and do not appear to discriminate from blasts.

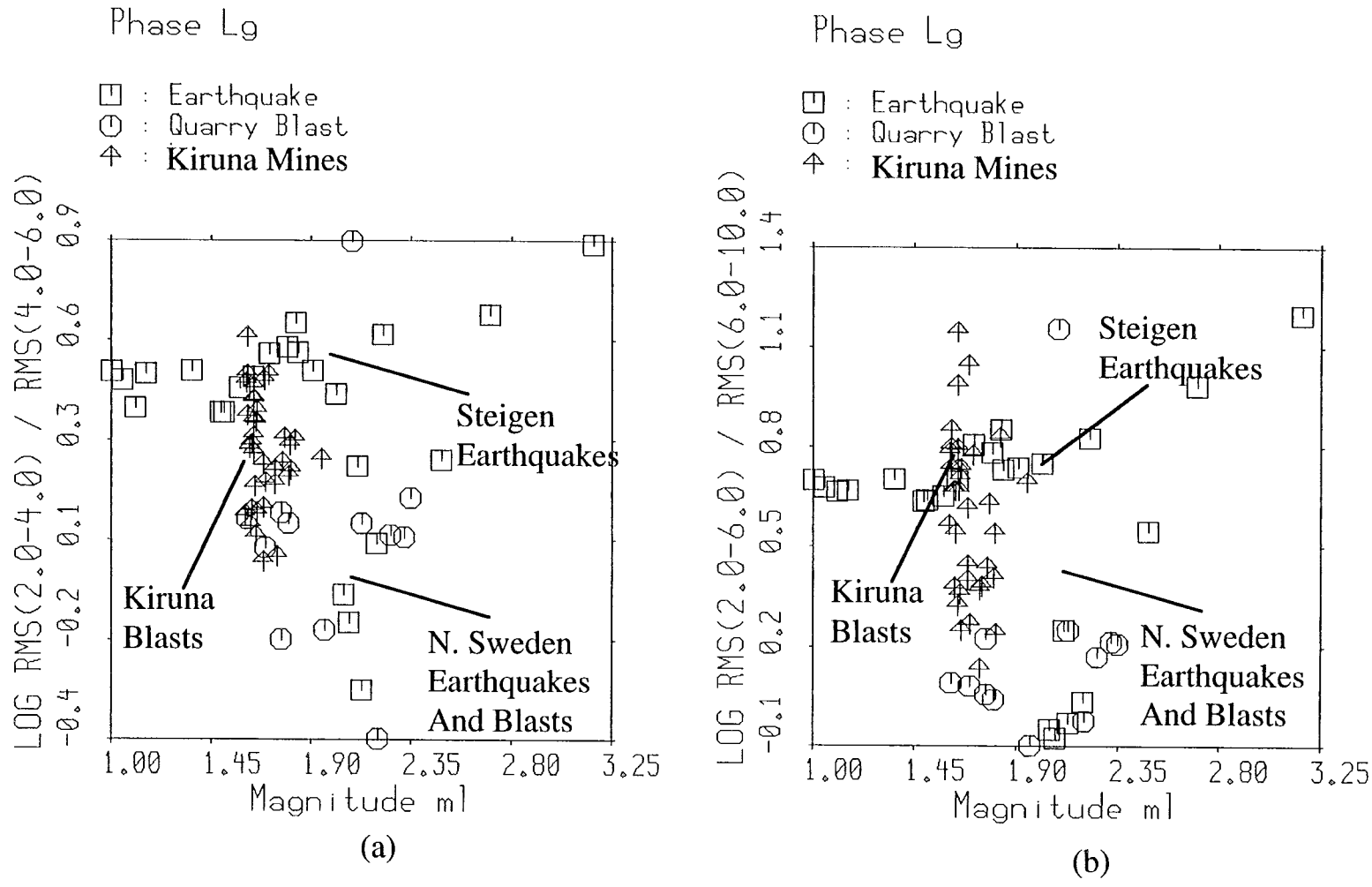

Figure 28: Two spectral ratio scatter plots for ARCESS recordings of Scandinavian earthquakes and explosions. Kiruna mine blasts completely overlap the Steigen earthquake swarm, which seems to scale with frequency. Northern Sweden blasts seem to have lower ratios (higher frequencies than earthquakes which is the reverse of the situation in the Vogtland region in Figure 27.

with the spectral ratio increasing with magnitude. The earthquakes in northern Sweden, which are not part of the Steigen swarm, do not seem to share the same magnitude scaling and have generally lower spectral ratios than the Steigen swarm. Part of this difference may be due to differences in propagation paths. The Kiruna events are all about the same magnitude, centered around 1.6, but have a wide range of spectral ratio. Clearly, these variations must be due to localized source effects and are not due to magnitude scaling.

Finally, Figure 29 shows the magnitude scaling against mb of the two *Lg* spectral ratios for the Urals event, recorded at ARU, compared with Chinese nuclear explosion, Chinese earthquakes, and Kazakh nuclear explosions recorded at the Chinese station, WMQ. There appears to be some indication of magnitude scaling of these spectral ratios, with the spectral ratio increasing with distance. However, the scatter is quite large, particularly around the magnitude of 4.7 for the Lop Nor events. Given the scatter in the data, there appears to be no evident discrimination between explosions and earthquakes.

We conclude from this analysis that there is limited evidence of strong magnitude scaling of the *Lg* spectral ratio at magnitudes below 3.0, although the Steigen swarm showed some evidence for this scaling. Perhaps because the Steigen events were in a swarm, they all had about the same source mechanism and source excitation spectrum, and the only variations are those due to magnitude scaling of the spectral ratios. The other earthquakes and rockbursts occurred in different locations at different times so that source differences and propagation effects could strongly affect the values of the spectral ratios. *Lg* spectral ratio only works for discriminating blasts and earthquakes in Germany but doesn't work in Scandinavia. It also did not work for larger earthquakes and nuclear explosions in China.

5.3 A Distance Correction Scheme for Spectral Ratios

We now address the problem of the distance scaling of *Lg* spectral ratios which is evident in Figure 25 (a). The ratios for the rockbursts in Poland increase with distance, as we might

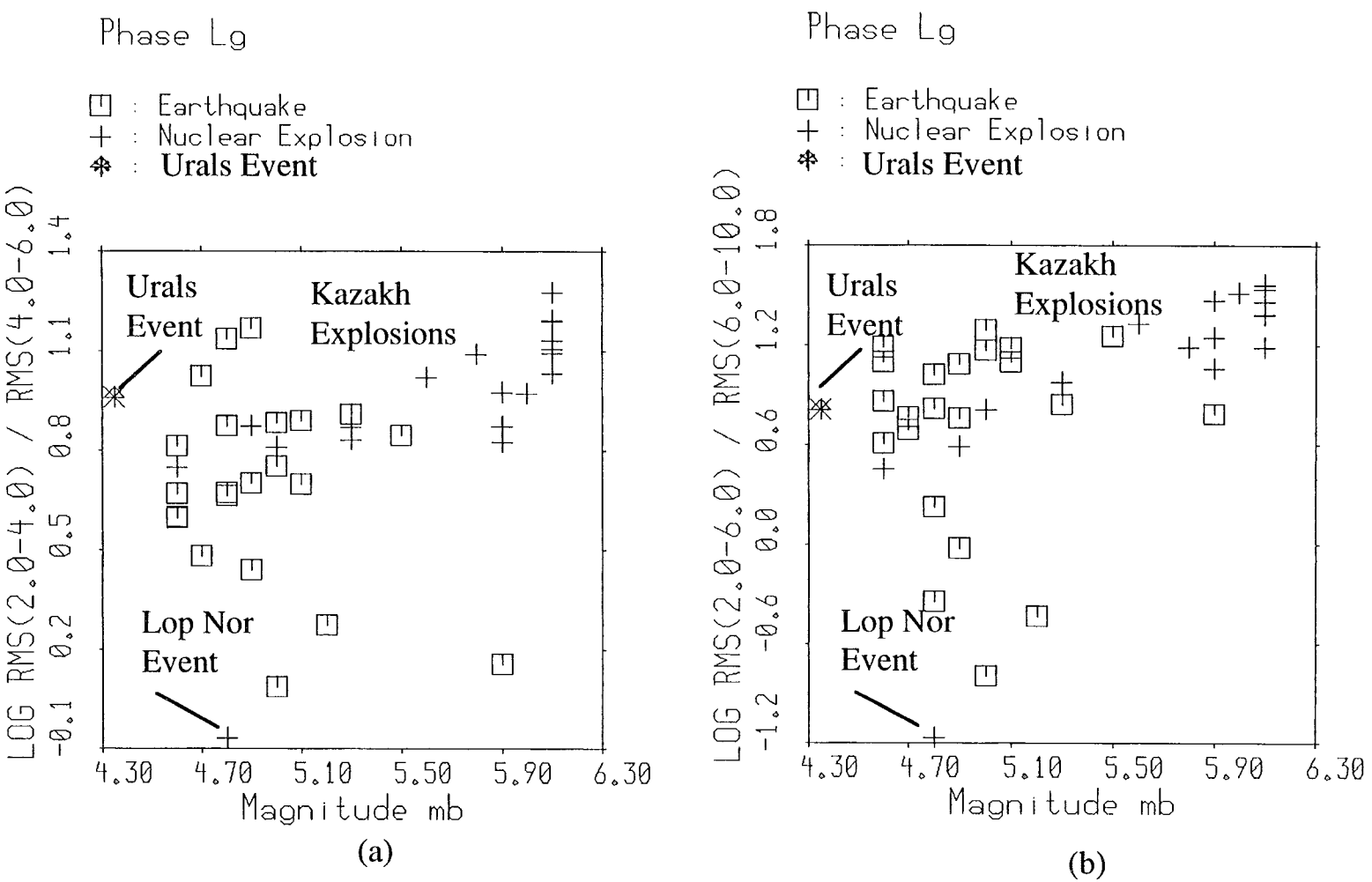

Figure 29: Two spectral ratio scatter plots for WMQ recordings of Chinese earthquakes, Lop Nor nuclear blast, and Kazakh nuclear blasts, versus mb. Also shown is the ARU recording of the January 5, 1995 Southern Urals event. Spectral ratios do appear to scale with magnitude. As in Scandinavia in Figure 20, there appears to be very little discrimination between blasts and earthquakes.

expect since increasing attenuation of high frequencies with distance will reduce the high frequency energy in the *Lg* spectrum and cause the spectral ratio to increase.

In order to reduce the systematic bias and scatter due to variations in propagation path distances, we have included in ISEIS a simple scheme for correcting the spectral ratio for anelastic attenuation. We model the attenuation of the regional phase with the standard anelastic attenuation relation

$$A^{TH}(f,D) = A_o(f)\exp\left[\frac{-\pi f D}{QU}\right], \tag{13}$$

where A^{TH} is the theoretical spectral amplitude at frequency f and distance D, A_o is the initial source excitation, D is the distance in km, Q is the attenuation quality factor, U is the group velocity of the regional phase and f is the frequency in Hz. We assume the commonly used power-law frequency dependence for attenuation

$$Q = Q_o\left(\frac{f}{f_o}\right)^{\zeta} \tag{14}$$

where Q_o is quality factor at the reference frequency f_o and ζ specifies the frequency dependence. Generally, f_o is 1 Hz and ζ ranges from 0.0 to 1.0.

Specifying a certain frequency band Δf and breaking it up into N frequency intervals, we compute the rms spectral level as

$$A^{TH}{}_{rms}(\Delta f, D) = \sqrt{\frac{1}{N}\sum_{i=1}^{N} A^{TH}(f_i, D)^2} \tag{15}$$

where the values of f_1 to f_N are the low and high frequency limits in the band Δf. For the theoretical rms spectral ratio, we have

$$R^{TH}(\Delta f_1, \Delta f_2, D) = \frac{A^{TH}{}_{RMS}(\Delta f_1, D)}{A^{TH}{}_{RMS}(\Delta f_2, D)}. \quad (16)$$

Given observed values of the rms spectral ratio, $R(\Delta f_1,\Delta f_2,D)$, at distances D, we wish to correct the ratios to the same reference distance, D_{ref}. Assuming values of Q_o, ζ, and U, we have for the distance corrected spectral ratio

$$R(\Delta f_1, \Delta f_2, D_{ref}) = R(\Delta f_1, \Delta f_2, D) \frac{R^{TH}(\Delta f_1, \Delta f_2, D_{ref})}{R^{TH}(\Delta f_1, \Delta f_2, D)} . \quad (17)$$

Group velocities, U, of 8.1, 6.5, 4.7, and 4.0 km/sec were assumed for major regional phases, *Pn*, *Pg*, *Sn*, and *Lg*, respectively. Values of *Qo* and z are dependent on the path and must be determined by direct inversion of *Lg* spectra or coda, or by trial and error by fitting trends by eye to spectral-ratio-versus-distance plots. In this study, we use the latter approach.

Figures 30, 31, and 32 show examples of theoretical spectral ratio curves for different values of Q_o and frequency dependence, ζ, plotted over the GERESS points from Figure 25 (a). We also include the measurements for the Swiss earthquake swarm, shown in the map in Figure 24. Increasing values of Q_o increases the intercept of the correction curves and smaller values of the frequency dependence exponent, ζ, produces large slopes.

Based on trial and error plotting of different attenuation correction curves, we conclude that the curve for Q_o = 200 and ζ = 0.2 seems to pass through the extreme values of the earthquakes and rockbursts, as shown in Figure 33 (a). Assuming this correction curve, and using (17), we get the distance-corrected spectral ratios shown plotted in Figure 33 (b). After correction, the rockburst points at larger distance are shifted downward and more closely resemble the values of Vogtland earthquakes. Thus, in this instance at least, the increased scatter of the rockbursts may have been due to their increased distance. We conclude that, after distance corrections, the rockbursts in Poland are similar to earthquakes and that both *Pn/Lg* ratios and *Lg* spectral ratios can classify events in this region.

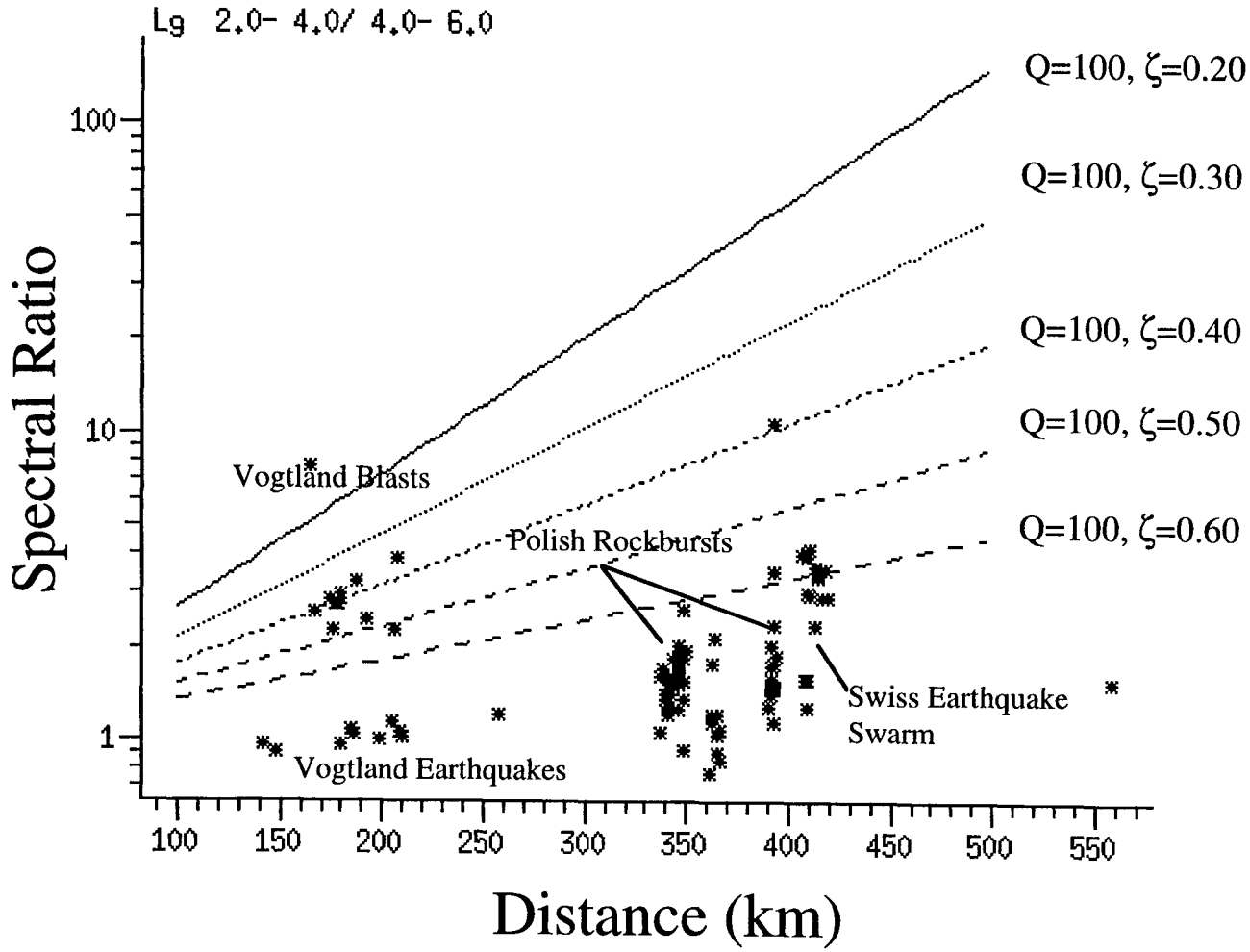

Figure 30: Examples of theorectical distance correction curves for Q=100 for the 2-4Hz/4-6Hz *Lg* spectral ratio overlaid on measurements from the GERESS array shown in Figure 25 a.

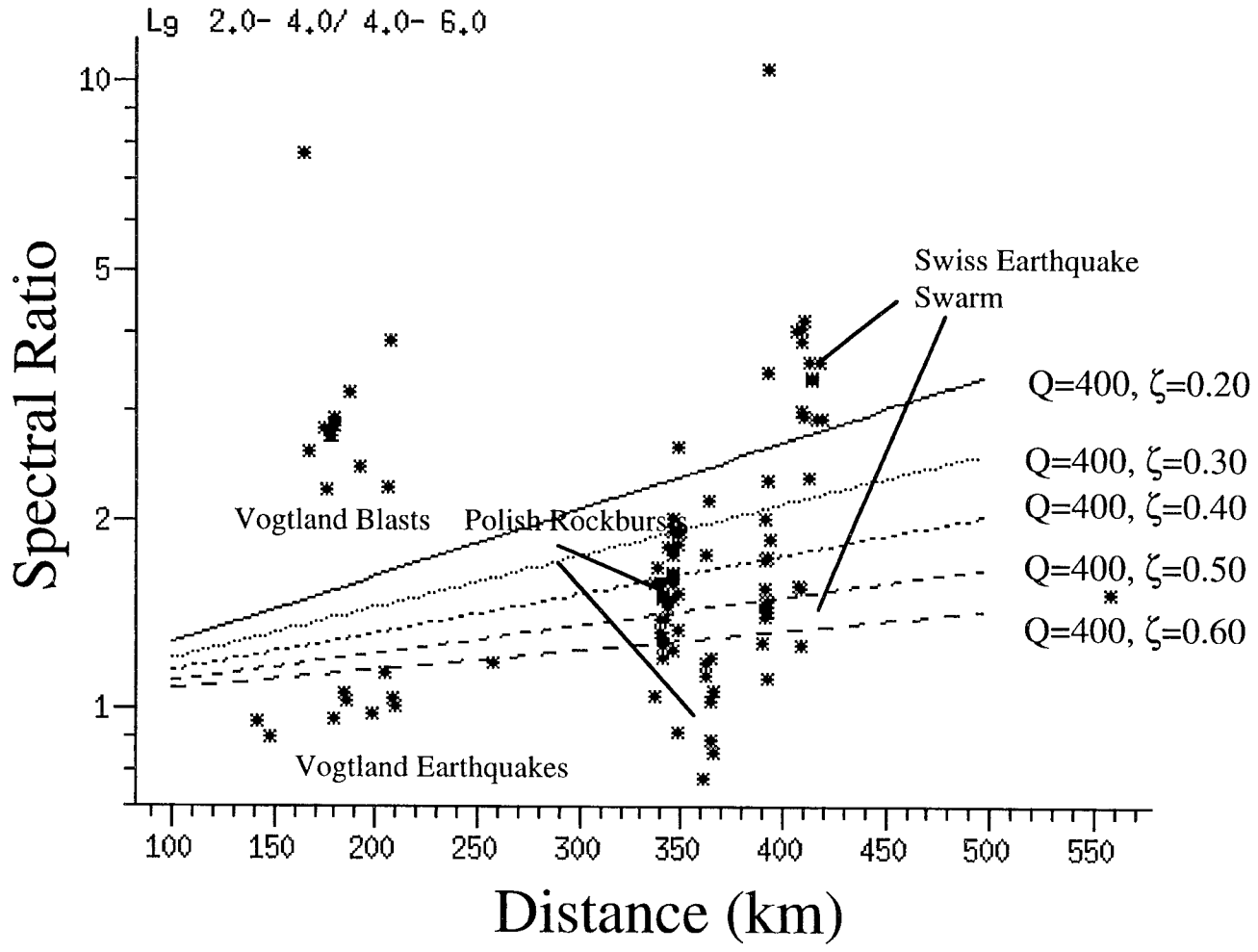

Figure 31: Examples of theorectical distance correction curves for Q=400 for the 2-4Hz/4-6Hz *Lg* spectral ratio overlaid on measurements from the GERESS array shown in Figure 25 (a.).

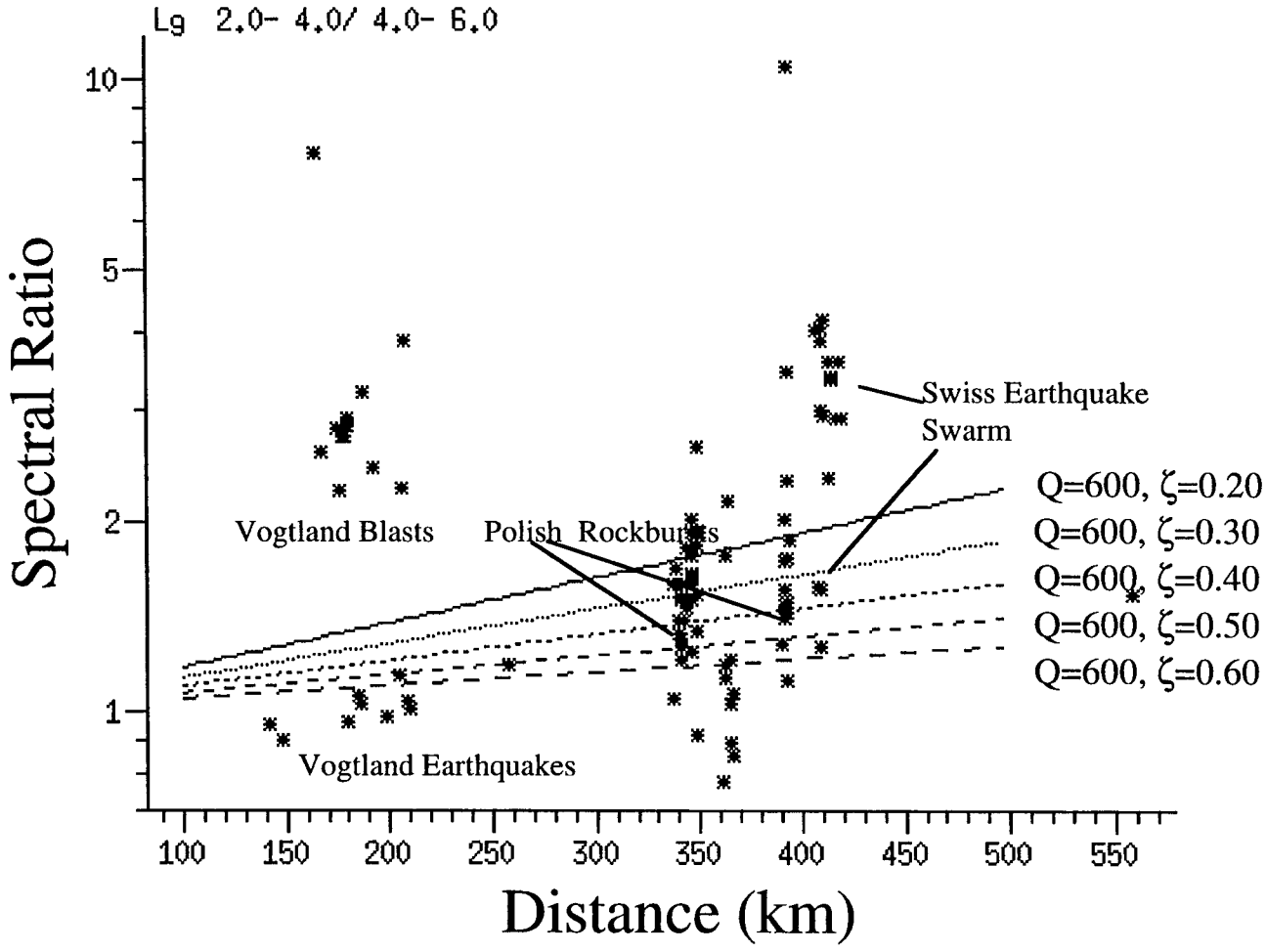

Figure 32: Examples of theorectical distance correction curves for Q=600 for the 2-4Hz/4-6Hz *Lg* spectral ratio overlaid on measurements from the GERESS array shown in Figure 25 (a).

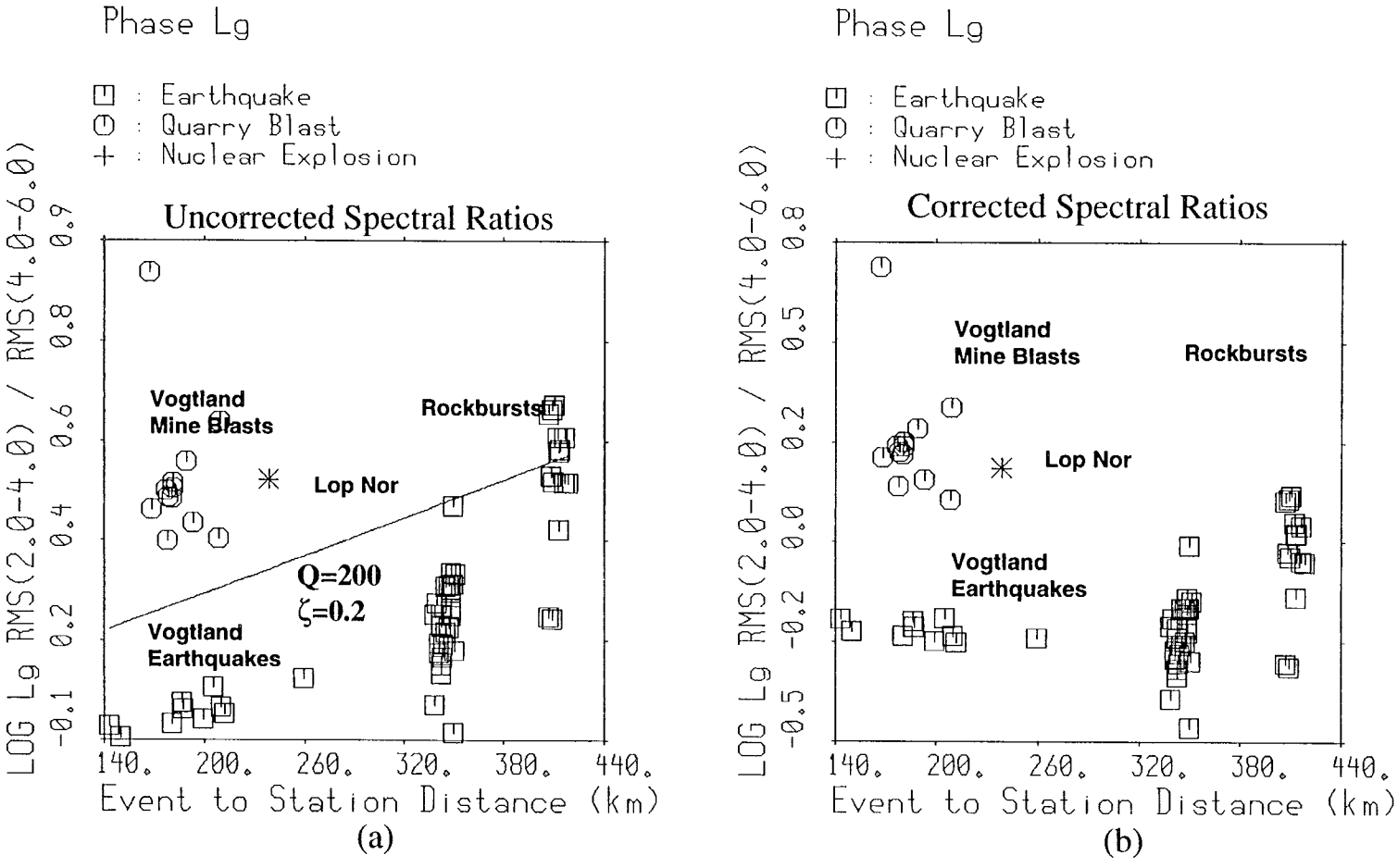

Figure 33: (a) GERESS spectral ratios for Vogtland and Polish rockbursts with distance correction curve for Q=200 and ζ=0.2. (b) Result of correcting the spectral ratios for anelastic attenuation. Note now that the rockburst points are lowered and discriminate from the mine blasts.

6.0 CONCLUSIONS

With the shifting of priorities in test ban treaty monitoring from focusing on a single country, the former Soviet Union, to taking into account the entire world for monitoring comprehensive test ban and non-proliferation treaties, global networks of seismic stations are being deployed and seismic data from sources over a variety of propagation paths must be understood. Global seismic event identification requires discriminants which are insensitive to propagation path effects or can be corrected for these effects. In our research in regional discriminant transportability from regions we have studied which have historical data for explosions and earthquakes, to new regions of the world where there may be limited historical data, we have tried to understand the effects of propagation path effects, with our main focus on the regional *P/S* amplitude ratio discriminant and spectral ratio.

Performance of discriminants in different regions is based on other factors besides propagation path effects. One of the main conclusions of this project, based on our analyses of frequency dependent *Pn/Sn* and *Pn/Lg* amplitude ratios for events in a number of mines, is that mine blasts can have large *S* wave amplitudes, comparable to those observed from small earthquakes. This might be expected since mine blasts are designed to induce fracture in rocks. Ripplefired blasting near the bench face of a mine shears off rock fragments and ejects rock fragments into ballistic free fall. The rock shearing and spallation can induce arbitrarily large shear waves. Thus, mine blasts will look much more earthquake-like than single explosions, including, for example, nuclear explosions. In essence, mine blasts may be classified as another kind of rockburst, which, as shown in our studies and those of Bennett et al (1994), have *P/S* amplitude ratios similar to earthquakes.

In test ban treaty monitoring, such events should not present a severe problem. As we noted in Section 2.0, the large *S*-wave events in the Kiruna mine were very small events. We have

yet to observe a known large mine blast (i.e., ML > 3.0) with very large *S* waves although such events could conceivable exist.

However, high magnitude rockbursts with large *S* waves are well observed which Bennett et al (1994) have suggested may be manipulated so as to obscure a decoupled nuclear explosion. Perhaps mine blasts could be ripplefired in such a way as to induce large shear waves which would be an easier way of hiding a decoupled blast than trying to induce a rockburst. The issue then becomes whether a decoupled blast could still be identified with the large *P* wave it would produce.

We have found that *Pn/Lg* ratios have a systematic increasing trend with distance, which appears to be due to differential attenuation of the phases. In our earlier report (Baumgardt and Der, 1994), we described our development of a set of empirical distance correction curves for *Pn/Sn* and *Pn/Lg* which removes the distance trend in these ratios. We have studied these corrections, as well as those derived from those of Sereno (1990), and we find that the corrections remove some of the frequency dependence scatter. However, there still remains a large residual scatter over the distance correction trend. For mine blasts, we have argued that the high variation in the *P/S* ratios would result from rock cracking and spalling induced by the blasting. Baumgardt and Der (1994) also investigated blockage effects due to crustal structure heterogeneities, and structure features can be correlated with signal features to correct for these effects.

The most effective discriminant for identifying multiple shooting in mines, either due to ripplefire or attempted "hide-in-mine blast/rockburst" evasion, is the time-independent spectral scalloping signature, discovered by Baumgardt and Ziegler (1988). In this report and in Der and Baumgardt (1994), we have emphasized the importance of signal correlation on the nature of spectral scalloping. The correlation of multiple superimposed blast signals, not source finiteness, produces spectral scalloping, and the effects of signal decorrelation can reduce the scalloping and eliminate it altogether. By studying the nature and intensity of spectral scalloping for different phases, it should be possible to very simply characterize the maximum dimensions of a blasting

pattern, which may be very important for detecting possible hide-in-mine blast/rockburst evasion attempts.

Finally, this study also has assessed the variability in performance of the spectral ratio discriminant which earlier appeared to be very promising. The variability of the performance of the discriminant points to a geological cause for the discriminant. If explosions and earthquakes occur in regions of strong vertical heterogeneity, such as at NTS where the explosions occur in rocks with variable gas porosity, and the earthquakes are at a greater depth below these effects, we expect the discriminant will work well. However, if earthquakes are shallow or if the blasts do not occur in near-surface geological heterogeneity, such as in shield regions like Scandinavia, the discriminant may fail.

In conclusion, this work shows that analysis of regional seismic data can reveal much about seismic events and be very valuable for identifying events. However, the whole picture must be considered, including the effects of source geology and propagation path effect on signals, to be able to fully understand the signals and use them to derive useful and reliable discriminants.

REFERENCES

Atakan, K. (1992). An unusual Earthquake Sequence in Steigen Northern Norway, Internal Report, 1992, Institute of Solid Earth Physics, University of Bergen, Norway.

Barker, T.G., M.L. McLaughin, and J.L. Stevens (1993). Numerical Simulation of Quarry Blast Sources, Technical Report, SSS-TR-93-13859, S-CUBED, La Jolla, CA.

Baumgardt, D.R. (1993a). Regional characterization of mine blasts, earthquakes, mine tremors, and nuclear explosions using the Intelligent Event Identification System, Final Report to ARPA, SAS-TR-94-12, ENSCO, Inc., Springfield, VA.

Baumgardt, D.R. (1993b). Seismic waveform feature and discrimination of the December 31, 1992 Novaya Zemlya event, Paper in volume compiled by Ryall (1993).

Baumgardt, D.R. (1995a). Identification of the January 5, 1995 Southern Urals special event, Topical Report, April 1995.

Baumgardt, D.R. (1995b). Identification of presumed shallow underwater chemical blasts using land-based regional seismic data, Topical Report, April 1995.

Baumgardt, D.R. and K.A. Ziegler (1988). Spectral evidence of source multiplicity in explosions: application to regional discrimination of earthquakes and explosions, *Bull. Seism. Soc. Am.*, **78**, 1773-1795.

Baumgardt, D.R. and G. Young (1990). Regional seismic waveform discriminants and case based event identification using regional arrays, *Bull. Seism. Soc. Am.*, **80**, Part B, 1874-1892.

Baumgardt, D.R. and Z.A. Der (1994). Investigation of the transportability of the P/S ratio discriminant to different tectonic regions, Scientific Report No. 1, PL-TR-94-2299, ENSCO, Inc., Springfield, VA, ADA292944.

Baumgardt, D.R., S. Carter, M. Maxson, J. Carney, K. Ziegler, and N. Matson (1991). Design and development of the intelligent event identification system, *PL-TR-91-22298(I)*, Final Report, ENSCO, Inc., Springfield, VA, ADA248381.

Baumgardt, D.R., J. Carney, M. Maxson, and S. Carter (1992). Evaluation of regional seismic discriminants using the Intelligent Seismic Event Identification System, Semiannual Technical Report, SAS-TR-93-38, ENSCO, Inc., Springfield, VA.

Bennett, T.J. and J.R. Murphy (1986). Analysis of seismic discrimination capabilities using regional data from western United States events, *Bull. Seism. Soc. Am.*, **76**, 1069-1086.

Bennett, T.J., B.W. Barker, K.L. McLaughlin, and J.R. Murphy (1989). Regional discrimination of quarry blasts, earthquakes, and underground nuclear explosions, Final Report, *GL-TR-89-0114,* S-Cubed, La Jolla, CA, ADA223148.

Bennett, T.J., M.E. Marshall, B.W. Barker, and J.R. Murphy (1994). Characteristics of rockbursts for use in seismic discrimination, *PL-TR-94-2269*, Final Report to Phillips Laboratory, S-CUBED, La Jolla, CA, ADA290881.

Blandford, R.R. (1993). Discrimination of Earthquakes and Explosions at Regional Distances Using Complexity, *AFTAC-TR-93-044*, H.Q. Air Force Technical Applications Center, Patrick Air Force Base, FL.

Blandford, R., R. Hartenberger, and R. Naylor (1981). Regional amplitude-distance relations, discrimination and detection, *VSC-TR-81-15*, Teledyne Geotech, Alexandria, VA.

Der, Z. and D.R. Baumgardt (1994). Issues in regional monitoring of mining operations for the presence of hidden nuclear tests, 1994 ARPA CTBT Monitoring Technologies Conference, San Diego, CA.

Gitterman, Y. and T. van Eck (1993). Spectra of quarry blasts and microearthquakes recorded at local distances in Israel, *Bull. Seism. Soc. Am.*, **83**, 1799-1812.

Grant, L., J. Coyne, and F. Ryall (1993). CSS Ground-Truth Database: Version 1 Handbook, *C93-05*, August, 1993, Center for Seismic Studies, Arlington, VA.

Hedlin, M.A., J.B. Minster, and J.A. Orcutt (1989). The time-frequency characteristics of quarry blasts and calibration explosions recorded in Kazakhstan, USSR, *Geophys. J. Int.*, **99**, 109-121.

Hedlin, M.A., J.B. Minster, and J.A. Orcutt (1990). An automatic means to discriminate between earthquakes and quarry blasts, *Bull. Seism. Soc. Am.*, **80**, 2143-2160.

Kim, W.Y., D.W. Simpson, and P.G. Richards (1993). Discrimination of earthquakes and explosions in the eastern United States using regional high-frequency data, *Geophys. Res. Lett.*, **20**, 1507-1510.

Kim, W.Y., D.W. Simpson, and P.G. Richards (1994). High-frequency spectra of regional phases from earthquakes and chemical explosions, *Bull. Seism. Soc. Am.*, **84**, 1365-1386.

Lynnes, C. and R. Baumstark (1991). Phase and spectral discrimination in North America, *PL-TR-91-2212 (II)*, Teledyne Geotech, Alexandria, VA, ADA246673.

McLaughlin, K.L., T.G. Barker, and J.L. Stevens (1994). Numerical Simulation of Quarry Blast Sources, *SSS-FR-94-14418*, S-CUBED, La Jolla, CA.

Murphy, J.R. and T.J. Bennett (1982). A discrimination analysis of short-period regional seismic data recorded at Tonto Forest Observatory, *Bull. Seism. Soc. Am.*, **72**, 1351-1366.

Mykkeltveit, S., K. Astebol, K.J. Doornbos, and E.S. Husebye (1983). Array configuration optimization, *Bull. Seism. Soc. Am*, **73**, 173-186.

Nuttli, O.W. (1981). On the attenuation of *Lg* waves in western and central Asia and their use as a discriminant between earthquakes and explosions, *Bull. Seism. Soc. Am.*, **72**, 1351-1366.

Pomeroy, P.W., W.J. Best, and T.V. McEvilly (1982). Test ban treaty verification with regional data - A review, *Bull. Seism. Soc. Am.*, **72**, S89-S129.

Riviere-Barbier, F. (1993). Constructing a reference event list for ARCESS, Special Technical Report, C93-03, Center for Seismic Studies, Arlington, VA.

Sereno, T.J. (1990). Attenuation of regional phases in Fennoscandia and estimates of arrival time and azimuth uncertainty using data recorded by regional arrays, SAIC-90/1472, SAIC, San Diego, CA.

Smith, A.T. (1989). High-frequency seismic observations and models of chemical explosions: implications for the discrimination of ripple-fired mining blasts, *Bull. Seism. Soc. Am.*, **79**, 1089-1110.

Smith, A.T. (1993). Discrimination of explosions from simultaneous mining blasts, *Bull. Seism. Soc. Am.*, **83**, 160-179.

Stump, B.W. and R.E. Reinke (1988). Experimental confirmation of superposition from small-scale explosions, *Bull. Seism. Soc. Am.*, **78**, 1059-1073.

Taylor, S.R., N.W. Sherman, and M.D. Denny (1988). Spectral discrimination between NTS explosion and western United States earthquakes at regional distances, *Bull. Seism. Soc. Am.*, **78**, 1563-1579.

Taylor, S.R., M.D. Denny, E.S. Vergino, and R.E. Glaser (1989). Regional discrimination between NTS explosion and western United States earthquakes, *Bull. Seism. Soc. Am.*, **79**, 1142-1176.

Walter, W.R. (1995). Personal communication.

Walter, W.R., K. Mayeda, and H.J. Patton (1994). Regional seismic observations of the Non-Proliferation experiment at Livermore NTS Network, *Proceedings on the Non-Proliferation Experiment: Results and Implications for Test Ban Treaties*, Rockville, MD, April 19-21, 1994.

Walter, W.R., K. Mayeda, and H.J. Patton (1994). Phase and spectra ratio discrimination between NTS earthquakes and explosions, Part 1: Empirical observations, UCRL-JC-118551 Part 1, Lawrence Livermore National Laboratory, September 1994.

Wuster, J. (1993). Discrimination of chemical explosions and earthquakes in central Europe - a case study, *Bull. Seism. Soc. Am.*, **83**, 1184-1212.

Prof. Thomas Ahrens
Seismological Lab, 252-21
Division of Geological & Planetary Sciences
California Institute of Technology
Pasadena, CA 91125

Prof. Keiiti Aki
Center for Earth Sciences
University of Southern California
University Park
Los Angeles, CA 90089-0741

Prof. Shelton Alexander
Geosciences Department
403 Deike Building
The Pennsylvania State University
University Park, PA 16802

Dr. Thomas C. Bache, Jr.
Science Applications Int'l Corp.
10260 Campus Point Drive
San Diego, CA 92121 (2 copies)

Prof. Muawia Barazangi
Cornell University
Institute for the Study of the Continent
3126 SNEE Hall
Ithaca, NY 14853

Dr. Douglas R. Baumgardt
ENSCO, Inc
5400 Port Royal Road
Springfield, VA 22151-2388

Dr. T.J. Bennett
S-CUBED
A Division of Maxwell Laboratories
11800 Sunrise Valley Drive, Suite 1212
Reston, VA 22091

Dr. Robert Blandford
AFTAC/TT, Center for Seismic Studies
1300 North 17th Street
Suite 1450
Arlington, VA 22209-2308

Dr. Steven Bratt
ARPA/NMRO
3701 North Fairfax Drive
Arlington, VA 22203-1714

Dale Breding
U.S. Department of Energy
Recipient, IS-20, GA-033
Office of Arms Control
Washington, DC 20585

Dr. Jerry Carter
Center for Seismic Studies
1300 North 17th Street
Suite 1450
Arlington, VA 22209-2308

Mr Robert Cockerham
Arms Control & Disarmament Agency
320 21st Street North West
Room 5741
Washington, DC 20451,

Dr. Zoltan Der
ENSCO, Inc.
5400 Port Royal Road
Springfield, VA 22151-2388

Dr. Stanley K. Dickinson
AFOSR/NM
110 Duncan Avenue
Suite B115
Bolling AFB, DC

Dr Petr Firbas
Institute of Physics of the Earth
Masaryk University Brno
Jecna 29a
612 46 Brno, Czech Republic

Dr. Mark D. Fisk
Mission Research Corporation
735 State Street
P.O. Drawer 719
Santa Barbara, CA 93102

Dr. Cliff Frohlich
Institute of Geophysics
8701 North Mopac
Austin, TX 78759

Dr. Holly Given
IGPP, A-025
Scripps Institute of Oceanography
University of California, San Diego
La Jolla, CA 92093

Dr. Jeffrey W. Given
SAIC
10260 Campus Point Drive
San Diego, CA 92121

Dan N. Hagedon
Pacific Northwest Laboratories
Battelle Boulevard
Richland, WA 99352

Dr. James Hannon
Lawrence Livermore National Laboratory
P.O. Box 808, L-205
Livermore, CA 94550

Dr. Roger Hansen
University of Colorado, JSPC
Campus Box 583
Boulder, CO 80309

Prof. Danny Harvey
University of Colorado, JSPC
Campus Box 583
Boulder, CO 80309

Prof. Donald V. Helmberger
Division of Geological & Planetary Sciences
California Institute of Technology
Pasadena, CA 91125

Prof. Eugene Herrin
Geophysical Laboratory
Southern Methodist University
Dallas, TX 75275

Prof. Robert B. Herrmann
Department of Earth & Atmospheric Sciences
St. Louis University
St. Louis, MO 63156

Prof. Lane R. Johnson
Seismographic Station
University of California
Berkeley, CA 94720

Prof. Thomas H. Jordan
Department of Earth, Atmospheric &
Planetary Sciences
Massachusetts Institute of Technology
Cambridge, MA 02139

U.S. Dept of Energy
Max Koontz, NN-20, GA-033
Office of Research and Develop.
1000 Independence Avenue
Washington, DC 20585

Dr. Richard LaCoss
MIT Lincoln Laboratory, M-200B
P.O. Box 73
Lexington, MA 02173-0073

Prof. Charles A. Langston
Geosciences Department
403 Deike Building
The Pennsylvania State University
University Park, PA 16802

Jim Lawson, Chief Geophysicist
Oklahoma Geological Survey
Oklahoma Geophysical Observatory
P.O. Box 8
Leonard, OK 74043-0008

Prof. Thorne Lay
Institute of Tectonics
Earth Science Board
University of California, Santa Cruz
Santa Cruz, CA 95064

Dr. William Leith
U.S. Geological Survey
Mail Stop 928
Reston, VA 22092

Mr. James F. Lewkowicz
Phillips Laboratory/GPE
29 Randolph Road
Hanscom AFB, MA 01731-3010(2 copies)

Dr. Gary McCartor
Department of Physics
Southern Methodist University
Dallas, TX 75275

Prof. Thomas V. McEvilly
Seismographic Station
University of California
Berkeley, CA 94720

Dr. Keith L. McLaughlin
S-CUBED
A Division of Maxwell Laboratory
P.O. Box 1620
La Jolla, CA 92038-1620

Prof. Bernard Minster
IGPP, A-025
Scripps Institute of Oceanography
University of California, San Diego
La Jolla, CA 92093

Prof. Brian J. Mitchell
Department of Earth & Atmospheric Sciences
St. Louis University
St. Louis, MO 63156

Mr. Jack Murphy
S-CUBED
A Division of Maxwell Laboratory
11800 Sunrise Valley Drive, Suite 1212
Reston, VA 22091 (2 Copies)

Dr. Keith K. Nakanishi
Lawrence Livermore National Laboratory
L-025
P.O. Box 808
Livermore, CA 94550

Prof. John A. Orcutt
IGPP, A-025
Scripps Institute of Oceanography
University of California, San Diego
La Jolla, CA 92093

Dr. Howard Patton
Lawrence Livermore National Laboratory
L-025
P.O. Box 808
Livermore, CA 94550

Dr. Frank Pilotte
HQ AFTAC/TT
1030 South Highway A1A
Patrick AFB, FL 32925-3002

Dr. Jay J. Pulli
Radix Systems, Inc.
6 Taft Court
Rockville, MD 20850

Prof. Paul G. Richards
Lamont-Doherty Earth Observatory
of Columbia University
Palisades, NY 10964

Mr. Wilmer Rivers
Multimax Inc.
1441 McCormick Drive
Landover, MD 20785

Dr. Alan S. Ryall, Jr.
Lawrence Livermore National Laboratory
L-025
P.O. Box 808
Livermore, CA 94550

Dr.Chandan K. Saikia
Woodward Clyde- Consultants
566 El Dorado Street
Pasadena, CA 91101

Mr. Dogan Seber
Cornell University
Inst. for the Study of the Continent
3130 SNEE Hall
Ithaca, NY 14853-1504

Secretary of the Air Force
(SAFRD)
Washington, DC 20330

Office of the Secretary of Defense
DDR&E
Washington, DC 20330

Thomas J. Sereno, Jr.
Science Application Int'l Corp.
10260 Campus Point Drive
San Diego, CA 92121

Dr. Michael Shore
Defense Nuclear Agency/SPSS
6801 Telegraph Road
Alexandria, VA 22310

Prof. David G. Simpson
IRIS, Inc.
1616 North Fort Myer Drive
Suite 1050
Arlington, VA 22209

Dr. Jeffrey Stevens
S-CUBED
A Division of Maxwell Laboratory
P.O. Box 1620
La Jolla, CA 92038-1620

Prof. Brian Stump
Los Alamos National Laboratory
EES-3
Mail Stop C-335
Los Alamos, NM 87545

Prof. Tuncay Taymaz
Istanbul Technical University
Dept. of Geophysical Engineering
Mining Faculty
Maslak-80626, Istanbul Turkey

Prof. M. Nafi Toksoz
Earth Resources Lab
Massachusetts Institute of Technology
42 Carleton Street
Cambridge, MA 02142

Dr. Larry Turnbull
CIA-OSWR/NED
Washington, DC 20505

Dr. Karl Veith
EG&G
5211 Auth Road
Suite 240
Suitland, MD 20746

Prof. Terry C. Wallace
Department of Geosciences
Building #77
University of Arizona
Tuscon, AZ 85721

Dr. William Wortman
Mission Research Corporation
8560 Cinderbed Road
Suite 700
Newington, VA 22122

ARPA, OASB/Library
3701 North Fairfax Drive
Arlington, VA 22203-1714

HQ DNA
ATTN: Technical Library
Washington, DC 20305

Defense Technical Information Ctr
8725 John J. Kingman Road
Ft Belvoir, VA 22060-6218
(2 copies)

TACTEC
Battelle Memorial Institute
505 King Avenue
Columbus, OH 43201 (Final Report)

Phillips Laboratory
ATTN: GPE
29 Randolph Road
Hanscom AFB, MA 01731-3010

Phillips Laboratory
ATTN: TSML
5 Wright Street
Hanscom AFB, MA 01731-3004

Phillips Laboratory
ATTN: PL/SUL
3550 Aberdeen Ave SE
Kirtland, NM 87117-5776 (2 copies)

Dr. Michel Campillo
Observatoire de Grenoble
I.R.I.G.M.-B.P. 53
38041 Grenoble, FRANCE

Prof. Hans-Peter Harjes
Institute for Geophysic
Ruhr University/Bochum
P.O. Box 102148
4630 Bochum 1, GERMANY

Prof. Eystein Husebye
IFJF
Jordskjelvstasjonen
Allegaten 41, 5007 BERGEN NORWAY

David Jepsen
Acting Head, Nuclear Monitoring Section
Bureau of Mineral Resources
Geology and Geophysics
G.P.O. Box 378, Canberra, AUSTRALIA

Ms. Eva Johannisson
Senior Research Officer
FOA
S-172 90 Sundbyberg, SWEDEN

Dr. Peter Marshall
Procurement Executive
Ministry of Defense
Blacknest, Brimpton
Reading FG7-FRS, UNITED KINGDOM

Dr. Bernard Massinon, Dr. Pierre Mechler
Societe Radiomana
27 rue Claude Bernard
75005 Paris, FRANCE (2 Copies)

Dr. Svein Mykkeltveit
NTNT/NORSAR
P.O. Box 51
N-2007 Kjeller, NORWAY (3 Copies)

Dr. Jorg Schlittenhardt
Federal Institute for Geosciences & Nat'l Res.
Postfach 510153
D-30631 Hannover , GERMANY

Dr. Johannes Schweitzer
Institute of Geophysics
Ruhr University/Bochum
P.O. Box 1102148
4360 Bochum 1, GERMANY

Trust & Verify
VERTIC
Carrara House
20 Embankment Place
London WC2N 6NN, ENGLAND